HEAVY METAL DETECTION METHODS IN WATER USING QUARTZ CRYSTAL MICROBALANCE

by

Jiexiong Xu

A Thesis

Submitted to the Faculty of Purdue University

In Partial Fulfillment of the Requirements for the degree of

Master of Science

School of Engineering Technology

West Lafayette, Indiana

May 2022

THE PURDUE UNIVERSITY GRADUATE SCHOOL
STATEMENT OF COMMITTEE APPROVAL

Dr. Suranjan Panigrahi
School of Engineering Technology

Dr. Linda Lee
Department of Agronomy

Dr. Jennifer L. Freeman
School of Health Sciences

Approved by:
Dr. John Sheffield

Dedication

ACKNOWLEDGMENTS

I would like to acknowledge multiple individuals for their support and contributions to this thesis. First, I would like to express my gratitude to Dr. Suranjan Panigrahi for his tireless work and guidance throughout the entirety of this research. Second, I would like to thank my committee professors Dr. Linda Lee and Dr. Jennifer Freeman for their time and effort. In addition, I would also like to thank Heiner Castro, Anusha Hettiyadura, Ryan Hilger, and Lyu Yixuan for their contributions to this research. Finally, I would like to thank my parents, Purdue School of Engineering Technology, Purdue physics department, Purdue rowing team for their support and encouragement throughout my career at Purdue University.

TABLE OF CONTENTS

LIST OF TABLES

LIST OF FIGURES

LIST OF ABBREVIATIONS

AAS	Atomic Absorption Spectroscopy
As	Arsenic
CGL	Chitosan - Glutaraldehyde and lead ionophore ii
DTT	Dithiothreitol
FDA	Food and Drug Administration
Pb	Lead
Ppb	Parts per billion (micrograms / liter)
Ppm	Parts per million (milligrams / liter)
ICP-MS	Inductively Coupled Plasma Mass Spectrometry
ICP-OES	Inductively Coupled Optical Emission Spectrometry
WHO	World Health Organization

GLOSSARY

Dithiothreitol – “A Chelating sulfur-containing ligand.” (Kalluri et al., 2009, p. 1)

Glutaraldehyde – “Acts as the crosslinking agent, is added to improve the chemical stabilities of Chitosan.” (Lokman et al., 2019, p. 2)

Quartz Crystal Microbalance – “Piezoelectric crystals utilizes piezoelectric effect to measure the mass.” (Alassi et al., 2017, p. 1)

ABSTRACT

According to the World Health Organization, long-term exposures to heavy metal toxicants such as arsenic (As) and lead (Pb), even at the parts per billion (ppb, μg/L) level, can cause severe health problems such as cancer, skin lesions, and cardiovascular diseases. Therefore, an accurate and rapid heavy metal toxicant monitoring technique is needed. This research investigated the proof-of-the concept of a portable sensor for detecting As and Pb in water. The sensor system utilized a Quartz Crystal Microbalance - QCM (openQCM w-i2) system interfaced with a computer as the sensing platform. It was further integrated with a peristaltic pump and required tubing to create the integrated sensing system. It used a 10 MHz AT-cut quartz crystal gold electrode as the sensing substrate. For the determination of As in water, dithiothreitol (DTT) was used as the ligand to be deposited on the gold electrode using the Self-assembly-monolayer method (SAM). For the determination of Pb, a combination of ligands (Chitosan, Glutaraldehyde, and lead ionophore II - CGL) was used and deposited on the gold electrode using the spin-coating method. The system was tested for As in water with specific concentrations (0, 50, 100, and 200 ppb) under laboratory conditions. Similarly, the system was tested for Pb in water with different concentrations (0, 10, 25, 50, and 100 ppb) under laboratory conditions. The resulted change of frequency (with respect to time, in seconds) of the QCM system to different concentrations of the individual analyte was recorded. Subsequently, the recorded data were analyzed to determine the correlation model and coefficient of determination, R^2. The maximum R^2 values for detecting As and Pb were 0.963 and 0.991, respectively. Thus, this proof-of-the-concept study using the developed QCM-based sensing system for detecting As and Pb in water was successful.

CHAPTER 1-INTRODUCTION

1.1 Problem Statement

Heavy metal pollution causes a variety of health concerns around the world. According to the World Health Organization (WHO), health problems such as cancer, skin lesions, cardiovascular diseases, and cognitive disorders have correlations with long-term exposure to heavy metal particles such as arsenic from water and food (World Health Organization, 2018). According to the WHO, no level of lead exposure was free from harmful effects, and heavy metal toxicants such as lead accounted for 900,000 deaths in 2019 (World Health Organization, 2021). According to research by (Fasinu & Orisakwe, 2013), urbanization, mining, and lack of waste control were the primary reasons for increased heavy metal pollution in sub-Sahara Africa. Surface water in some African countries had arsenic concentrations up to 10,000 parts per billion (ppb, μg/L) (Ahoulé et al., 2015). The surface water value was 1,000 times higher than the 10 ppb lower limit regulated by the WHO. Arsenic-contaminated water could also mitigate into food crops. Heavy metal contaminated food and water posed a serious health risk; even the World Health Organization called for actions to reduce human exposure to heavy metal toxicants such as arsenic and lead (WHO & World Health Organization, 2019).

Monitoring of drinking water was the first step in preventing humans from consuming heavy metal toxicants. Conventional methods for detecting arsenic samples such as atomic absorption spectrometry (Shen et al., 2018), inductively coupled plasma optical emission spectroscopy (Yao et al., 2017), and inductively coupled plasma with mass spectrometry (Galiová et al., 2008) provided highly accurate detection. However, these methods required a long wait for the results, complicated sample preparation, and experienced hand for operation.

The following research presents a portable, low-cost heavy metal (As, Pb) detection sensor in water with sensing capability at the ppb level. The sensor systems utilized Quartz Crystal Microbalance (QCM) system.

1.2 Significance

The rapid industrialization in developing countries continues to accelerate. However, the benefit of rapid industrialization also comes with the cost of heavy metal toxicant pollution. On average, rapid industrializing countries such as China discharge 21.8 billion m^3 of heavy metal contaminated wastewater in natural water bodies per year (Yang et al., 2022). However, developing countries cannot perfect environmental regulations overnight.

Sensors with selective detection capability and ppb level limit of detection can prevent people from consuming waters with heavy metal toxicants and prevent death and illnesses. Therefore, a cost-effective, portable sensor is necessary with acceptable accuracy.

1.3 Goal of the Project

The goal of this research was to develop a proof of the concept for the QCM-based heavy metal sensor to detect arsenic and lead in water.

1.4 Objectives

The associated objectives are to develop and test a QCM-based sensor to detect arsenic in ultra-pure water. Subsequently, Develop and test a QCM-based sensor to detect lead in ultra-pure water.

CHAPTER 2-REVIEW OF LITERATURE

The research aimed to develop QCM based heavy metal sensor that specifically detected arsenic and lead particles in water. Therefore, the literature review focused on QCM sensor applications in heavy metal sensing in water. The following sections included a review of QCM sensing principles, heavy metal detection methods, quartz crystal gold electrode cleaning methods, ligand modification techniques, general components of QCM sensing systems, and sample preparation methods. The information acquired from the review was incorporated into the development of QCM based heavy metal sensor that detected arsenic and lead particles.

2.1 QCM Based Mass Sensor

The Quartz Crystal Microbalance (QCM) measured the frequency value of a vibrating crystal in an anti-parallel manner. The relationship between the change of frequency and mass change was linear (Reviakine et al., 2011). The relationship between the change of frequency and mass change in a liquid environment was best described by the resonance frequency shift equation (Alassi et al., 2017). The equation is primarily used to describe frequency shift for liquid measurement and shows the negative correlation between the shift of frequency and increase of mass.

$$\frac{\Delta f_M}{f_0} = -\frac{2Nf_0\Delta m}{A_e\sqrt{\mu_q\rho_q}}$$

Resonance frequency shift equation, A_e is the surface area of the crystal, ρ_p is the density, η_q is crystal's the shear modulus (Alassi et al., 2017).

The QCM's detection sensitivity for mass was as low as 4.42 ng/cm^2 (Jahnke et al., 2016). Therefore it was used for microscopic mass detection (Reviakine et al., 2011).

However, not all mass sensing from QCM produced a negative correlation between the shift of frequency and mass increase. For example, the frequency value increased with a thick ligand as the mass value increased (Sadman et al., 2018).

2.2 QCM based Heavy Metal Sensors

QCM sensor detected verities of heavy metal particles and achieved a reasonable detection limit. The following review examined the application of the QCM instrument in heavy metal sensing and studied theories and methodologies behind the successful detection of ppb-level heavy metal detections. A QCM based copper (Cu), lead (Pb), chromium (Cr), and cadmium(Cd) liquid sensor utilized 5 MHz AT-cut quartz crystal gold electrodes coated with polymer chains and achieved 0.01 – 10000 parts per million (ppm, μg/L) detection sensitivity, cadmium being the highest and copper was the lowest (Sartore et al., 2011).

The QCM sensor also achieved single-digit ppb concentration detection on cadmium (Cd), which used spin-coater to deposit single-walled carbon nanotubes and beeswax on 5 MHz AT-cut quartz crystal 5.2 ppb cadmium (Taneja et al., 2018). Taneja's study also displayed an image of binding between (Cd) and single-walled carbon nanotubes from a field emission scanning electron microscope and reported a positive correlation between ligand density and sensor sensitivity.

The QCM sensor detected lead particles at ppm-level concentration with a Calixresorcinarenes coated 5 MHz AT-cut quartz crystal gold electrode detected lead particles in water at 0.89 ppm concentration (Eddaif et al., 2020).

In summary, QCM-based heavy metal sensors require selective ligand chemicals that bind with a specific element. Therefore, the quartz crystal gold electrode modification was crucial for successful heavy metal sensing.

2.3 QCM based Arsenic Sensor

Arsenic (As) poses a severe health effect on the human body (World Health Organization, 2018). A QCM-based arsenic sensor if developed successfully can quickly and accurately monitor the arsenic concentration in drinking water. The zirconia nanoparticle-loaded hydrogel coated on 9MHz AT-cut quartz crystal detected arsenic in liquid samples, and hydrogel selectively detected As (III) and As(V) and achieved a 0.57 mg/m^3 limit of detection (Tokuyama et al., 2020).

Another study reported by Li et al. (2013) mixed dithiothreitol (DTT) in the arsenic sample and detected Arsenate As(V) and Arsenite As (III) particles in water at 2-ppb concentration. The advantage of Li's research was that it utilized the self-assembled monolayer and allowed the DTT to bind the gold surface and arsenic during detection.

2.4 Quartz Crystal Gold Electrode Cleaning

Quartz Crystal Gold electrode cleaning was a crucial step in improve QCM detection sensitivity. The research result (Poitras & Tufenkji, 2009) reported cleaning AT-Cut, 5 MHz quartz crystal gold electrode with Hellmanex, hydrogen peroxide, and ammonia mixed with ultrapure deionized water for E.coli detection. Another cleaning method described by Sartore reported cleaning AT-Cut, 9 MHz quartz crystal gold electrode by soaking 0.222 M cystamine solution for 72 hours at room temperature (Sartore et al., 2011). Both two methods provided

quick and easy cleaning procedures for significant sensitivity increase. However, neither had reported the potential damages to the quartz crystal gold electrode.

A study on gold cleaning methods for electrodes reported by Fischer indicated solution mixture of potassium hydroxide and hydrogen peroxide was the optimal cleaning method with minimal damage to the gold surface (Fischer et al., 2009). On the other hand, the cleaning procedure utilized potassium hydroxide and hydrogen peroxide combination reported by Heiskanen boiled the electrode in acetone, then submerged the electrode in 50 mM potassium hydroxide dissolved in hydrogen peroxide with 25 % (v/v) concentration (Heiskanen et al., 2008). In addition, Heiskanen's research incorporated a potential sweep method from -200 mV to -1200 mV.

2.5 Arsenic Detection Ligand

The research reported by Li (Li et al., 2013) utilized dithiothreitol (DTT) as a sensing ligand. Li's research's advantage was the simplicity of DTT incorporation in arsenic and achieved a low limit of detection (0.6 ppb). Furthermore, the DTT as a thiol group can also bind to the surface of gold automatically using the self-assembled monolayer method and allow sensing of other chemicals (Creczynski-Pasa et al., 2009).

2.6 Lead Detection Ligand

The self-assembled monolayer method was also used for lead particle detection. The detection DNAzyme combined with nanomagnetic beads and deposited on the quartz crystal gold electrode using the self-assembled monolayer method detected lead particles in liquid samples (Zhang et al., 2018)

Drop cast calixaresorcinarene on quartz resonator also successfully detected lead particles in liquid samples and achieved a 300 ppb limit of detection(Eddaif et al., 2020). In addition, the thioglycolic acid-modified CdTe (nanospheres) on QCM also achieved a 0.096 ppb limit of detection for lead particles (Sun et al., 2020).

The research reported by Koksharov (Koksharov et al., 2019) utilized pectin to attract lead particles. Koksharov utilized the linear regression fitting method and concluded that pectic acid was the most effective agent when forming a bond with lead ions.

Chitosan film was another possible ligand for quartz crystal gold electrode deposition and lead sensing. Research reported by (Lokman et al., 2014) utilized chitosan-glutaraldehyde crosslink combined with lead ionophore and graphene oxidize nanosheets on surface plasmon resonance (SPR) to improve the detection sensitivity of Pb (II) ions. However, there has been no research utilizing chitosan film to detect lead nanoparticles using QCM. However, chitosan detected methylamine (Ayad & Minisy, 2016) and volatile organic compounds (Ayad et al., 2014).

2.7 Pump

The characteristics of the pump needed in QCM liquid sensing were important due to the sensor's sensitivity. The QCM sensor required a pump with minimal disturbance and a consistent flow rate for successful measurement. *Table 2.1* shows the number of pump choices used in the QCM system for the liquid sensing experiment.

Table 2.1 selection of liquid pumps used in QCM based sensing experiments

Type of Pump	Element	Flow rate (μL/min)	Circuit volume (μL)	Chamber pre-fill	Detection Limit (ppb)	Signal Stabilization time (sec)	Reference
Gilson Peristaltic pump	Cu^{2+} Cd^{2+} Pb^{2+}	50	Did not mention	Prefilled with double-distilled deionized water	10,000	2400	(Cao et al., 2011)
Knauer Volumetric Pump	Cu Pb Cr Cd	400	Did not mention	5-10min natural water as mobile, the fill the chamber with consecutive injections of HMS	10 -1000000	300-600	(Sartore et al., 2011)
Fluidic Pump	Cd, Cr, Cu, Fe, Ni, Pb, Se, Zn	300-1000	150	Use the maximum flow rate of the pump to clean the chamber with distilled water	1	600	(Cimpoca et al., 2010)
Peristaltic pump	P. putida biofilm	200	N/A	N/A	N/A	36000	(Sprung et al., 2009)
Peristaltic pump	Al^{+3}	3,000	5000	Pure water and 50 μM ammonium chloride were alternatively injected into the chamber using the pump	N/A	900	(Kosaki et al., 2012)
peristaltic pump (made by Gilson)	salivary α-amylase	3	200	N/A	1000	1000	(Ventura et al., 2017)
syringe pump	Bacteria	1-5	N/A	N/A	N/A	N/A	(Jahnke et al., 2016)
Gilson peristaltic pump	synthetic thrombin aptamer	N/A	30	N/A	N/A	N/A	(Politi et al., 2016)
Gilson peristaltic pump	Pb^{+2} Cd^{+2} AS^{+2}	N/A	30	N/A	1.2	N/A	(Politi et al., 2017)

CHAPTER 3-RESEARCH METHODOLOGY

The focus of this research was proof of the concept that the Quartz Crystal Microbalance (QCM) based heavy metal sensors had capabilities to selectively detect ppb concentration arsenic (As) and lead (Pb) in ultra-pure water. The research had two parts. The first part of this research focused on developing an arsenic detecting QCM system. The arsenic sensor development included combining hardware and software, modifying quartz crystal gold electrodes with ligand, and data analysis.

The subsequent research for lead detection included quartz crystal gold electrode modification with a different ligand specific for lead detection and analyzed data acquired from lead concentrations.

3.1 QCM Based Arsenic Sensor

The openQCM wi-2 device was purchased from openQCM Co. (openQCM, Italy). The device was integrated with electronic hardware, a microcontroller (internally), and a 50 μL sampling chamber. The openQCM wi-2 device also had a white release lever that must be at the minimum setting before removing the liquid cap from the device. Once the liquid chamber was exposed under the liquid cap, the quartz crystal gold electrode was placed at the center of the sampling chamber. Subsequently, we closed the liquid cap and pushed the lever to the medium setting for optimal chamber sealing. The openQCM wi-2 device also had a provision to be interfaced with a 14 mm diameter, 10 MHz, AT-cut circular quartz crystal gold electrode; and the QCM sensing system has provisions to be interfaced with a personal computer via a USB. In addition to frequency, the system also measures the temperature in the sampling chamber.

Therefore, the temperature fluctuation can be observed, and appropriation can be made to compensate for temperature fluctuation.

The wi-2 device required some modification to be ready for the sensing experiment. The modification included integrating a Masterflex 30μL/min Low-Flow peristaltic pump purchased from Cole Parmer Co. (Cole Parmer, USA), a modification of quartz crystal gold electrode with sensing ligand and adjusting the sampling chamber for optimal sealing. *Figure 3.1* shows an overview of QCM-based arsenic sensor system development.

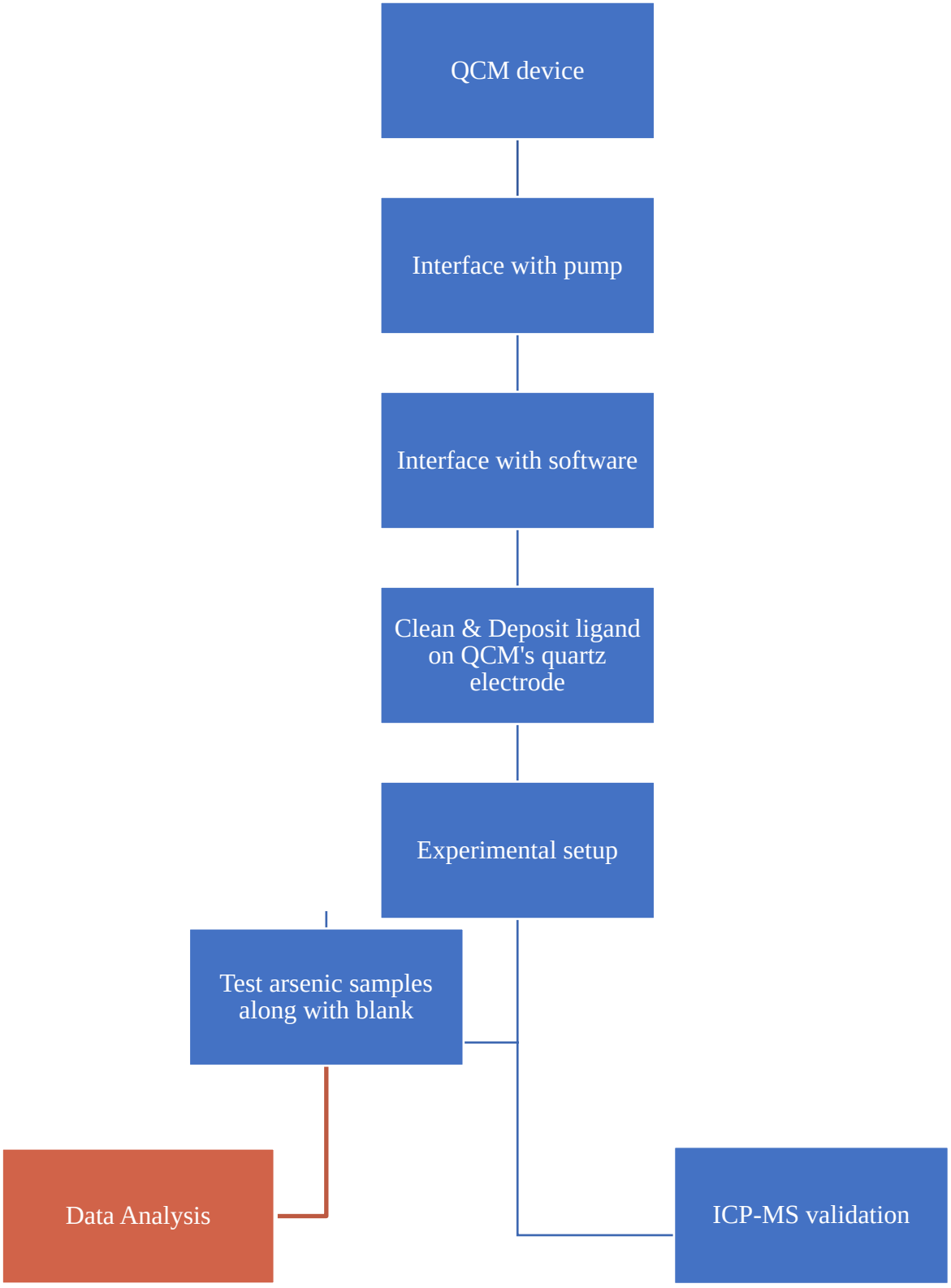

Figure 3.1 QCM-based arsenic sensor development and testing overview.

3.1.1 QCM System Integration

The QCM system integration followed the openQCM's user guide (Quartz & Microbalance, 2021). The liquid cap on QCM has two holes: the inlet and outlet. The inlet (larger diameter) was interfaced to an inlet tube connecting the container of the liquid sample to be analyzed. The outlet hole of the liquid cap was connected to an outlet tube which is intern interfaced with the inlet port of the peristaltic pump. Before each experiment, we used a conventional injection syringe (without a needle) to suck (pull) ultra-pure water from the sample container via the outlet port until the sample chamber was filled. Subsequently, the outlet tube was connected to the outlet port. We also used a specific barb connector to connect the inlet/outlet tube with a peristaltic pump. *Figure 3.2* shows a picture of the QCM system, which includes an openQCM wi-2 equipped with a liquid cap, a Masterflex 30µL/min Low-Flow peristaltic pump, an inlet tube connected to the larger hole of the liquid cap and sample container, outlet tube connected to the smaller hole of the liquid cap and peristaltic pump, a waste beaker, and a personal computer. *Figure 3.3* shows a side-by-side image of a quartz electrode and a quartz electrode installed in QCM's sampling chamber.

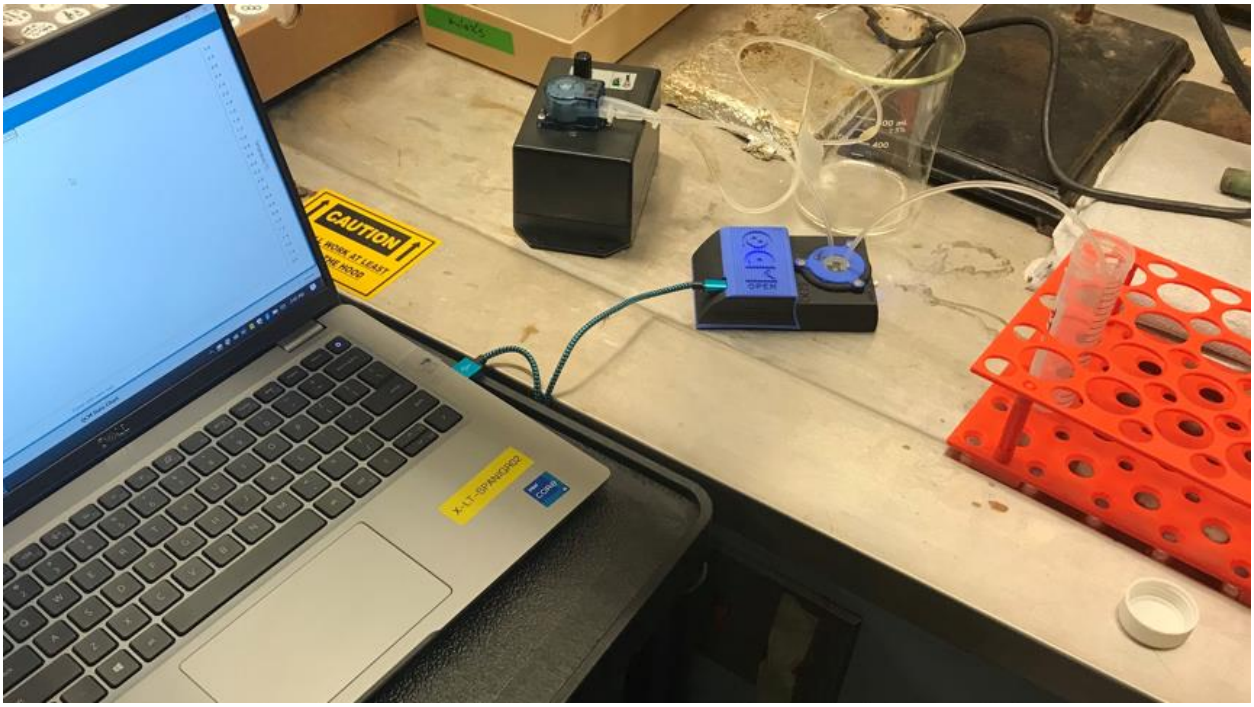

Figure 3.2 A picture of an integrated QCM system.

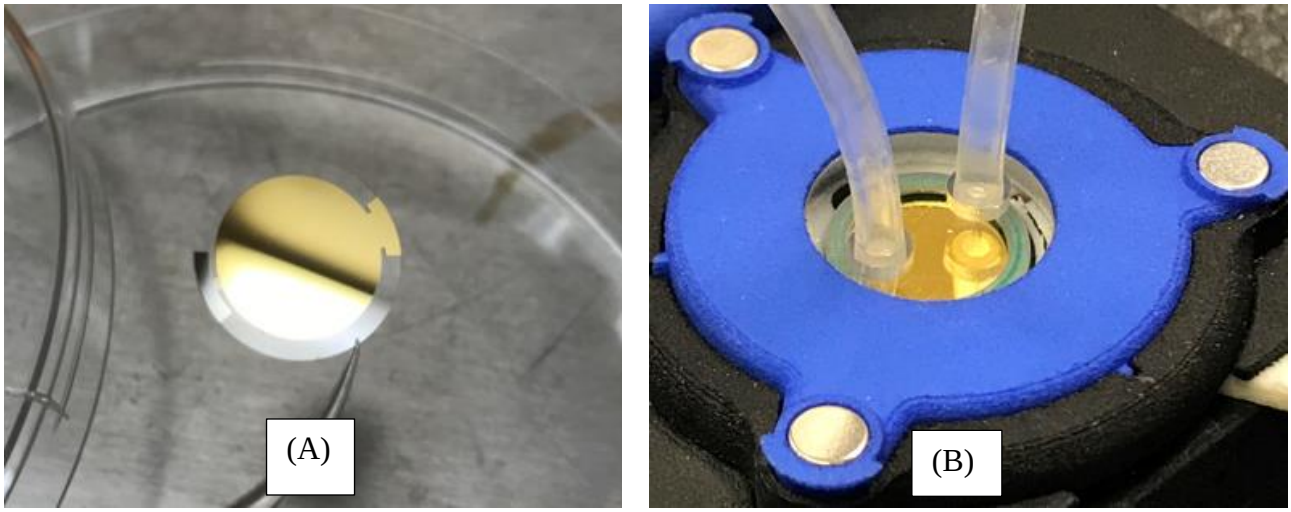

Figure 3.3 (A) Cleaned quartz crystal gold electrode. (B) A quartz crystal gold electrode was installed in QCM's liquid chamber.

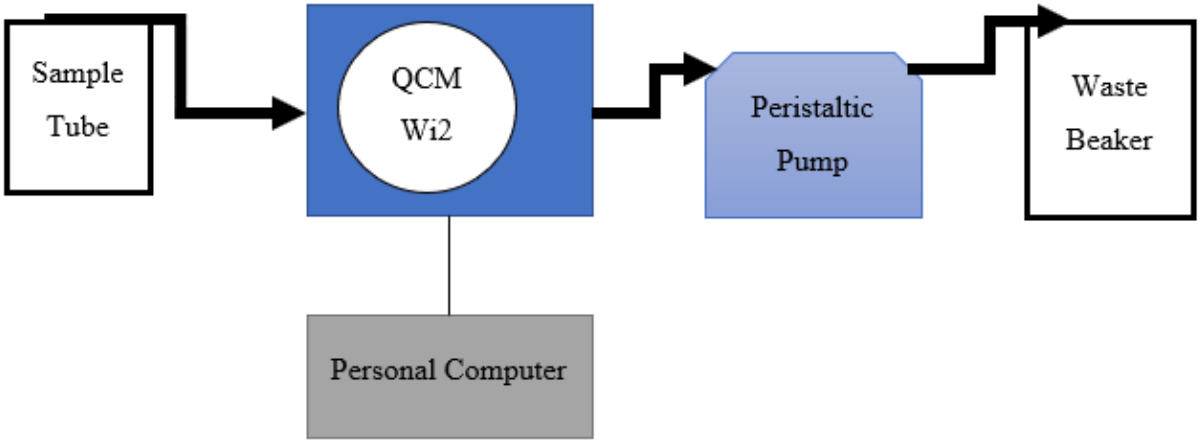

Figure 3.4 The schematic image of the QCM system. The black arrows represent connection tubes and the flow direction of liquid sample. The narrow black line represents the USB connection between openQCM wi-2 device and a personal computer.

3.1.2 Glucose Experimental Procedure

A preliminary glucose experiment (Mauro, 2015) was conducted using the QCM system. Glucose samples with different concentrations were used to assess the functionality of the integrated QCM system. The glucose samples were prepared by dissolving D-Glucose powders purchased from Fisher Chemical Co. (Fisher Chemical, USA) in ultra-pure water. In this research, we prepared three concentrations (0, 41.6, and 84.6 M) of glucose by dissolving 0, 7.5, and 15 grams of D-Glucose powder in three containers (centrifuge tube) of 50 ml ultra-pure water reservoir. The QCM system recorded the frequency signal of each three concentrations three times.

The sample injection time was 6 minutes after switching on the peristaltic pump. Once the sample injection was complete and the pump was switched off, the QCM needed 10 minutes of resting time to reach a stable frequency value. *Table 3.1* shows the glucose sample's sequences of injection.

Table 3.1 Glucose experiment's sequences of injection. (The pumping time for the sequence of injection 2 was 3 minutes due to an error of timing during the experiment).

Sequence of injection	Sample name	Pumping time (min)	Signal Resting (Stabilization) time (min)	Total Recording Time (min)
1	0M Glucose	6	15	20
2	41.6M Glucose	3	10	13
3	0M Glucose	6	10	16
4	41.6M Glucose	6	10	17
5	0M Glucose	6	10	16
6	41.6M Glucose	6	10	16
7	0M Glucose	6	10	16
8	84.6M Glucose	6	10	16
9	0M Glucose	6	10	16
10	84.6M Glucose	6	10	16
11	0M Glucose	6	10	16
12	84.6M Glucose	6	10	16

3.1.3 Quartz Crystal Gold Electrode Cleaning

The cleaning procedure was the first step of the quartz crystal gold electrode modification. The cleaning ensured the successful ligand deposition. In this research, the cleaning protocol (Heiskanen et al., 2008) was adopted, and it incorporated the use of boiling acetone and potassium hydroxide/ hydrogen peroxide mixture ($KOH+H_2O_2$). This method was the second-best cleaning method and was reported to cause minimum damage to quartz crystal gold electrodes (Fischer et al., 2009).

Reagents. The Acetone (Certified ACS), Potassium Hydroxide (KOH), and Hydrogen Peroxide 30% w/v (H_2O_2) were obtained from Fischer Chemical Co. (Fischer Chemical, USA).

Cleaning. Each quartz crystal gold electrode was placed in a glass beaker containing 20 mL of boiling acetone bath for 10 minutes. The acetone glass beaker was held by a clamp on a ring stand and soaked in a 100 ml beaker that contained deionized water on a hot plate. Then, the quartz crystal gold electrode was moved to 50mM Potassium Hydroxide dissolved in 25%

Hydrogen Peroxide contained in a glass beaker. Each quartz crystal gold electrode was cleaned in the ($KOH+H_2O_2$) mixture for 10 minutes. However, the damage was visible after 10 minutes of cleaning. Therefore, the cleaning time was reduced to 8 minutes for subsequent cleanings. Finally, the cleaned quartz crystal gold electrode was rinsed in ultra-pure water before ligand deposition.

3.1.4 Ligand Deposition

The dithiothreitol (DTT) demonstrated promising results when detecting arsenic in water with a QCM system (Li et al., 2013). In addition, the self-assembled monolayer successfully allowed the deposition of DTT onto the gold surface (Creczynski-Pasa et al., 2009). In this research, we incorporated methodologies from both Li and Creczynski-Pasa's and deposited DTT on the surface of the quartz crystal gold electrode by using the self-assembled monolayer (SAM) attracted arsenic in water. The SAM procedure followed the guideline provided by Sigma Aldrich (*Preparing Self-Assembled Monolayers*, n.d.).

Reagents. The ligand chemical dithiothreitol (DTT) was obtained from Sigma-Aldrich Co. (Sigma-Aldrich, USA), and 200 proof ethanol was obtained from Fischer Chemical Co. (Fischer Chemical, USA).

Ligand Deposition. An amount of 10 ml of 1mM DTT stock solution was prepared in a 15 ml centrifuge tube by mixing 0.154 g of DTT in 10 ml of 200 proof ethanol. Subsequently, 70 μL of DTT stock solution was added to a Nalgene bottle that contained 140 ml of 200 ethanol to make the 50 μM DTT solution. Then, a pre-cleaned quartz crystal gold electrode rinsed with 50uM DTT was placed in the Nalgene bottle with 50 μM DTT solution for 24 hours with the cap closed.

Finally, the quartz crystal gold electrode was taken out of the Nalgene bottle and dried in a petri-dish for 12 hours.

3.1.5 Arsenic Experimental Plan

In this research, the QCM system recorded frequency vs. time variation of arsenic in ultra-pure water prepared in laboratory conditions. Arsenic samples were diluted from 1,000-ppm arsenic in 2% HNO_3 stock solution purchased from Exaxol Co. (Exaxol, USA). We also prepared additional arsenic samples in 0.5% HNO_3 and validated the sample preparation methodology using ICP-MS. The sample preparation procedure followed the demonstration protocol by Dr. Anusha Priyadarshani Silva Hettiyadura from Purdue University's Department of Chemistry. All arsenic samples were prepared on the same day of the experiment.

Reagent. The ultra-pure HNO_3 for ICP analysis was obtained from Shimadzu Co. (Shimadzu, Japan). The 1,000-ppm arsenic in 2% HNO_3 stock solution was obtained from Exaxol Co. (Exaxol, USA).

Arsenic sample preparation. The Nalgene volumetric flasks (100 mL) were rinsed five times with ultra-pure water before they were used to dilute the arsenic stock solution. Each plastic volumetric flask was designated only for one arsenic concentration. The 0.5% HNO_3 solution was prepared in a 500 ml Nalgene volumetric flask by diluting 3.6 ml of HNO_3 in 496.4 ml of ultra-pure water. The concentrations of arsenic samples were 0, 50, 100, and 200 ppb. Additional sample preparation information can be found in Appendix F.

QCM measurement of arsenic. The QCM system installed with a DTT deposited quartz crystal gold electrode recorded frequency vs. time variation of arsenic samples prepared in the laboratory. The injection of the arsenic sample for each experiment was from low concentration

to high concentration. The injection time for all arsenic samples was 5 minutes and required 10 to 15 minutes for the frequency to stabilize overtime before the next sample injection. Initial experiments included injection of ultra-pure water between each measurement of samples. However, more injections caused bubbles to accumulate; therefore, the procedure was abandoned. *Table 3.2* shows the sequence of sample injection for the arsenic experiments with the injection of the ultra-pure water between each arsenic sample. *Table 3.3* shows the sequence of sample injection for the arsenic experiment without the injection of ultra-pure water between each arsenic sample.

Table 3.2 Arsenic sample injection sequences

Sequence of Injection	Sample Name	Pumping time (min)	Signal Resting (stabilization) time (min)	Total Recording time (min)
1	As 0 ppb	5	10	15
2	Ultra-pure water	5	10	15
3	As 50 ppb	5	10	15
4	Ultra-pure water	5	10	15
5	As 100 ppb	5	10	15
6	Ultra-pure water	5	10	15
7	As 200 ppb	5	10	15

Table 3.3 Arsenic sample injection sequences without injecting ultra-pure water between each sample and increased stabilization time.

Sequence of Injection	Sample Name	Pumping time (min)	Signal Resting (stabilization) time (min)	Total Recording time (min)
1	As 0 ppb	5	15	20
2	As 50 ppb	5	15	20
3	As 100 ppb	5	15	20
4	As 200 ppb	5	15	20

3.1.6 ICP-MS Operation Procedure

The ICP-MS in the Purdue Chemistry Department analyzed the arsenic samples prepared in 0.5% HNO_3. The ICP-MS was the Thermo Scientific Element 2 mass spectrometer. The injection of the arsenic sample utilized the Aridus II Desolvating Sample Introduction system, which had a concentric nebulizer flow rate of 100 μL/min (Teledyne Cetac Technologies, USA). The experiment also utilized a Teledyne Cetac Autosampler ASX-112FR. The tuning and calibration of the ICP-MS used 1 ppb arsenic Thermo Fisher Tune-Up solution.

3.2 QCM Based Lead Sensor

The QCM system setup for lead (Pb) detection was the same as arsenic (As) detection. However, the quartz crystal gold electrode required different ligand modifications. Initially, a ligand-based on chitosan was used. Subsequently, the quartz crystal gold electrode underwent chitosan-glutaraldehyde crosslink modification combined with lead ionophore II and this combination is called “CGL” for selective lead particle sensing.

3.2.1 Quartz Crystal Gold Electrode Modification for Lead Detection

To selectively attract lead (Pb) particles, the quartz crystal gold electrode needed deposition of recognition chemical. Chitosan was an ideal sensing ligand for biosensors (Koev et al., 2010). Initially, we considered chitosan as a sensing ligand for binding lead particles in water. However, the chitosan material was unstable in a liquid environment, and the sensor generated random signals. Therefore, a stablizing agent was necessary to incorporate chitosan as a liquid sensing ligand. Glutaraldehyde functioned as a stable chemical that ensured the stability of chitosan in a liquid environment (Lokman et al., 2019). The following section describes the protocol for the chitosan-glutaraldehyde crosslink ligand combined with lead ionophore II (CGL). The ligand preparation recipe was based on a previous study on Pb (II) detection using chitosan-graphene oxide nanocomposite (Lokman et al., 2019).

Reagent. Both the chitosan and lead ionophore II were obtained from Sigma Aldrich Co. (Sigma Aldrich, USA). The glutaraldehyde was obtained from Fischer Chemical Co. (Fischer Chemical, USA)

Preparation of CGL ligand. The chitosan solution was prepared in a Falcon centrifuge tube by dissolving 0.4 g of chitosan in 50 ml of 1% acidic acid and stirred continuously on a magnetic stirrer for 12 hours. Then, we added 0.2 ml of glutaraldehyde to the chitosan solution and continued stirring for another 12 hours. Subsequently, 10 mg of lead ionophore II was dissolved in 1 ml of 200 proof ethanol in a separate Falcon centrifuge tube, then 4 ml of ultra-pure water was added. Finally, in a new 50 ml Falcon tube, 45 ml of chitosan/glutaraldehyde solution was mixed with 5 ml of lead ionophore solution.

Drop Casting. A cleaned quartz crystal gold electrode was placed at the center of a petri-dish. (See 3.1.3 for cleaning protocol). Subsequently,we pipetted 0.05 ml of CGL ligand solution

at the center of the quartz crystal gold electrode. Finally, the quartz crystal gold electrode was baked in an oven for 20 minutes at 65 degrees Celsius.

The QCM sensor installed with a drop-casted quartz crystal gold electrode did not generate a proper resonant frequency response after injection of ultra-pure water. Therefore, the sensor did not work as intended. The film thickness reduction was necessary for the CGL sensing ligand to function. Therefore, we chose the spin-coating method as an alternative deposition method to reduce the thickness of CGL ligand film.

Spin Coating. The spin coating recipe was adapted from another application of chitosan-based ligand on copolyester; which the spin coater produced uniform thickness on the surface (Niemczyk et al., 2015). First, the quartz crystal gold electrode was cleaned with the same cleaning protocol described in section 3.1.3. Then, a cleaned quartz crystal gold electrode was placed at the vacuum center of the SPIN 150i spin coater manufactured by SPS Co. (SPS, Germany). Then the 0.05 ml of CGL ligand was deposited on the center part of a quartz crystal gold electrode using a micropipette. Subsequently, a spin coating operation was performed (*Table 3.4*). Then the coated quartz crystal gold electrode was removed and stored in a petri-dish with a cover.

Table 3.4 Spin coating recipe for CGL deposition (Niemczyk et al., 2015)

The sequence of spinning action	Time (sec)	Spin Velocity (rpm)	Spin Acceleration (rpm/sec)
1	5	250	50
2	30	1000	100
3	30	1500	200
4	30	240	50

3.2.2 Lead Experimental Plan

In this research, the frequency vs. time variation of lead samples in ultra-pure water was recorded by the QCM system installed with CGL spin-coated quartz crystal gold electrode. Lead samples were diluted from a 100 ppm lead stock solution purchased from Exaxol Chemical Co. (Exaxol, USA). We recorded three sets of frequency vs. time variation of three different lead concentrations in 0, 100, and 200 ppb. Subsequently, we recorded three sets of frequency vs. time variation of five more lead concentrations in 0, 10, 25, 50, and 100 ppb. All samples were prepared on the same day of the experiment.

Reagent. The stock solution (100 ppm lead in 2% HNO_3) was obtained from Exaxol Chemical Co. (Exaxol, USA).

Lead stock dilution. Nalgene volumetric flasks (100 ml) were rinsed five times with ultra-pure water before they were used to dilute 100 ppm lead in 2% HNO_3 stock solution. We prepared 100 ml of 0, 100, 200 ppb lead solution and 100 ml of 0, 10, 25, 50, and 100 ppb lead solution. Additional information on sample preparation can be found in Appendix F.

QCM measurement of lead. We used QCM system installed with a spin-coated CGL ligand deposited quartz crystal gold electrode recorded frequency vs. time variation of lead samples prepared in the laboratory. The injection of lead sample for each experiment was from low concentration to high concentration. The injection time for all lead samples was 5 minutes and the resting time before the injection of subsequent sample was 15 minutes. The resting time allowed frequency value stabilize overtime. *Table 3.5* and *Table 3.6* show the lead sample injection sequence for three different lead concentrations in ultra-pure water and five different lead concentrations in ultra-pure water.

Table 3.5 Lead sample injection sequence for three different concentrations of lead samples.

Sequence of injection	Sample Name	Pumping time (min)	Signal resting time (stabilization) (min)	Total Recording time (min)
1	Pb 0 ppb	5	15	20
2	Pb 100 ppb	5	15	20
3	Pb 200 ppb	5	15	20

Table 3.6 Lead sample injection sequence for five different concentrations of lead samples.

Sequence of injection	Sample Name	Pumping time (min)	Signal resting time (stabilization) (min)	Total Recording Time (min)
1	Pb 0 ppb	5	15	20
2	Pb 10 ppb	5	15	20
3	Pb 25 ppb	5	15	20
4	Pb 50 ppb	5	15	20
5	Pb 100 ppb	5	15	20

CHAPTER 4-RESULTS

4.1 QCM Based Arsenic Sensor

The dithiothreitol (DTT) compound was used as a thiol, which attracted arsenic (As) in water and then attached to the quartz crystal gold surface, which caused the change of mass and frequency of a QCM (Li et al., 2013). Based on Li's research, modifying the measuring methodology was necessary to better suit the openQCM wi-2 hardware. *Figure 4.1* shows an image of the integrated QCM system for arsenic sensing used for this research.

4.1.1 QCM System Assembling

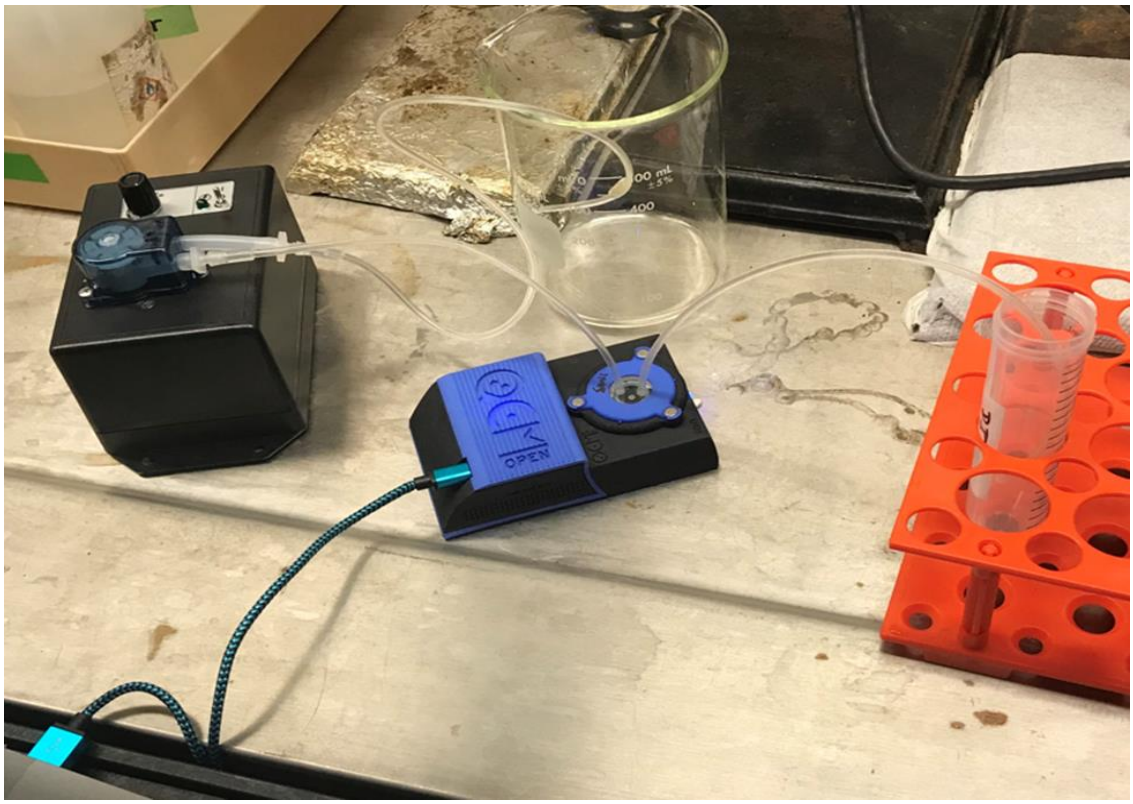

Figure 4.1 QCM system with a peristaltic pump, wi-2 QCM device, centrifuge tube with sample, waste beaker, and connection tubes.

Figure 4.2 – Figure 4.6 show components of the QCM sensing system. The sensing system comprised with openQCM wi-2 QCM device, a 10 MHz AT-cut quartz crystal gold electrode, a peristaltic pump, three connection tubes, centrifuge tubes for samples, a waste beaker, and a personal computer.

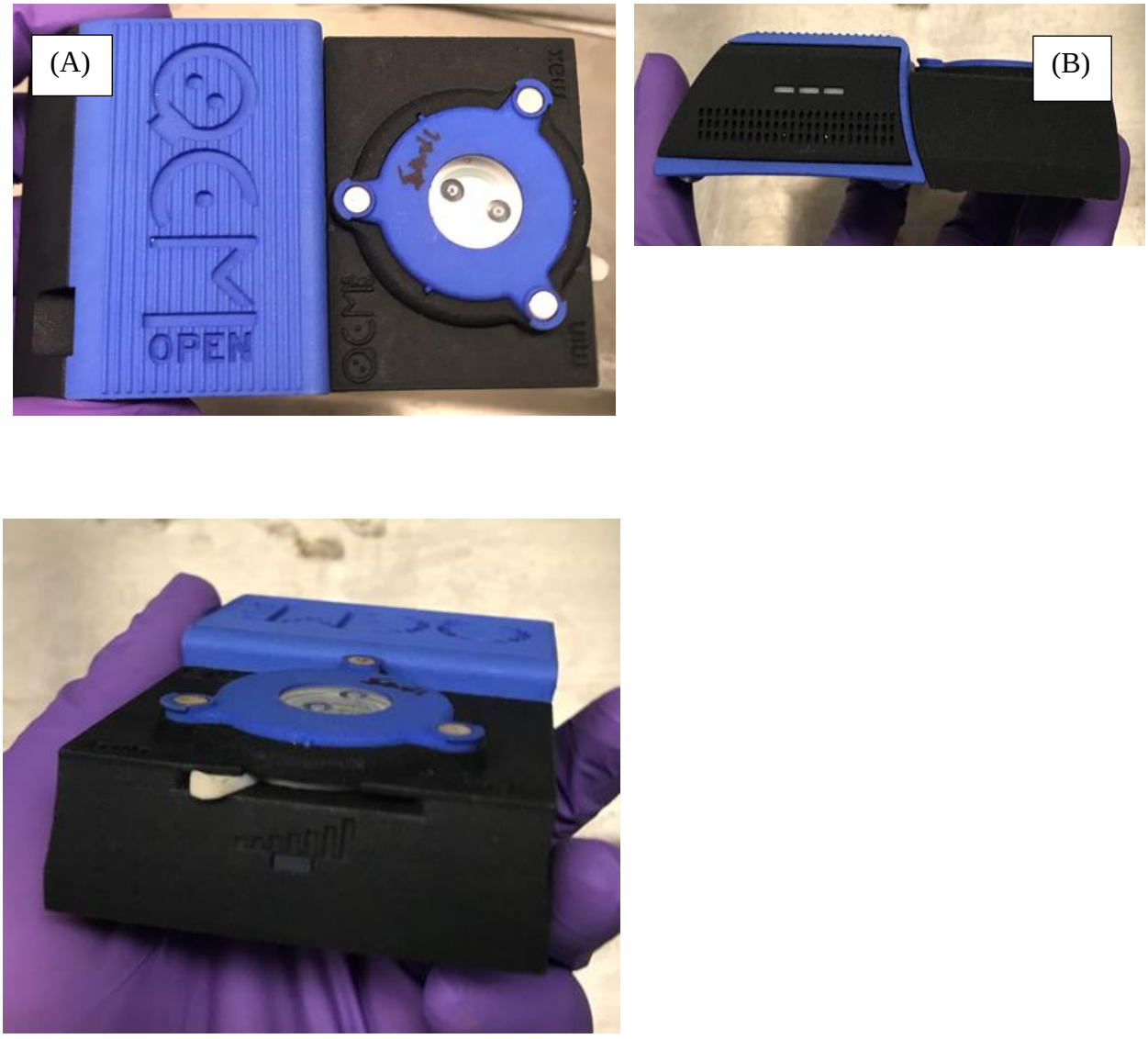

Figure 4.2 Different views of the openQCM wi-2 device. (A) top view (b) side view (C) front view.

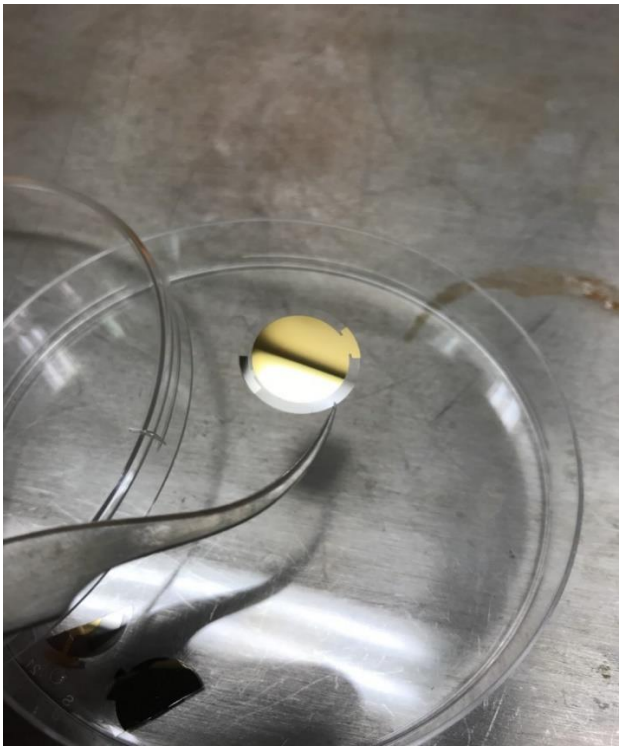

Figure 4.3 Image of an AT-cut 10 MHz quartz crystal gold electrode (openQCM, Italy).

Figure 4.4 Masterflex 30µL/min Low-Flow peristaltic pump (Cole-Parmer, USA). (A) Top view. (B) Side view.

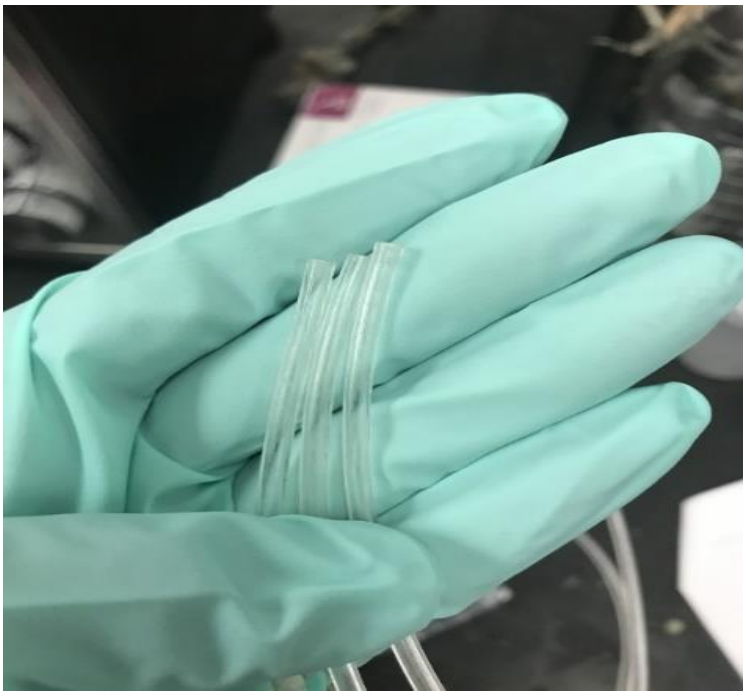

Figure 4.5 Connection tubes with 0.9 mm inner diameter and 1.8 mm outer diameter.

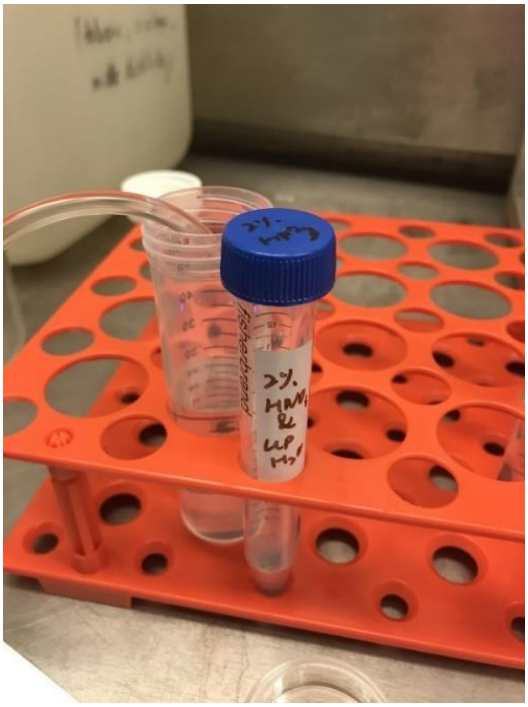

Figure 4.6 Falcon 15 ml and 50 ml centrifuge tubes for holding samples.

4.1.2 Scanning Electrode Microscope Picture of Quartz Crystal Gold Electrode

The deposition of DTT on the quartz crystal gold electrode was at a microscopic level. The distinction between the clean quartz crystal gold electrode and DTT deposited quartz crystal gold electrode was impossible with the naked eye. The cross-sectional view of a quartz crystal gold electrode scanned by scanning electron microscope (SEM) allowed visualization of DTT deposition in nanometers. *Figure 4.7* shows a cross-sectional image of the dithiothreitol deposited quartz crystal gold electrode (Heiner Castro Gutierrez), and the thickness of DTT was 211.8 nm, which was considered a thick film. Still, this was acceptable for this study.

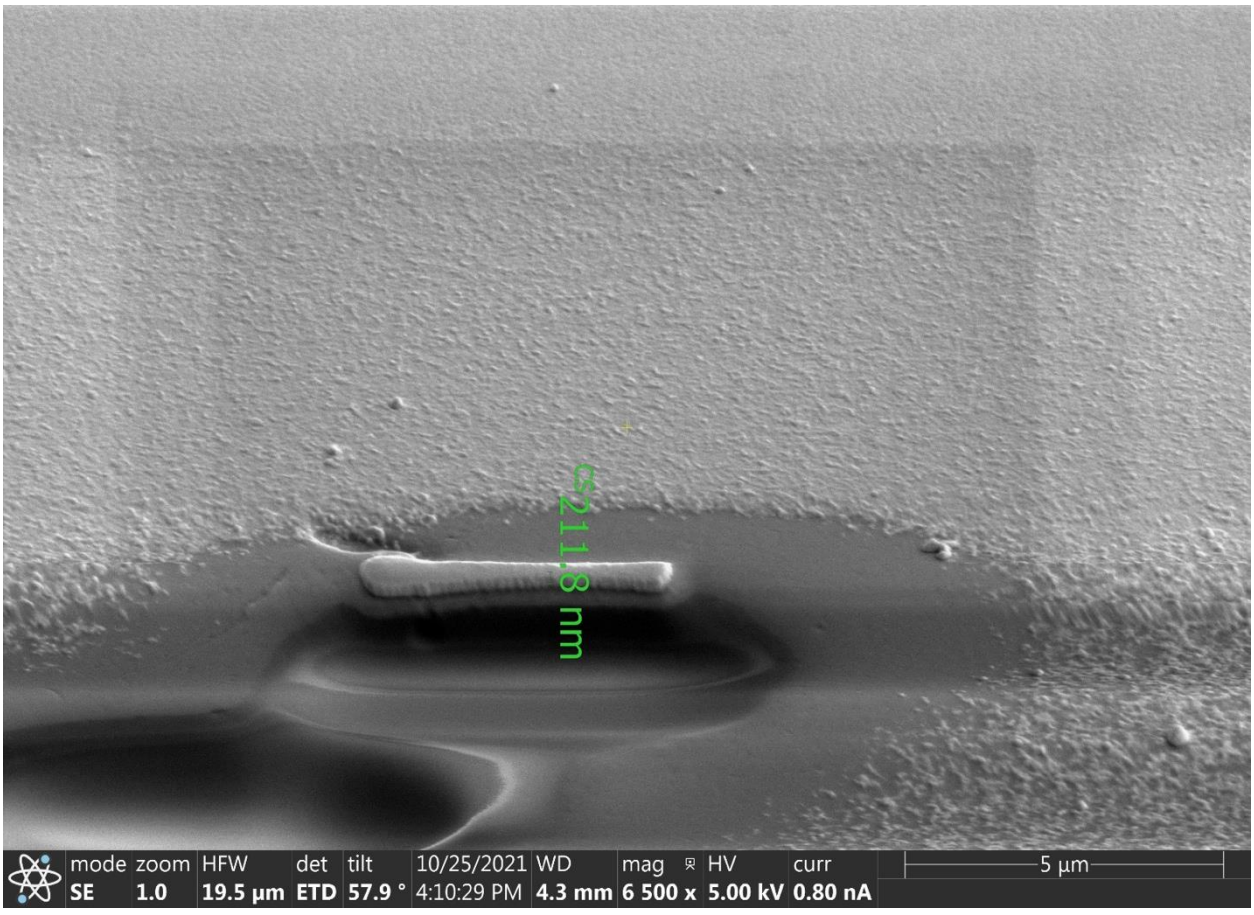

Figure 4.7 The cross-sectional image of quartz crystal gold electrode deposited with dithiothreitol, DTT. The segment highlighted in green was the thickness of the DTT ligand.

4.2 Glucose Experimental Results

4.2.1 Raw Data Results from Glucose Experiment

The openQCM system recorded frequency vs. time variation of ultra-pure water and glucose in a sequenced order. *Figure 4.8* shows the frequency vs. time variation for a series of experiments. The data highlighted represented the responses of QCM's frequency after injection of the 0 M glucose.

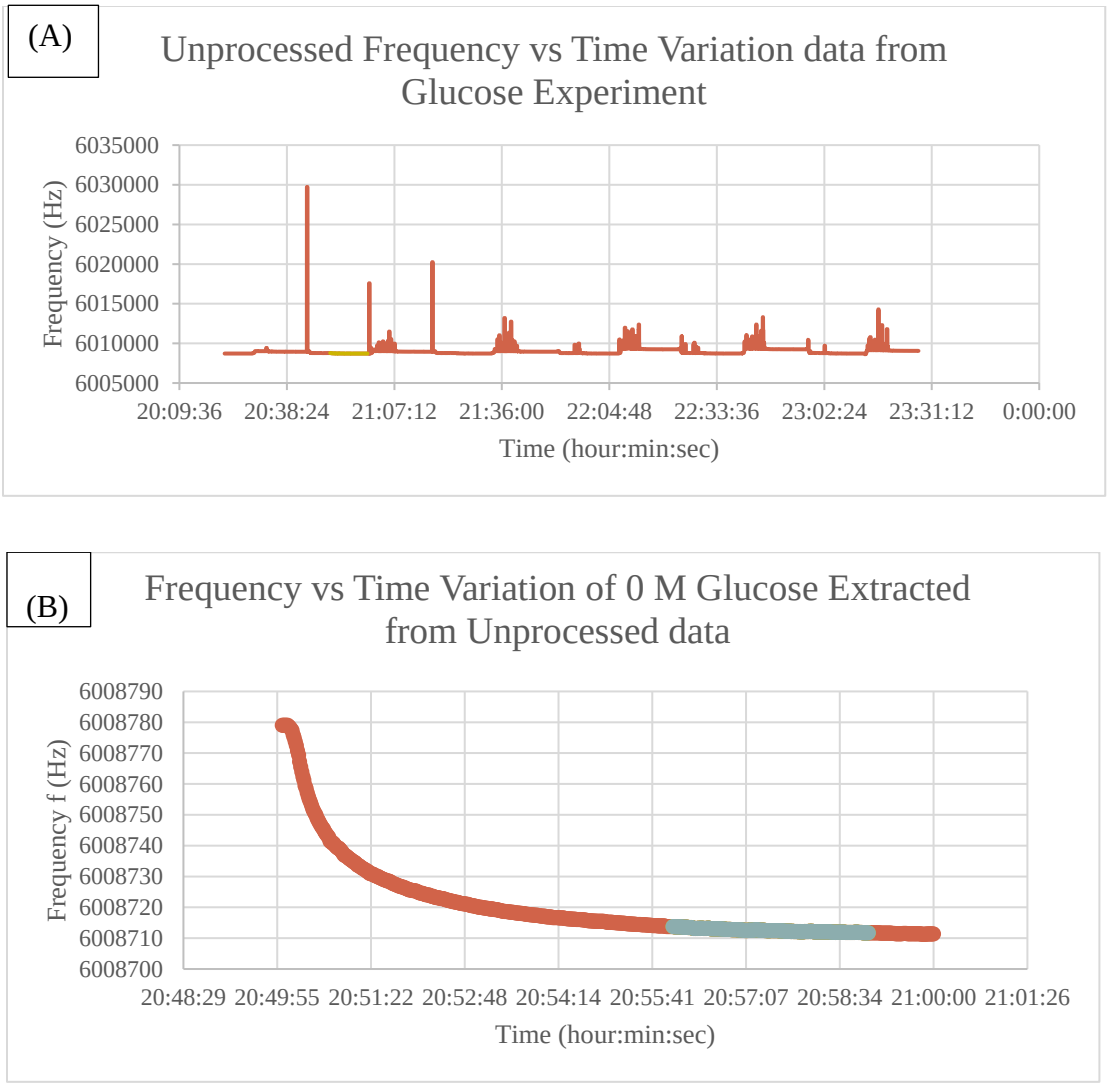

Figure 4.8 (A) Unprocessed frequency vs. time variation from the glucose experiment. The area highlighted represents the time domain after the injection of 0 M glucose and before the injection of the following sample. (B) Zoomed in highlight of 0M glucose, the area highlighted represents the three minutes frequency values for average (f).

4.2.2 Data Analysis Logic

The analytical logic was consistent across all QCM results for this research. Across all QCM results during the glucose experiment, the frequency value decreased exponentially right after the sample injection and reached an equilibrium stage. The frequency stabilization process required roughly 10 minutes to become horizontal after the pumping stopped. Therefore, to conduct data analysis, we extracted the frequency vs. time variation value right after the injection of the corresponding sample and the time right before the injection of the following sample. *Figure 4.8* shows the extraction of frequency vs. time variation of the 0 M glucose sample.

Subsequently, to analyze the results, we took 4 minutes of frequency signal from the end of stabilization time, discarded the last 1 minute, then calculated the average value of the remaining 3 minutes. The average frequency responses of each concentration were then subtracted from the average frequency response of blank. The average 3 minutes of frequency differences (Δf) and standard deviation in a sample set of data values for each concentration across all experiments were then used to plot the average frequency differences vs. theoretical concentration linear correlation curve and their error bars. If the correlation model shows a strong coefficient of determination for linear correlation ($R^2 > 0.99$), then the limit of detection (LOD) value was calculated.

The limit of detection equation shown in *Figure 4.9* required the slope of the linear correlation equation model, the standard deviation of the intercept. *Table 4.1* shows the regression statistics output table that generated the standard error intercept for the standard deviation of the intercept calculation.

$$\text{Limit of Detection(LOD)} = 3(\,^{S_{yx}}/_{b})$$

Figure 4.9 Limit of detection equation, where the Syx is the standard deviation of intercept from the linear correlation equation, b is the slope of the linear correlation curve (Indrayanto et al., 2018).

Table 4.1 Regression statistic output of glucose experiment.

SUMMARY OUTPUT								
Regression Statistics								
Multiple R	0.999911							
R Square	0.999821							
Adjusted R Square	0.999643							
Standard Error	4.4586							
Observations	3							
ANOVA								
	df	*SS*	*MS*	*F*	*Significance F*			
Regression	1	111325.9	111325.9	5600.144	0.008507			
Residual	1	19.87912	19.87912					
Total	2	111345.8						
	Coefficients	*Standard*	*t Stat*	*P-value*	*Lower 95%*	*Upper 95%*	*Lower 95.0%*	*Upper 95.0%*
Intercept	-1.82153	4.06954	-0.4476	0.732074	-53.5299	49.88688	-53.5299	49.88688
X Variable 1	5.667307	0.075732	74.83411	0.008507	4.705046	6.629568	4.705046	6.629568

4.2.3 Glucose Results

The average frequency value (f) from each concentration was calculated in excel. *Table 4.2* shows average frequency for each glucose concentration. *Table 4.3* shows average frequency differences (Δf) between each glucose concentration and the blank. The Δf between 0M and blank was always 0. The values were then used to construct the correlation curves. *Figure 4.10* also shows a linear correlation line between frequency difference and glucose concentration. The average frequency differences from three glucose experiments provided an R^2 value of 0.9998 and the limit of detection of 3.73 M.

Table 4.2 Average frequency (f) value from three glucose concentrations (0, 41.6, 83.26 M) in ultra-pure water.

(f) / Experiment	0 M Glucose (Hz)	41.6 M Glucose (Hz)	83.26 M Glucose (Hz)
1 (Glucose in ultra-pure water)	6008716	6008943	6009251
Standard deviation of three-minute frequency value within experiment 1	0.19	0.82	0.56
2 (Glucose in ultra-pure water)	6008712	6008943	6009253
Standard deviation of three-minute frequency value within experiment 2	0.55	0.71	0.98
3 (Glucose in ultra-pure water)	6008715	6008948	6009055
Standard deviation of three-minute frequency value within experiment 3	0.62	0.69	0.88

Table 4.3 Average frequency difference (Δf) between three glucose concentrations (0, 41.6, 83.26 M) in ultra-pure and blank sample.

|Δf| / Experiment	$\|f_{0M} - f_{0M}\|$ (Hz)	$\|f_{41.6M} - f_{0M}\|$ (Hz)	$\|f_{83.26M} - f_{0M}\|$ (Hz)
1 (Glucose in ultra-pure water)	0	227.50	535.68
Standard deviation of observation within experiment 1	0.27	0.85	0.59
2 (Glucose in ultra-pure water)	0	230.84	540.24
Standard deviation of observation within experiment 2	0.78	0.90	1.12
3 (Glucose in ultra-pure water)	0	232.56	339.66
Standard deviation of observation within experiment 3	0.88	0.93	1.07
Mean of average frequency difference across four experiments	0	230.30	472.03
Standard deviation of mean of average frequency difference across four experiments	0	2.49	93.37

Figure 4.10 shows a linear correlation trendline based on calculation from *Table 4.3*. The x-axis displays glucose concentration M and the y-axis displays the average frequency difference Δf across three experiments and their standard deviation error bars. The limit of detections was 3.73 M.

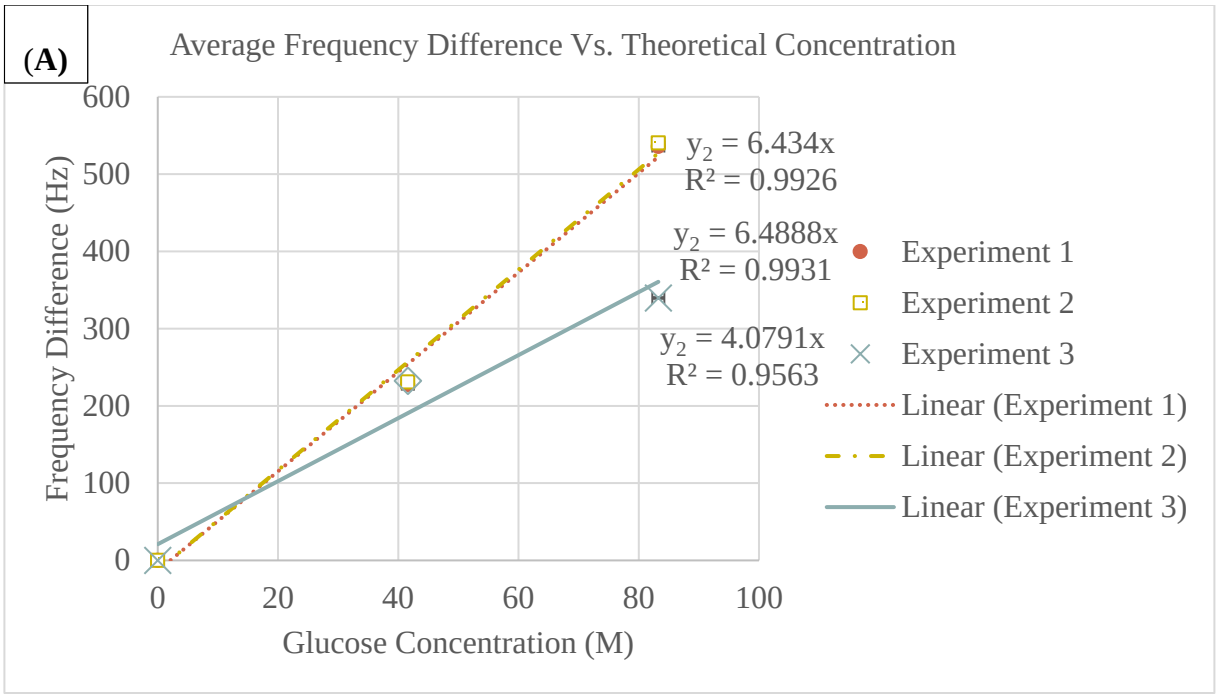

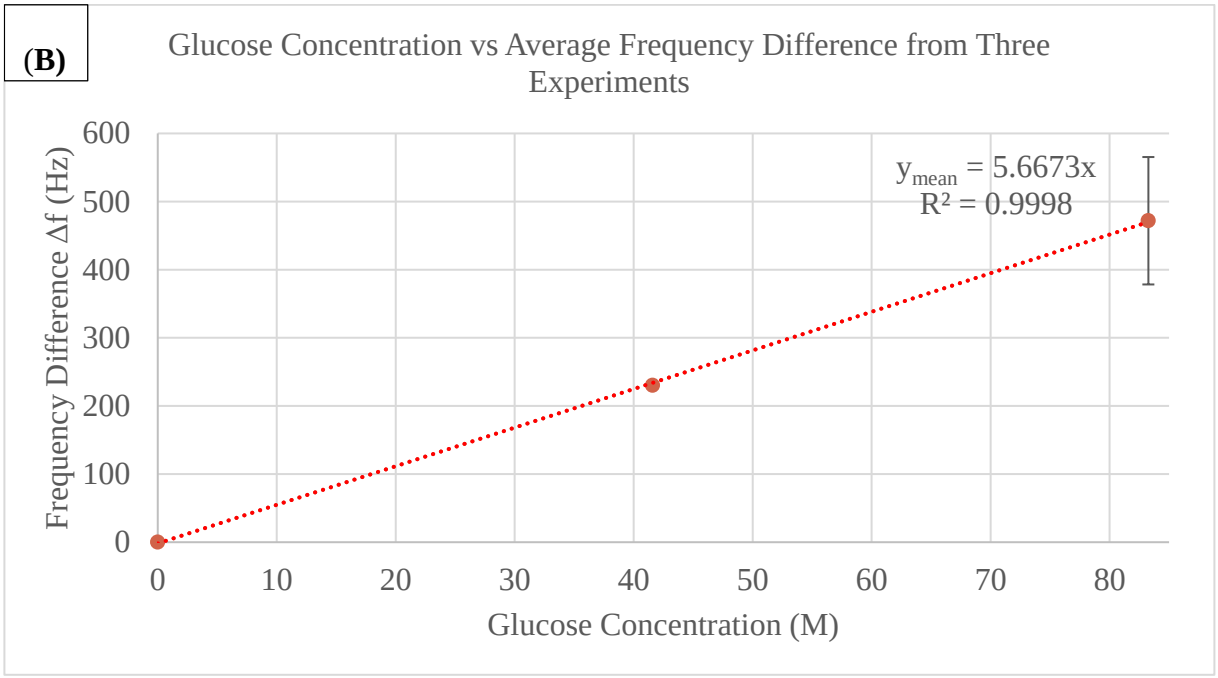

Figure 4.10 (A) Linear correlation curve for three glucose experiments and their standard deviation. (B) Mean of average frequency difference of three glucose experiments and their standard deviations. The limit of detection for the mean was 3.73 M. (Error bars show the standard deviations and are not visible for some concentrations as their standard deviations are very low.)

4.3 Arsenic Experimental Results

The following sections reported results from six different arsenic experiments. Four of the six experiments detected arsenic in ultra-pure water. Two of the six experiments detected arsenic in 0.5% HNO_3. The data analysis procedure followed the same protocols described in section 4.2.2. The arsenic particles in 0.5% HNO_3 samples were also analyzed by ICP-MS, which was used to validate the arsenic sample preparation procedures.

4.3.1 Arsenic in Ultra-Pure Water Results

The arsenic experiments were conducted separately based on the solvent of the arsenic samples. As a result, the QCM acquired four sets of frequency vs. time variation of four arsenic concentrations (0, 50, 100, and 200 ppb) in ultra-pure water. The frequency vs. time variation plot can be found in Appendix A. The data were extracted and analyzed using the same analysis logic mentioned in section 4.2.2. *Table 4.4* shows the average frequency value (f) from each arsenic concentration in ultra-pure water and their standard deviations. Subsequently, the differences between the average frequency from each arsenic concentration and the average frequency of blank (Δf) were also calculated (*Table 4.5*). *Figure 4.11* shows linear correlation curves between frequency difference and concentration for individual experiments and the mean correlation curve of four experiments.

Figure A.5 – A.8 - (APPENDIX A) show the linear correlation curves plotted separately for four arsenic concentrations in the ultra-pure water.

Table 4.4 Average frequency (f) value from four arsenic concentrations (0, 50, 100, 200 ppb) in ultra-pure water.

(f) / Experiment	$f_{0\ ppb}$ (Hz)	$f_{50\ ppb}$ (Hz)	$f_{100\ ppb}$ (Hz)	$f_{200\ ppb}$ (Hz)
1 (As in Ultra-Pure water experiment 1 conducted on September 29, 2021)	5992367.91	5992360.36	5992351.82	5992344.07
Standard deviation of three-minute frequency value within experiment 1	0.96	0.38	0.45	0.28
2 (As in Ultra-Pure water experiment 2 conducted on October 8, 2021)	5992348.81	5992343.61	5992339.27	5992336.50
Standard deviation of three-minute frequency value within experiment 2	0.37	0.49	0.12	0.13
3 (As in Ultra-Pure water experiment 3 conducted on October 21, 2021)	5992264.04	5992259.26	5992254.83	5992254.21
Standard deviation of three-minute frequency value within experiment 3	0.17	0.59	0.05	0.26
4 (As in Ultra-Pure water experiment 4 conducted on November 15, 2021)	5984291.22	5984286.64	5984285.27	5984282.19
Standard deviation of three-minute frequency value within experiment 4	0.10	0.05	0.14	0.06

Table 4.5 Average frequency difference (Δf) between four arsenic concentrations (0, 50, 100, 200 ppb) in ultra-pure and blank sample.

|Δf| / Experiment	$\|f_{0ppb} - f_{0ppb}\|$ (Hz)	$\|f_{50ppb} - f_{0ppb}\|$ (Hz)	$\|f_{100ppb} - f_{0ppb}\|$ (Hz)	$\|f_{200ppb} - f_{0ppb}\|$ (Hz)
1 (As in Ultra-Pure water experiment 1 conducted on September 29, 2021)	0	7.55	16.09	23.84
Standard deviation of observation within experiment 1	1.35	1.03	1.06	0.99
2 (As in Ultra-Pure water experiment 2 conducted on October 8, 2021)	0	5.20	9.54	12.31
Standard deviation of observation within experiment 2	0.53	0.62	0.39	0.16
3 (As in Ultra-Pure water experiment 3 conducted on October 21, 2021)	0	4.78	9.20	9.82
Standard deviation of observation within experiment 3	0.24	0.62	0.18	0.31
4 (As in Ultra-Pure water experiment 4 conducted on November 15, 2021)	0	4.58	5.94	9.02
Standard deviation of observation within experiment 4	0.2	0.11	0.17	0.12
Mean of average Frequency Difference across four experiments	0	5.53	10.20	13.75
Standard deviation of Mean of average frequency differences across four experiments	0	1.06	3.29	1.06

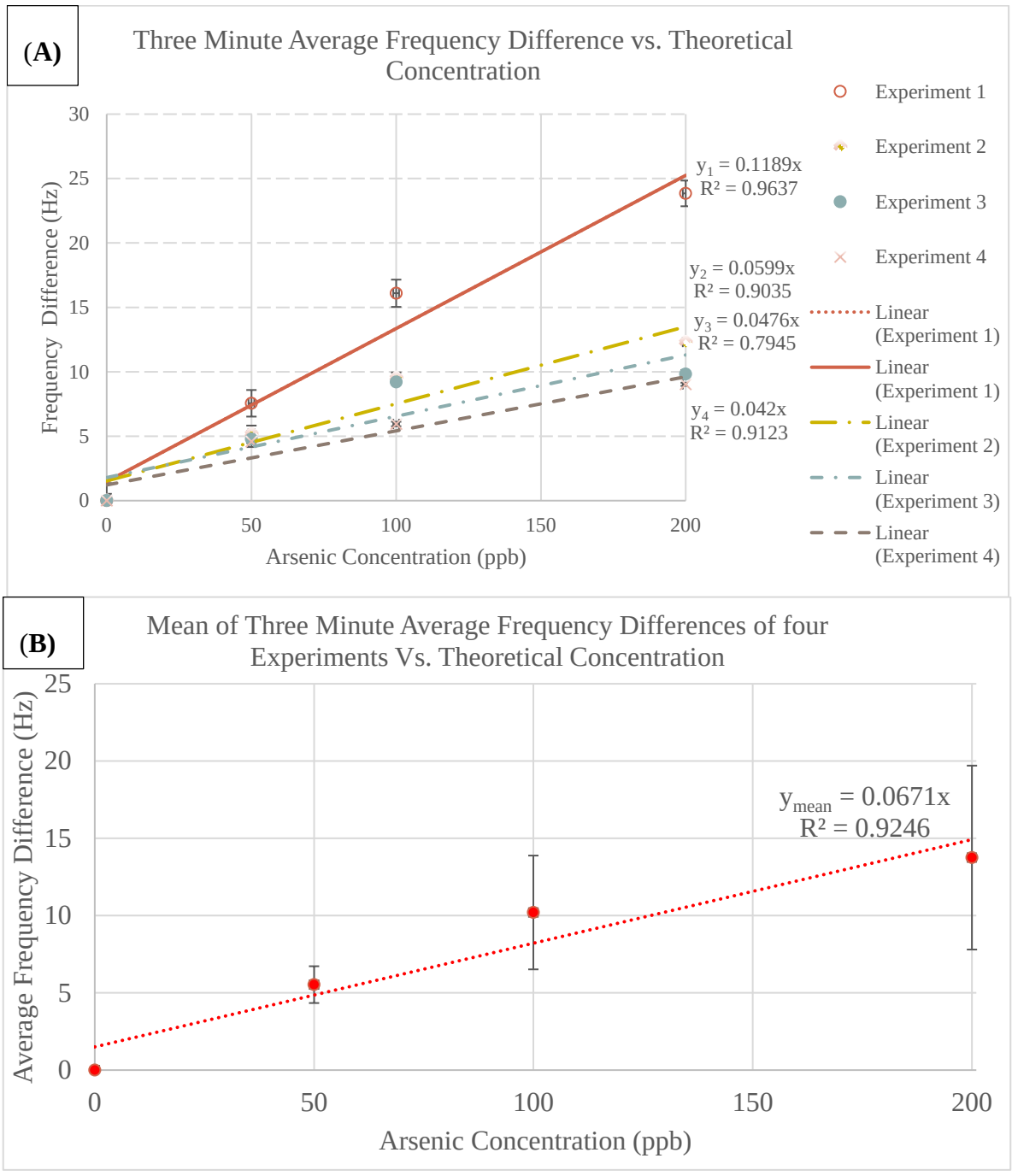

Figure 4.11 (A) Linear correlation curves of four arsenic experiments in ultra-pure water and their standard deviations. (B) Mean linear correlation curve of four arsenic experiments and standard deviation error bars.

4.3.2 Arsenic in 0.5% HNO_3 Results

The QCM also acquired two sets of frequency vs. time variations of four arsenic concentrations (0, 50, 100, 200 ppb) in 0.5% HNO_3. The frequency vs. time variation plots can be found in APPENDIX B. The data were extracted and analyzed using the same analysis logic mentioned in section 4.2.2. *Table 4.6* shows the average frequency value (f) and the standard deviation from each arsenic concentration in 0.5% HNO_3 and their standard deviations. Subsequently, the average frequency difference between each arsenic concentration and blank (Δf) was also calculated (*Table 4.7*). *Figure 4.12* shows linear correlation curves between frequency difference and concentration for individual experiments and the mean correlation curve of two experiments. The arsenic in 0.5% HNO_3 samples were also analyzed by ICP-MS. *Figure 4.13* shows R^2 of 0.9946, which validated the arsenic sample preparation methodology.

Figure B.3- Figure B.4 – (APPENDIX B) show the linear correlation curves plotted separately for four arsenic concentrations in the 0.5% HNO_3.

Table 4.6 Average frequency value (f) from four arsenic concentrations (0, 50, 100, 200 ppb) in 0.5% HNO_3.

(f) / Experiment	$f_{0\ ppb}$ (Hz)	$f_{50\ ppb}$ (Hz)	$f_{100\ ppb}$ (Hz)	$f_{200\ ppb}$ (Hz)
1 (As in 0.5% HNO_3 experiment 1 conducted on September 17, 2021)	6006777.79	6006764.16	6006757.52	6006746.05
Standard deviation of three-minute frequency value within experiment 1	1.59	0.71	0.75	0.33
2 (As in 0.5% HNO_3 experiment 2 conducted on October 1, 2021)	5991554.100	5991519.28	5991513.29	5991510.22
Standard deviation of three-minute frequency value within experiment 2	1.09	0.49	0.09	0.28

Table 4.7 Average frequency difference (Δf) between four arsenic concentrations (0,50, 100, 200 ppb) in 0.5% HNO_3 and blank sample.

|Δf| Experiment	$\|f_{0ppb} - f_{0ppb}\|$ (Hz)	$\|f_{50ppb} - f_{0ppb}\|$ (Hz)	$\|f_{100ppb} - f_{0ppb}\|$ (Hz)	$\|f_{200ppb} - f_{0ppb}\|$ (Hz)
1 (As in 0.5% HNO_3 experiment 1 conducted on September 17, 2021)	0	13.629	20.267	31.742
Standard deviation of observation within experiment 1	2.25	1.74	1.76	1.62
2 (As in 0.5% HNO_3 experiment 2 conducted on October 1, 2021)	*0	36.64	42.63	45.69
Standard deviation of observation within experiment 2	1.55	1.20	1.09	1.13
Mean of average frequency difference across two experiments	0	24.22	30.54	37.80
Standard deviation of mean of average frequency difference across two experiments	0	14.99	14.52	8.58

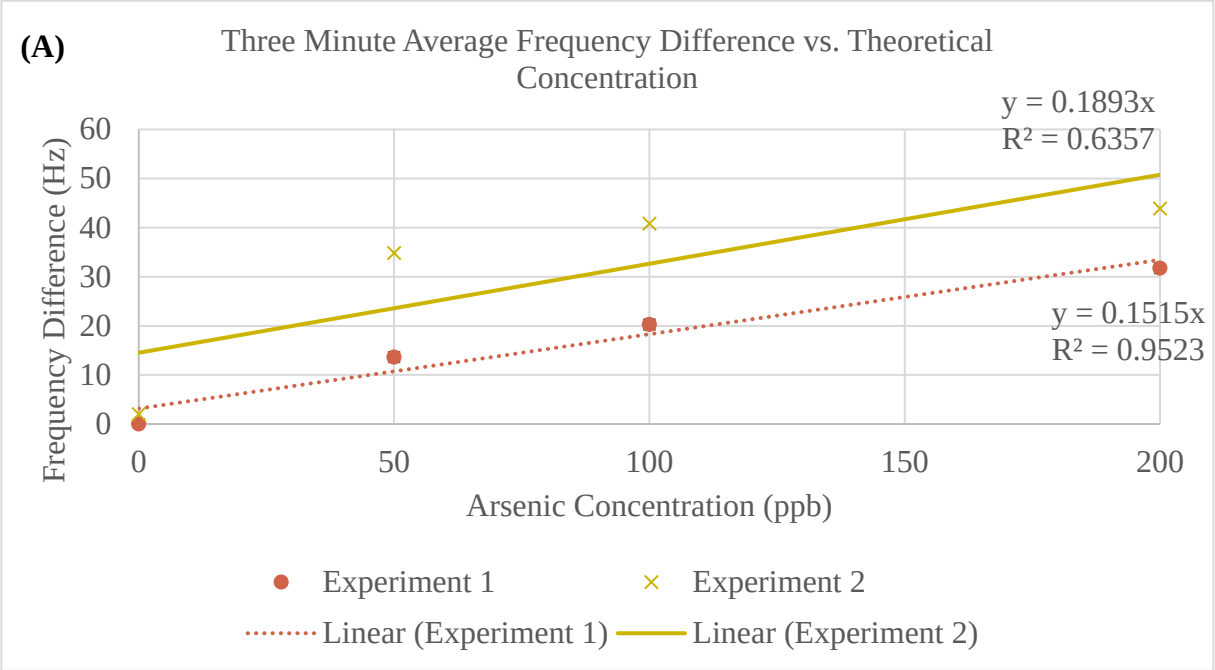

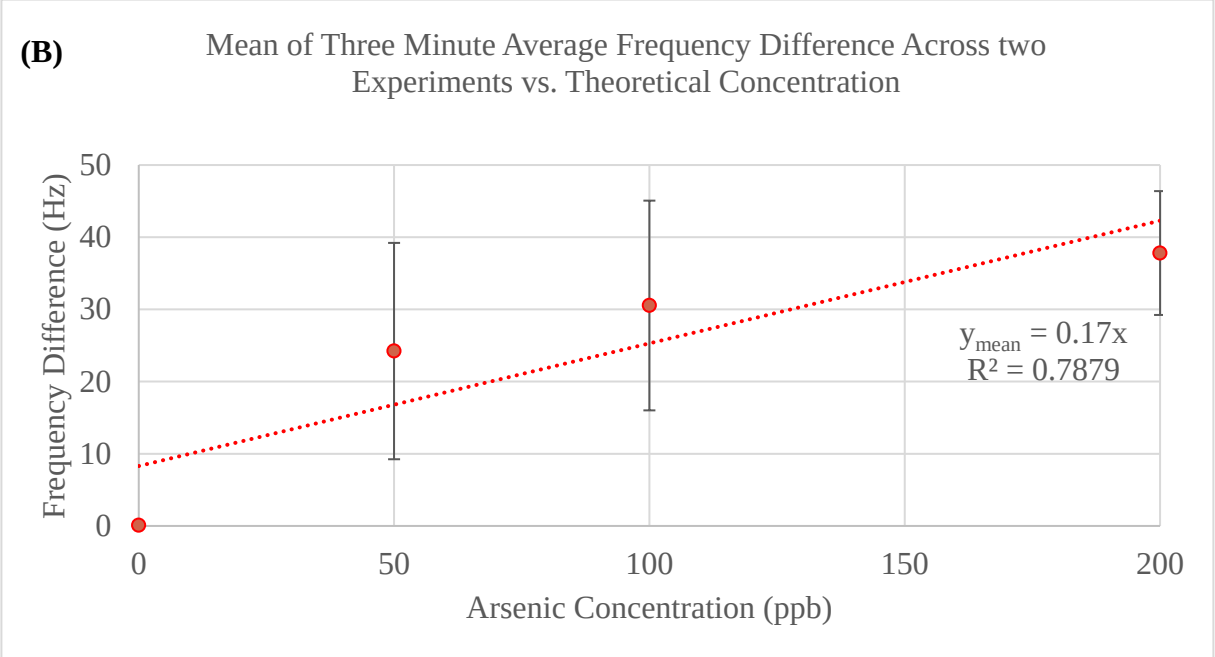

Figure 4.12 (A) Linear correlation curve for arsenic experiments in 0.5% HNO_3. (B) Mean linear correlation curve of two arsenic experiments in 0.5% HNO_3. (Error bars show the standard deviations and are not visible for some concentrations as their standard deviations are very low.)

Figure 4.13 shows the linear correlation curve of the arsenic sample prepared in 0.5% HNO_3 analyzed by ICP-MS. The correlation line shows the R^2 value of 0.9946, validating the arsenic sample preparation methods we used.

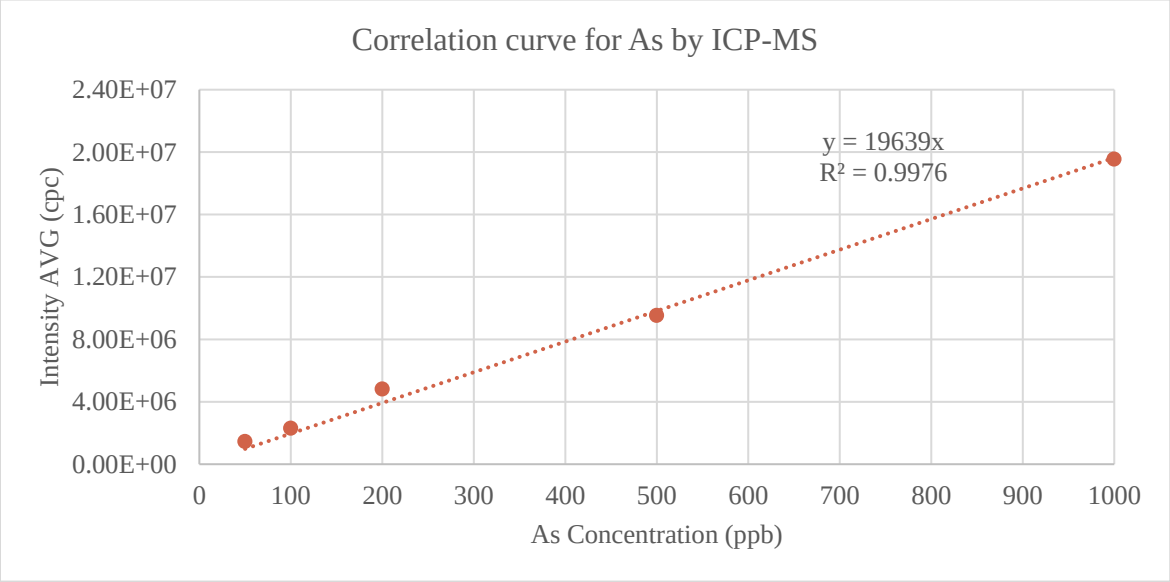

Figure 4.13 The linear correlation curve for arsenic samples prepared in 0.5% HNO_3 (ICP-MS analysis conducted by Anusha Priyadarshani Silva Hettiyadura at Purdue Chemistry facility).

4.4 Lead Experimental Results

The quartz crystal gold electrode modification with Chitosan-Glutaraldehyde ligand used the drop-casting method at first. However, the QCM frequency signal raised to the maximum value (16,000,000 Hz). The communication with openQCM (openQCM, Italy) indicated that one of the possible reasons for the maximum frequency response was the ligand chemical's high thickness, which caused oversaturation. Therefore, we chose spin-coating to create thin-film ligand deposition as an alternative method. The QCM's frequency vs. time variation to each lead sample in ultra-pure water was analyzed. Section 4.4.1 demonstrated results acquired from QCM system installed with drop-casted quartz crystal gold electrodes, and Section 4.4.2 demonstrated results acquired from QCM system installed with spin-coated gold electrodes.

4.4.1 Drop-Casting Coated Quartz Crystal Gold Electrode Raw Data

The quartz crystal gold electrode underwent drop-casting ligand modification with CGL ligand before the experiment. The openQCM software recorded frequency vs. time variation of the ultra-pure water.

The frequency value (y-axis) after the injection of the sample immediately reached the maximum value of 16,000,000 Hz after the injection of ultra-pure water. Therefore, it was not possible to continue the rest of the experiment. *Figure 4.14* shows frequency vs. time variation from QCM after injection of the ultra-pure water. The frequency vs. time variation plot from the rest of two quartz crystal gold electrodes can be found in *Figure C.1* – (Appendix C).

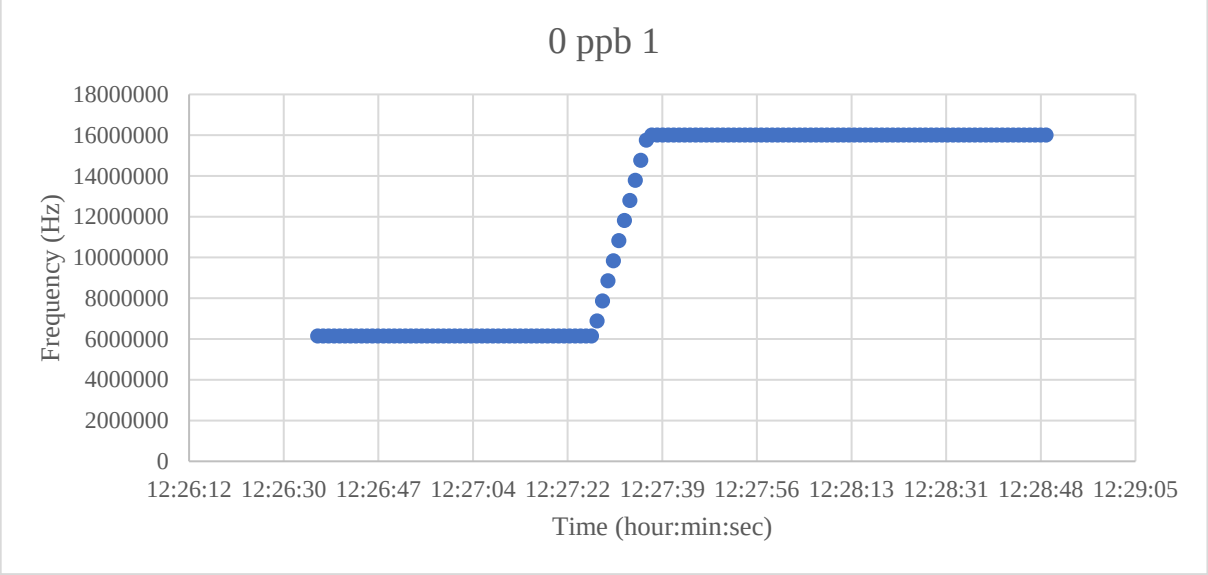

Figure 4.14 The frequency vs. time variation after injection of 0 ppb (blank) in ultra-pure water Experiment 1was conducted on February 24, 2022.

4.4.2 Spin-Coater Coated Quartz Crystal Gold Electrode Measurement of Lead in Ultra-Pure Water

The spin coating technique provided a quartz crystal gold electrode thinner layer of ligand deposition (Niemczyk et al., 2015). *Figure 4.15* shows an image comparison between drop-casted and spin-coated quartz crystal gold electrodes.

We conducted three experiments using QCM installed with quartz crystal gold electrodes (spin-coated with CGL). Each experiment contained three concentrations of lead (0, 100, 200 ppb) in ultra-pure water. The frequency vs. time variation plot can be found in APPENDIX D. The data were extracted and analyzed using the same analysis logic mentioned in section 4.2.2. *Table 4.8* shows the average frequency values (f) from each lead concentration in ultra-pure water and their standard deviations. Subsequently, the differences between the average frequency from each lead concentration and the average frequency of blank (Δf) were also calculated (*Table 4.9*). *Figure 4.16* shows linear correlation curves between frequency difference and concentration for individual experiments and the mean correlation curve of three experiments.

Figure C.1 – Figure C.3 - (APPENDIX C) show the linear correlation curves plotted separately for three lead concentrations in the ultra-pure water.

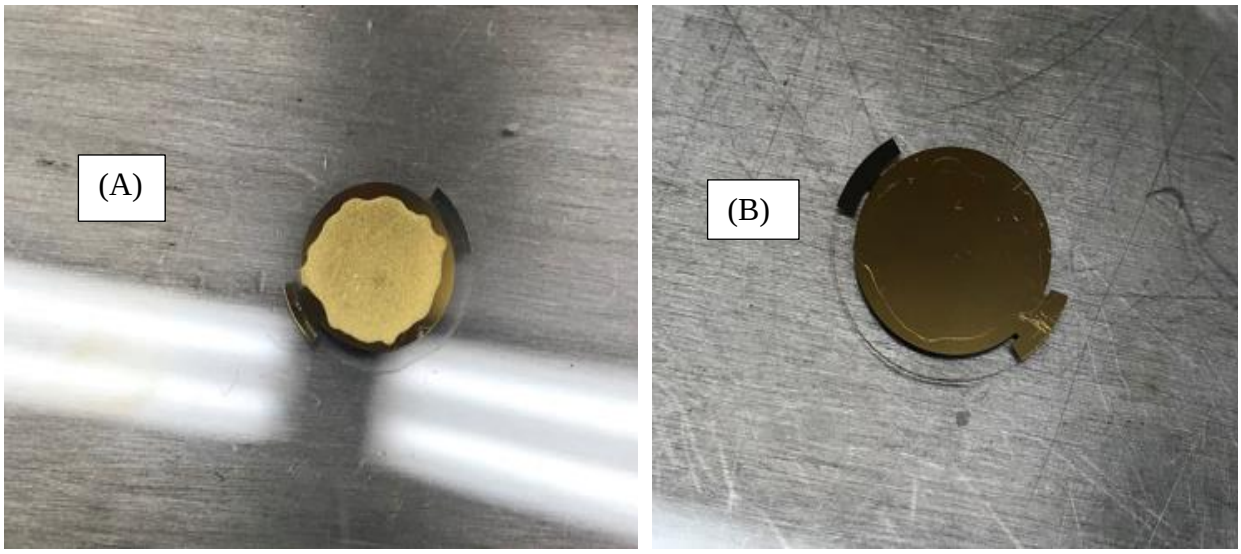

Figure 4.15 (A) A quartz crystal gold electrode modified with CGL ligand using drop-casting method. (B) A quartz crystal gold electrode modified with CGL ligand using spin coating method.

Table 4.8 Average frequency values (f) from three lead concentrations (0, 100, 200 ppb) in ultra-pure water.

(f) / Experiment	$f_{0\ ppb}$ (Hz)	$f_{100\ ppb}$ (Hz)	$f_{200\ ppb}$ (Hz)
Pb three concentrations in ultra-pure water experiment 1 conducted on March 7, 2022	5991805.36	5992160.17	5992506.10
Standard Deviations of three-minute frequency value within experiment 1	0.55	4.92	7.73
Pb three concentrations in ultra-pure water experiment 2 conducted March 7, 2022	6000548.17	6001095.71	6001645.78
Deviations of three-minute frequency value within experiment 2	0.25	6.95	11.31
Pb three concentrations in ultra-pure water experiment 3 conducted March 8, 2022	6007668.87	6007797.93	6007896.08
Deviations of three-minute frequency value within experiment 3	0.25	0.98	1.75

Table 4.9 Average frequency difference (Δf) between the three lead concentrations (0, 100, 200 ppb) in ultra-pure water and blank.

|Δf| / Experiment	$\|f_{0ppb}-f_{0ppb}\|$ (Hz)	$\|f_{0ppb}-f_{100ppb}\|$ (Hz)	$\|f_{0ppb}-f_{200ppb}\|$ (Hz)
Pb three concentrations in ultra-pure water experiment 1 conducted on March 7, 2022	0	354.80	700.73
Standard deviations of observation within experiment 1	0.79	4.95	7.75
Pb three concentrations in ultra-pure water experiment 2 conducted March 7, 2022	0	547.54	1097.60
Standard deviations of observation within experiment 2	0.36	6.96	11.32
Pb three concentrations in ultra-pure water experiment 3 conducted March 8, 2022	0	129.05	227.21
Standard deviations of observation within experiment 3	0.13	1.04	3.14
Mean of average frequency average Difference across three experiments	0	343.80	675.18
Standard deviations of Mean of average frequency difference across three experiments	0	209.46	435.76

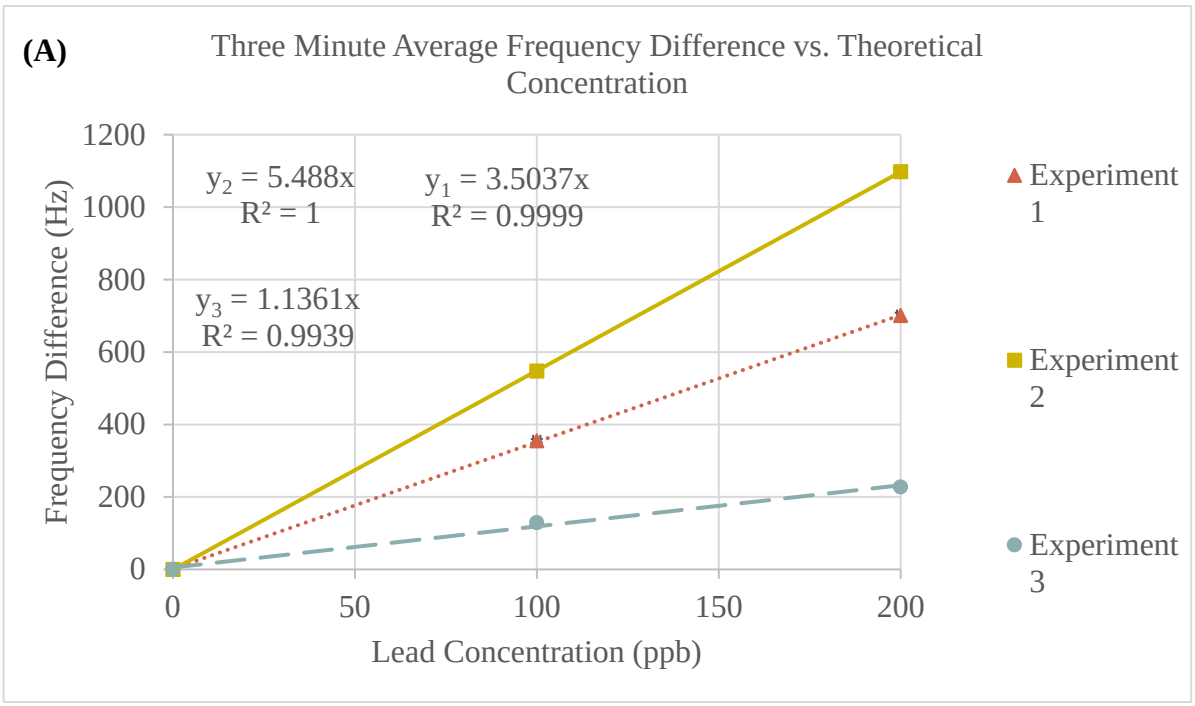

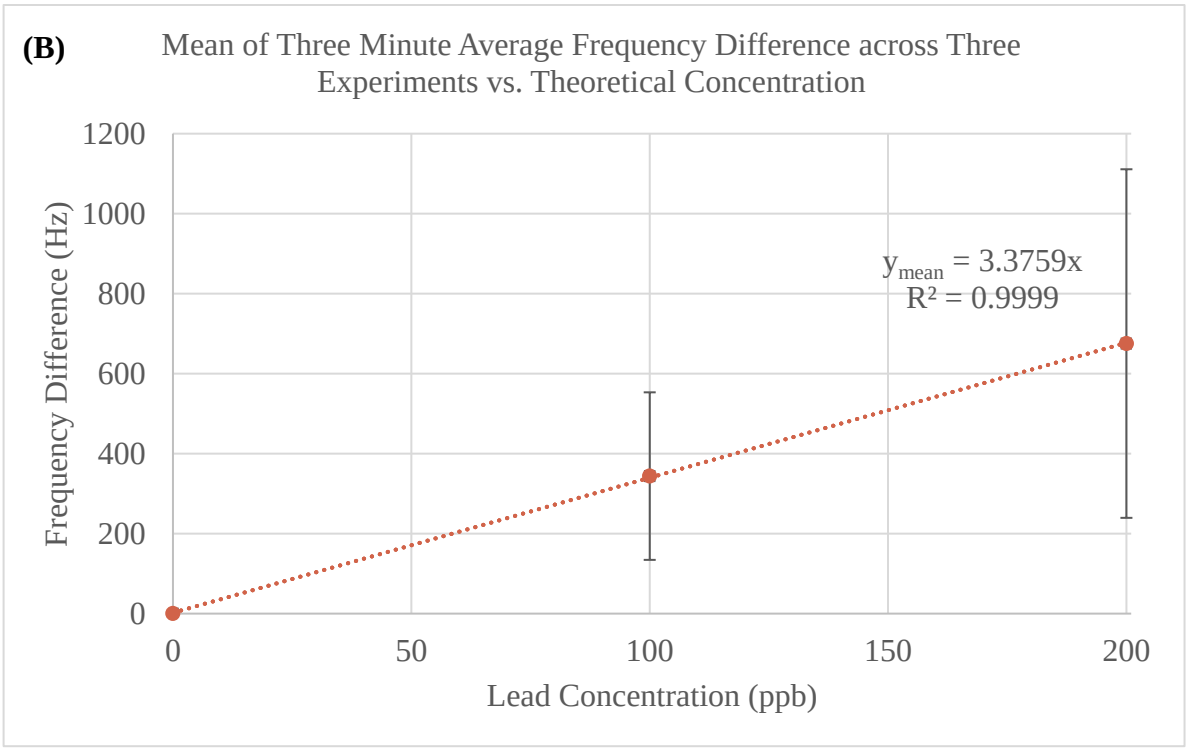

Figure 4.16 (A) Linear correlation curve for three concentrations of lead in ultra-pure water. (B) Mean correlation curve from three concentrations of lead in ultra-pure water. (Error bars show the standard deviations and are not visible for some concentrations as their standard deviations are very low.)

Subsequently, we conducted three additional experiments with five different concentrations of lead (0, 10, 25, 50, and 100 ppb) in ultra-pure water. The frequency vs. time variation of each experiment can be found in APPENDIX E. The data were extracted and analyzed using the same analysis logic mentioned in section 4.2.2. *Table 4.10* shows the average frequency values (f) from each experiment concentration and their standard deviations. Subsequently, the differences between the average frequency from each lead concentration and the average frequency of blank (Δf) were also calculated (*Table 4.11*). *Figure 4.17* shows linear correlation curves between frequency difference and concentration for individual experiments and the mean correlation curve of three experiments.

Figure E.4-Figure E.6 – (APPENDIX E) show the linear correlation curves plotted separately for five lead concentrations in the ultra-pure water.

Table 4.10 Average frequency values (f) from five lead concentrations (0, 10, 25, 50, 100 ppb) in ultra-pure water.

(f) / Experiment	$f_{0\ ppb}$ (Hz)	$f_{10\ ppb}$ (Hz)	$f_{25\ ppb}$ (Hz)	$f_{50\ ppb}$ (Hz)	$f_{100\ ppb}$ (Hz)
Pb concentration in ultra-pure water experiment 1 conducted on March 8, 2022	5992139.44	5992146.54	5992267.70	5992378.06	5992539.06
Standard deviations of three-minute frequency value within experiment 1	0.88	0.38	1.62	2.33	3.38
Pb concentration in ultra-pure water 2 conducted on March 8, 2022	5997591.21	5997605.22	5997647.61	5997734.82	5997844.90
Standard deviations of three-minute frequency value within experiment 2	0.36	0.36	0.39	0.35	0.73
Pb concentration in ultra-pure water 3 conducted on March 9, 2022	5996837.46	5996891.90	5996961.02	5997060.70	5997185.14
Standard deviations of three-minute frequency value within experiment 3	2.12	1.41	0.99	0.99	1.18

Table 4.11 Average frequency difference (Δf) between five lead concentrations (0, 10, 25, 50, 100 ppb) in ultra-pure water and blank sample.

|Δf| / Experiment	$\|f_{0ppb}-f_{0ppb}\|$ (Hz)	$\|f_{0ppb}-f_{10ppb}\|$ (Hz)	$\|f_{0ppb}-f_{25ppb}\|$ (Hz)	$\|f_{0ppb}-f_{50ppb}\|$ (Hz)	$\|f_{0ppb}-f_{100ppb}\|$ (Hz)
Pb concentration in ultra-pure water 1 conducted on March 8, 2022	0	7.09	128.26	238.62	399.62
Standard deviation of observation within experiment 1	1.25	0.96	1.85	2.49	3.50
Pb concentration in ultra-pure water 2 conducted on March 8, 2022	0	14.01	56.40	143.61	253.68
Standard deviation of observation within experiment 2	0.51	0.52	0.53	0.51	0.67
Pb concentration in ultra-pure water 3 conducted on March 9, 2022	0	54.44	123.56	223.24	347.68
Standard deviation of observation within experiment 3	2.99	2.54	2.34	2.34	2.42
Mean of average frequency difference across three experiments	0	25.18	102.74	201.82	333.66
Standard deviation of Mean of average frequency difference across three experiments	0	25.57	40.20	50.99	73.96

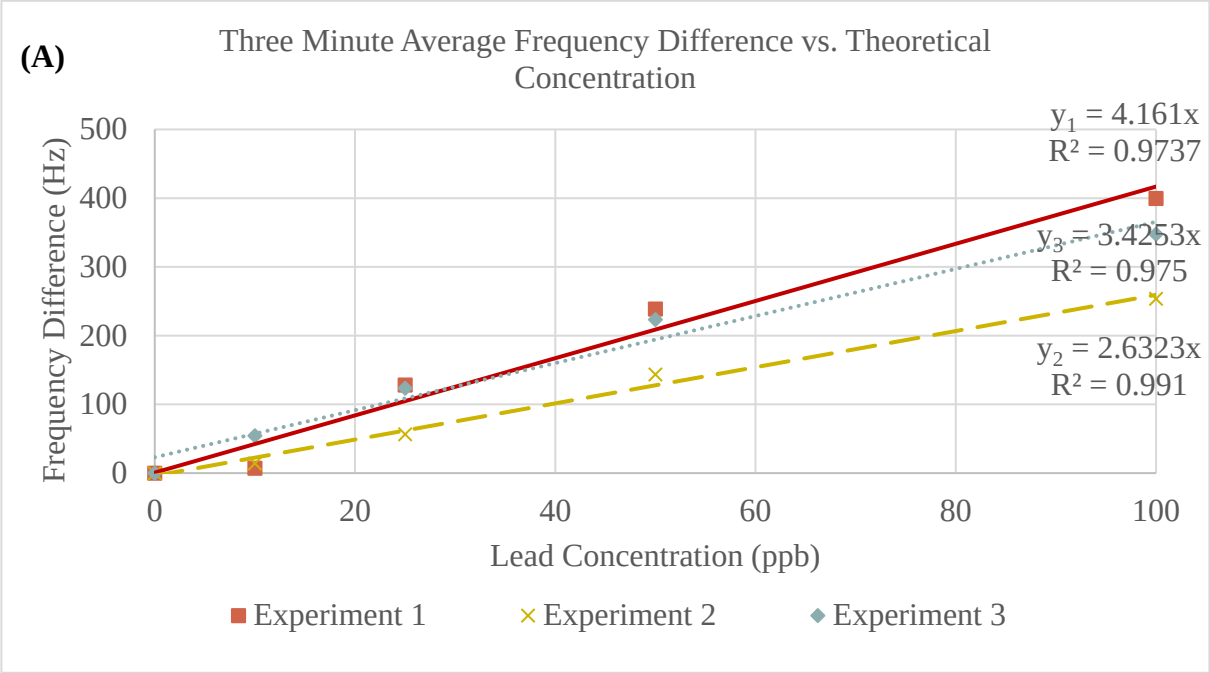

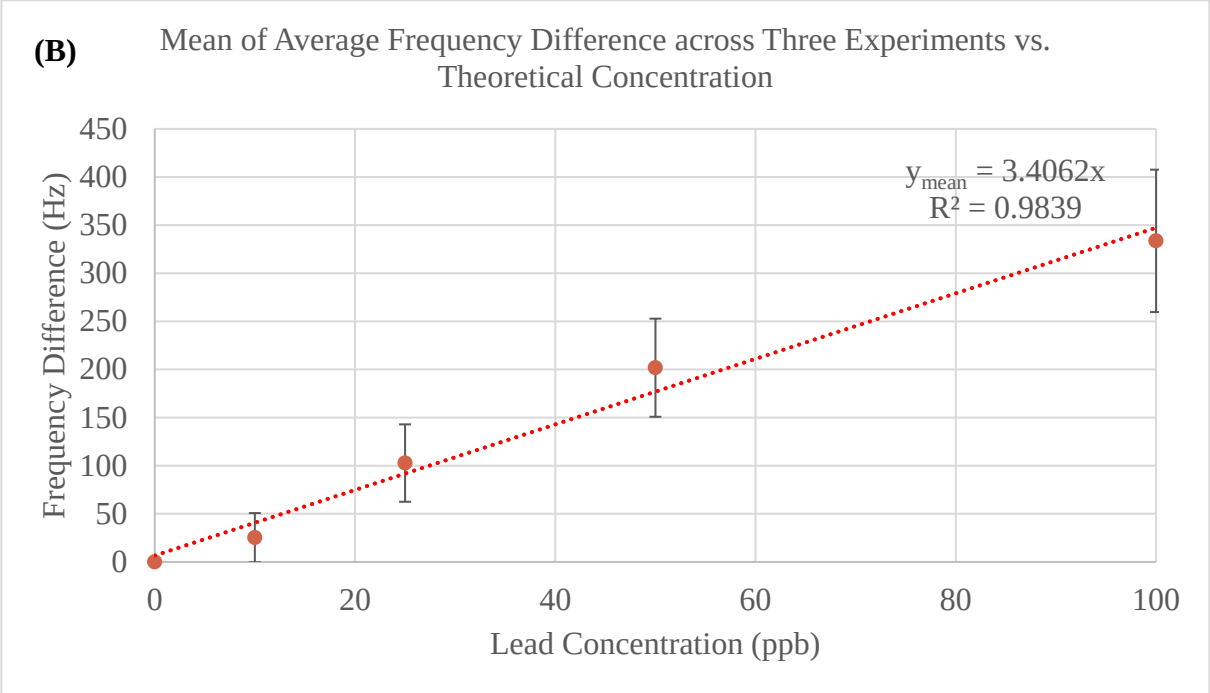

Figure 4.17 (A) Linear correlation curve for five concentrations of lead in ultra-pure water. The limit of detection values are 32.726 ppb, 18.964 ppb, and 31.888 ppb for experiment 1, 2, 3 respectively. (B) Linear correlation curve of mean average frequency differences of five concentrations and limit of detection is 7.58 ppb. (Error bars show the standard deviations and are not visible for some concentrations as their standard deviations are very low.)

CHAPTER 5-SUMMARY, CONCLUSIONS, AND RECOMMENDATIONS

5.1 Summary and Conclusions

The integrated QCM system was developed using openQCM wi 2 device. The integrated system consisted of a 10 MHz AT-cut quartz crystal gold electrode, a peristaltic pump, connecting tubes, a container for the samples, a waste beaker, and a personal computer. For arsenic determination in water, dithiothreitol (DTT) was used as a ligand and deposited onto quartz crystal gold electrode using the self-assembly monolayer (SAM) method. We conducted two types of experiments to determine the responsiveness of the QCM system for detecting arsenic in water. The first type conducted four experiments using arsenic-contaminated samples in ultra-pure water and the second type conducted two experiments using arsenic-contaminated samples in 0.5% HNO_3. The concentrations of arsenic-contaminated samples were 0, 50, 100, and 200 ppb. For arsenic samples prepared with ultra-pure water, the R^2 value obtained from the linear correlation curve with 0 intercepts between frequency difference and concentration value ranged from 0.795 and 0.964. The arsenic samples prepared with 0.5% HNO_3, the R^2 value obtained from the linear correlation curve between frequency difference and concentration value ranged from 0.636 to 0.952.

Initial experiments using chitosan as the ligand did not show promising results. Subsequently, we used a combination of chitosan, glutaraldehyde, and lead ionophore (II) (CGL) and deposited it onto the quartz crystal gold electrode using a spin coater. Two sets of lead experiments in ultra-pure water were conducted based on the number of concentrations. The first set conducted three experiments using three concentrations (0, 100, and 200 ppb) of lead. The second set conducted three experiments using five concentrations (0, 10, 25, 50, and 100 ppb) of

lead. Similarly, the data were recorded, and the correlation curve with 0 intercepts between frequency difference and concentration values was obtained. The R^2 value from the first set of experiments ranged from 0.994 to 1. For the second set of experiments, the R^2 value ranged from 0.974 to 0.991.

5.2 Future Work

The sensing capability of the QCM system can be further improved by integrating a peristaltic pump with a faster and more accurate flow rate. Additional research was necessary to incorporate DTT as a sensing ligand for arsenic detection. A different ligand can be explored to improve its sensing accuracy and range of detection. In addition, a technique that can help the ligand bind with arsenic and un-bind after injection of ultra-pure water would improve the user experience of the sensing system. For future work, a non-linear correlation model can be developed for arsenic results. Also, the bubble trapper can be integrated into the QCM system. Furthermore, the thickness of DTT deposition can also be reduced. Finally, an algorithm can be developed for interpreting the QCM data.

LIST OF REFERENCES

Ahoulé, D. G., Lalanne, F., Mendret, J., Brosillon, S., & Maïga, A. H. (2015). Arsenic in African Waters: A Review. *Water, Air, and Soil Pollution*, *226*(9). https://doi.org/10.1007/s11270-015-2558-4

Alassi, A., Benammar, M., & Brett, D. (2017). Quartz crystal microbalance electronic interfacing systems: A review. *Sensors (Switzerland)*, *17*(12), 1–41. https://doi.org/10.3390/s17122799

Ayad, M. M., & Minisy, I. M. (2016). Detection and kinetics of methylamine on chitosan film coated quartz crystal microbalance electrode. *Progress in Organic Coatings*, *100*, 76–80. https://doi.org/10.1016/j.porgcoat.2016.01.012

Ayad, M. M., Salahuddin, N., & Minisy, I. M. (2014). Detection of some volatile organic compounds with chitosan-coated quartz crystal microbalance. *Designed Monomers and Polymers*, *17*(8), 795–802. https://doi.org/10.1080/15685551.2014.918019

Cao, Z., Guo, J., Fan, X., Xu, J., Fan, Z., & Du, B. (2011). Detection of heavy metal ions in aqueous solution by P(MBTVBC-co-VIM)- coated QCM sensor. *Sensors and Actuators, B: Chemical*, *157*(1), 34–41. https://doi.org/10.1016/j.snb.2011.03.023

Cimpoca, G. V., Radulescu, C., Popescu, I. V., Dulama, I. D., Bancuta, I., Gheboianu, A. I., Ionita, I., Cimpoca, M., & Cernica, I. (2010). Monitoring of the drinking water using of alternative analytical techniques. *AIP Conference Proceedings*, *1203*(February), 409–414. https://doi.org/10.1063/1.3322477

Creczynski-Pasa, T. B., Millone, M. A. D., Munford, M. L., De Lima, V. R., Vieira, T. O., Benitez, G. A., Pasa, A. A., Salvarezza, R. C., & Vela, M. E. (2009). Self-assembled dithiothreitol on Au surfaces for biological applications: Phospholipid bilayer formation. *Physical Chemistry Chemical Physics*, *11*(7), 1077–1084. https://doi.org/10.1039/b811964c

Eddaif, L., Shaban, A., Telegdi, J., & Szendro, I. (2020). A piezogravimetric sensor platform for sensitive detection of lead (II) ions in water based on calix[4]resorcinarene macrocycles: Synthesis, characterization and detection. *Arabian Journal of Chemistry*, *13*(2), 4448–4461. https://doi.org/10.1016/j.arabjc.2019.09.002

Fasinu, P. S., & Orisakwe, O. E. (2013). Heavy metal pollution in sub-saharan africa and possible implications in cancer epidemiology. *Asian Pacific Journal of Cancer Prevention*, *14*(6), 3393–3402. https://doi.org/10.7314/APJCP.2013.14.6.3393

Fischer, L. M., Tenje, M., Heiskanen, A. R., Masuda, N., Castillo, J., Bentien, A., Émneus, J., Jakobsen, M. H., & Boisen, A. (2009). Gold cleaning methods for electrochemical detection applications. *Microelectronic Engineering*, *86*(4–6), 1282–1285. https://doi.org/10.1016/j.mee.2008.11.045

Galiová, M., Kaiser, J., Novotný, K., Novotný, J., Vaculovič, T., Liška, M., Malina, R., Stejskal, K., Adam, V., & Kizek, R. (2008). Investigation of heavy-metal accumulation in selected plant samples using laser induced breakdown spectroscopy and laser ablation inductively coupled plasma mass spectrometry. *Applied Physics A: Materials Science and Processing*, *93*(4), 917–922. https://doi.org/10.1007/s00339-008-4747-0

Heiskanen, A. R., Spégel, C. F., Kostesha, N., Ruzgas, T., & Emnéus, J. (2008). Monitoring of Saccharomyces cerevisiae cell proliferation on thiol-modified planar gold microelectrodes using impedance spectroscopy. *Langmuir*, *24*(16), 9066–9073. https://doi.org/10.1021/la800580f

Indrayanto, G. (2018). Validation of Chromatographic Methods of Analysis: Application for Drugs That Derived From Herbs. In *Profiles of Drug Substances, Excipients and Related Methodology* (1st ed., Vol. 43). Elsevier Inc. https://doi.org/10.1016/bs.podrm.2018.01.003

Jahnke, J. P., Terrell, J. L., Smith, A. M., Cheng, X., & Stratis-Cullum, D. N. (2016). Influences of adhesion variability on the "living" dynamics of filamentous bacteria in microfluidic channels. *Molecules*, *21*(8). https://doi.org/10.3390/molecules21080985

Kalluri, J. R., Arbneshi, T., Khan, S. A., Neely, A., Candice, P., Varisli, B., Washington, M., McAfee, S., Robinson, B., Banerjee, S., Singh, A. K., Senapati, D., & Ray, P. C. (2009). Use of gold nanoparticles in a simple colorimetric and ultrasensitive dynamic light scattering assay: Selective detection of arsenic in groundwater. *Angewandte Chemie - International Edition*, *48*(51), 9668–9671. https://doi.org/10.1002/anie.200903958

Koev, S. T., Dykstra, P. H., Luo, X., Rubloff, G. W., Bentley, W. E., Payne, G. F., & Ghodssi, R. (2010). Chitosan: An integrative biomaterial for lab-on-a-chip devices. *Lab on a Chip*, *10*(22), 3026–3042. https://doi.org/10.1039/c0lc00047g

Koksharov, S. A., Aleeva, S. V., & Lepilova, O. V. (2019). Description of adsorption interactions of lead ions with functional groups of pectin-containing substances. *Journal of Molecular Liquids*, *283*, 606–616. https://doi.org/10.1016/j.molliq.2019.03.109

Kosaki, Y., Takano, K., Citterio, D., Suzuki, K., & Shiratori, S. (2012). Quartz crystal microbalance sensor using ionophore for ammonium ion detection. *Journal of Nanoscience and Nanotechnology*, *12*(1), 563–567. https://doi.org/10.1166/jnn.2012.5386

Li, C., Başaran, A. E., & Tyson, J. F. (2013). Determination of inorganic arsenic in water by a quartz crystal microbalance. *Analytical Methods*, *5*(22), 6286–6291. https://doi.org/10.1039/c3ay40876k

Lokman, N. F., Azeman, N. H., Suja, F., Arsad, N., & Bakar, A. A. A. (2019). Sensitivity enhancement of Pb(II) ion detection in rivers using SPR-based Ag metallic layer coated with chitosan–graphene oxide nanocomposite. *Sensors (Switzerland)*, *19*(23). https://doi.org/10.3390/s19235159

Lokman, N. F., Bakar, A. A. A., Suja, F., Abdullah, H., Rahman, W. B. W. A., Huang, N. M., & Yaacob, M. H. (2014). Highly sensitive SPR response of Au/chitosan/graphene oxide nanostructured thin films toward Pb (II) ions. *Sensors and Actuators, B: Chemical*, *195*, 459–466. https://doi.org/10.1016/j.snb.2014.01.074

Mauro, M. (2015). *Sweet openQCM Tasting Water Sucrose Solutions*. https://openqcm.com/sweet-openqcm-water-sucrose-solutions.html

Niemczyk, A., Kaczorowski, P., & El Fray, M. (2015). Spin-coated chitosan on copolyester substrates. *Progress on Chemistry and Application of Chitin and Its Derivatives*, *20*(September), 236–245. https://doi.org/10.15259/PCACD.20.23

Poitras, C., & Tufenkji, N. (2009). A QCM-D-based biosensor for E. coli O157:H7 highlighting the relevance of the dissipation slope as a transduction signal. *Biosensors and Bioelectronics*, *24*(7), 2137–2142. https://doi.org/10.1016/j.bios.2008.11.016

Politi, J., Dardano, P., Caliò, A., Iodice, M., Rea, I., & De Stefano, L. (2017). Reversible sensing of heavy metal ions using lysine modified oligopeptides on porous silicon and gold. *Sensors and Actuators, B: Chemical*, *244*, 142–150. https://doi.org/10.1016/j.snb.2016.12.132

Politi, J., Rea, I., Nici, F., Dardano, P., Terracciano, M., Oliviero, G., Borbone, N., Piccialli, G., & De Stefano, L. (2016). Nanogravimetric and optical characterizations of thrombin interaction with a self-assembled thiolated aptamer. *Journal of Sensors*, *2016*. https://doi.org/10.1155/2016/3561863

Preparing Self-Assembled Monolayers. (n.d.). Retrieved June 4, 2022, from https://www.sigmaaldrich.com/US/en/technical-documents/protocol/materials-science-and-engineering/organic-electronics/preparing-self-assembled

Quartz, Q., & Microbalance, C. (2021). *openQCM Q -1 User ' s Guide*. 1–48.

Reviakine, I., Johannsmann, D., & Richter, R. P. (2011). Hearing what you cannot see and visualizing what you hear: Interpreting quartz crystal microbalance data from solvated interfaces. *Analytical Chemistry*, *83*(23), 8838–8848. https://doi.org/10.1021/ac201778h

Sadman, K., Wiener, C. G., Weiss, R. A., White, C. C., Shull, K. R., & Vogt, B. D. (2018). Quantitative Rheometry of Thin Soft Materials Using the Quartz Crystal Microbalance with Dissipation. *Analytical Chemistry*, *90*(6), 4079–4088. https://doi.org/10.1021/acs.analchem.7b05423

Sartore, L., Barbaglio, M., Borgese, L., & Bontempi, E. (2011). Polymer-grafted QCM chemical sensor and application to heavy metal ions real time detection. *Sensors and Actuators, B: Chemical*, *155*(2), 538–544. https://doi.org/10.1016/j.snb.2011.01.003

Sprung, C., Wählisch, D., Hüttl, R., Seldel, J., Meyer, A., & Wolf, G. (2009). Detection and monitoring of biofilm formation in water treatment systems by quartz crystal microbalance sensors. *Water Science and Technology*, *59*(3), 543–548. https://doi.org/10.2166/wst.2009.001

Taneja, P., Manjuladevi, V., & Gupta, R. K. (2018). Detection of cadmium ion in water using films of nanocomposite of functionalized carbon nanotubes and anionic polymer. *AIP Conference Proceedings*, *1953*(May), 30096–30099. https://doi.org/10.1063/1.5032433

Tokuyama, H., Kitamura, E., & Seida, Y. (2020). Development of zirconia nanoparticle-loaded hydrogel for arsenic adsorption and sensing. *Reactive and Functional Polymers*, *146*. https://doi.org/10.1016/j.reactfunctpolym.2019.104427

Ventura, B. Della, Iannaccone, M., Funari, R., Ciamarra, M. P., Altucci, C., Capparelli, R., Roperto, S., & Velotta, R. (2017). Effective antibodies immobilization and functionalized nanoparticles in a quartzcrystal microbalance-based immunosensor for the detection of parathion. *PLoS ONE*, *12*(2), 1–14. https://doi.org/10.1371/journal.pone.0171754

WHO, & World Health Organization. (2019). Preventing Disease through Healthy Environment. Exposure to Arsenic: A Major Public Health Concern. *Preventing Disease through Healthy Environment*, 1–5. http://www.who.int/ipcs/features/arsenic.pdf?ua=1

World Health Organization. (2018). *No Title*. Arsenic. https://www.who.int/news-room/fact-sheets/detail/arsenic

World Health Organization. (2021). *No Title*. Lead Poisoning. https://www.who.int/news-room/fact-sheets/detail/lead-poisoning-and-health

Yang, Z., Li, B., Xia, R., Ma, S., Jia, R., Ma, C., Wang, L., Chen, Y., & Bin, L. (2022). Understanding China's industrialization driven water pollution stress in 2002–2015—A multi-pollutant based net gray water footprint analysis. *Journal of Environmental Management*, *310*(October 2021), 114735. https://doi.org/10.1016/j.jenvman.2022.114735

Yao, M., Yang, H., Huang, L., Chen, T., Rao, G., & Liu, M. (2017). Detection of heavy metal Cd in polluted fresh leafy vegetables by laser-induced breakdown spectroscopy. *Applied Optics*, *56*(14), 4070. https://doi.org/10.1364/ao.56.004070

Zhang, Q., Cui, H., Xiong, X., Chen, J., Wang, Y., Shen, J., Luo, Y., & Chen, L. (2018). QCM-nanomagnetic beads biosensor for lead ion detection. *Analyst*, *143*(2), 549–554. https://doi.org/10.1039/c7an01498h

APPENDIX A

The QCM system recorded frequency vs. time variation of 0, 50, 100, and 200 ppb arsenic in ultra-pure water. *Figure A.1 - Figure A.4* show frequency vs. time variation of arsenic samples in ultra-pure water from four arsenic experiments. The data highlighted in orange was the three- minute of frequency value used for data analysis.

Figure A.5 – Figure A.8 show individual linear correlation curve for four experiments with four different concentrations of arsenic in ultra-pure water.

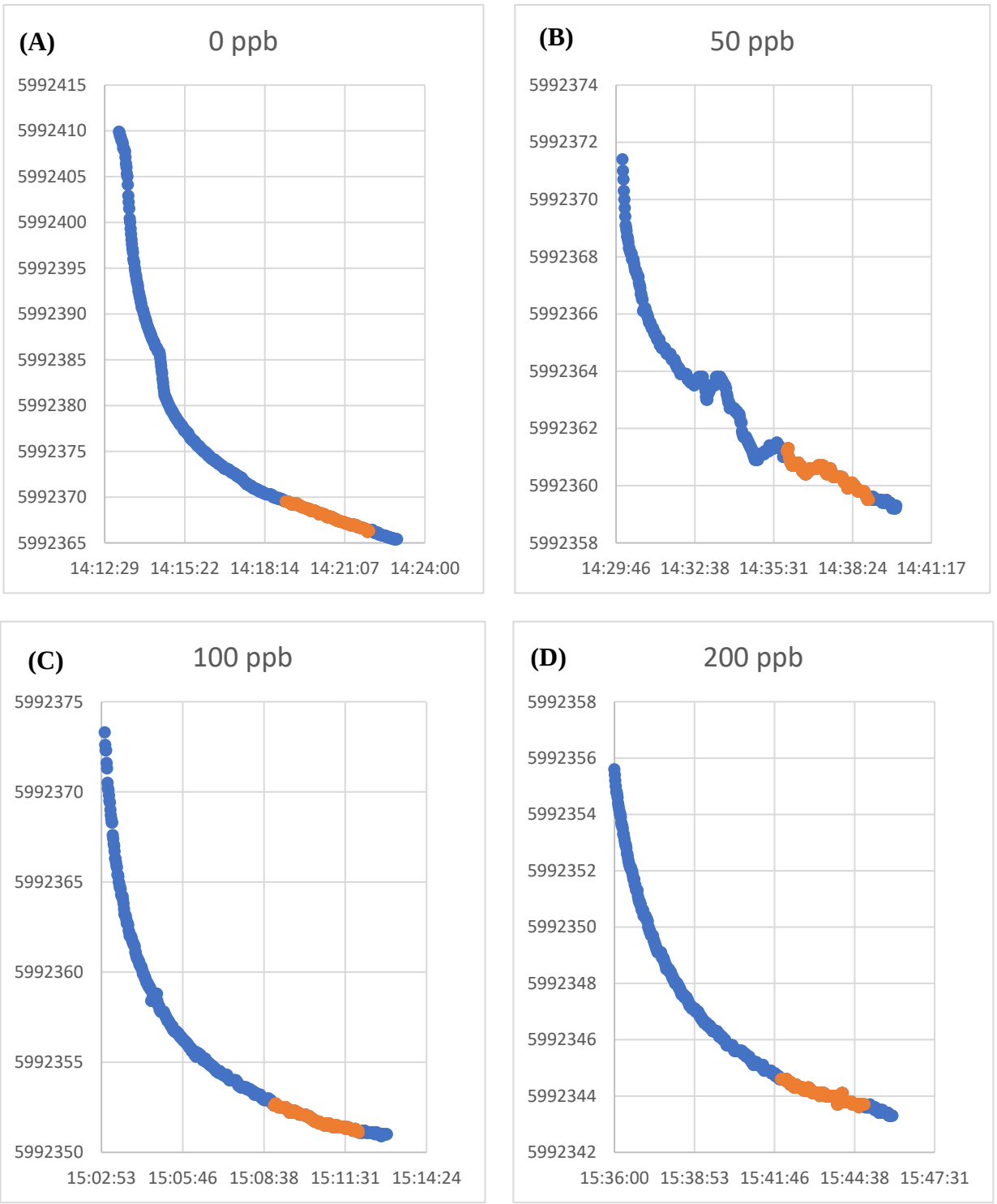

Figure A.1 Frequency vs. time variations for four concentrations of arsenic in ultra-pure water experiment 1 conducted on September 29, 2021, with 10 minutes stabilization time. (A) 0 ppb. (B) 50 ppb. (C)100 ppb. (D) 200 ppb.

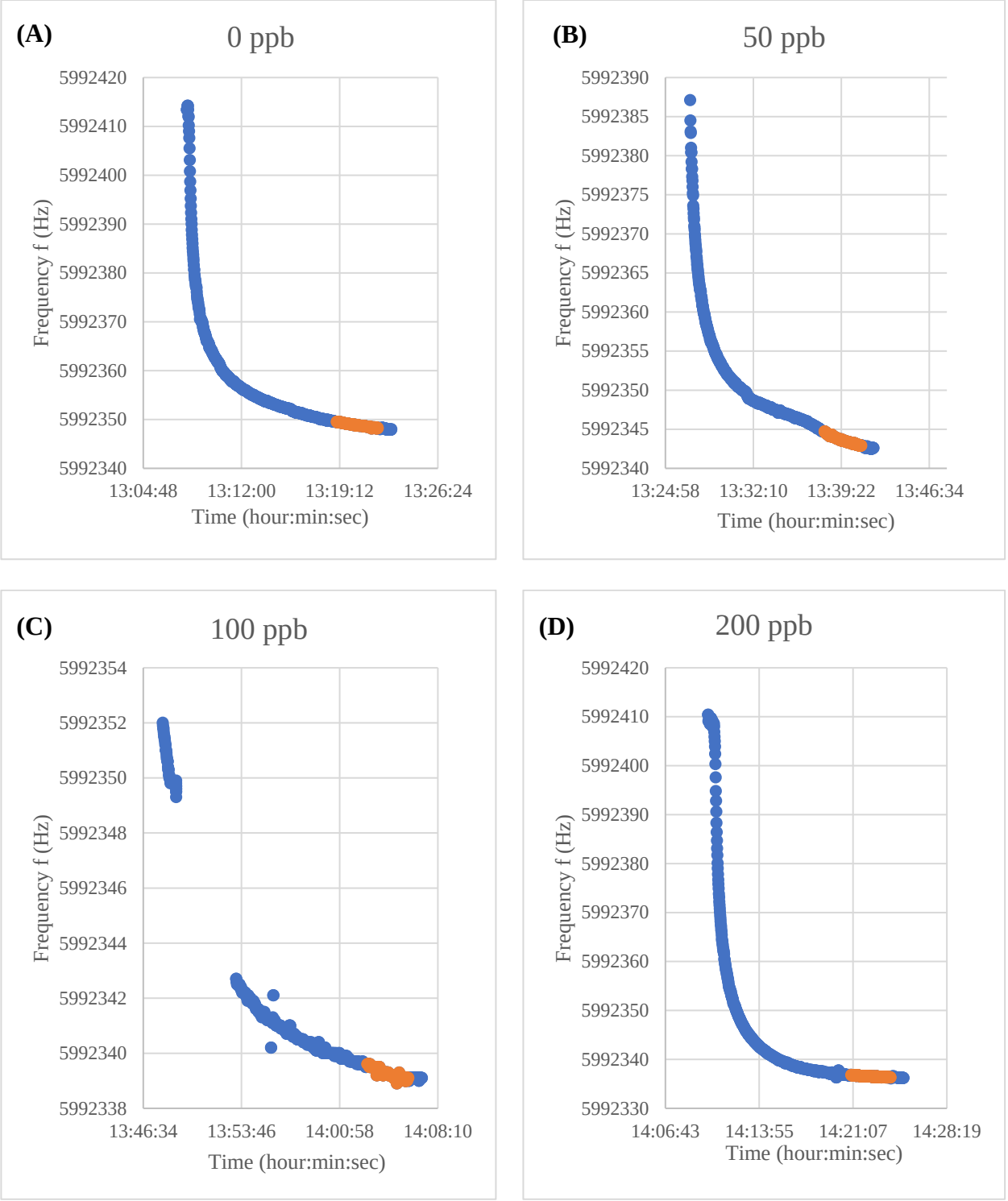

Figure A.2 Frequency vs. time variations for four concentrations of arsenic in ultra-pure water experiment 2 conducted on October 8, 2021, with 15 minutes stabilization time. (A) 0 ppb. (B) 50 ppb. (C)100 ppb. (D) 200 ppb.

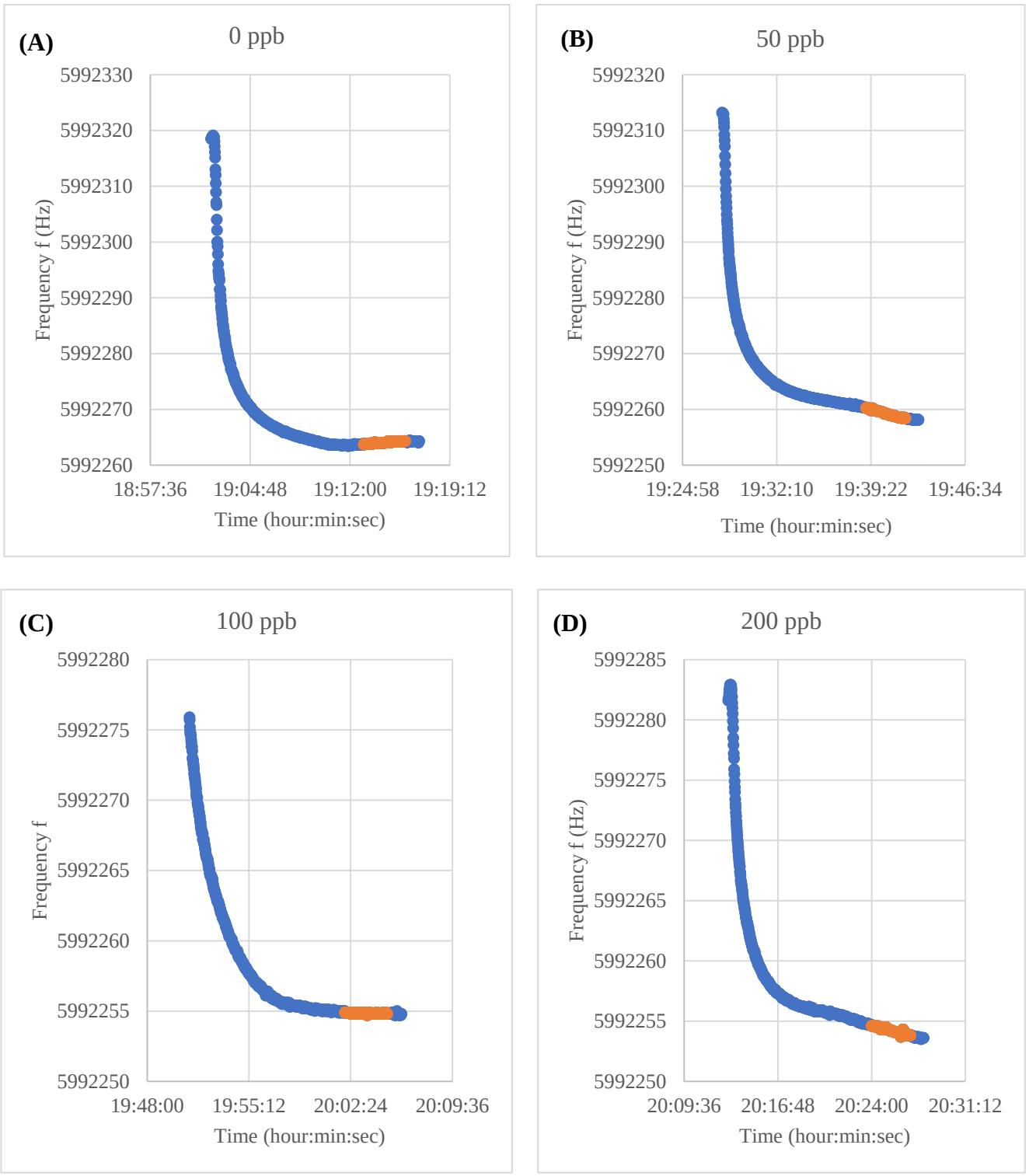

Figure A.3 Frequency vs. time variations for four concentrations of arsenic in ultra-pure water experiment 3 conducted on October 21, 2021, with 15 minutes stabilization time. (A) 0 ppb. (B) 50 ppb. (C)100 ppb. (D) 200 ppb.

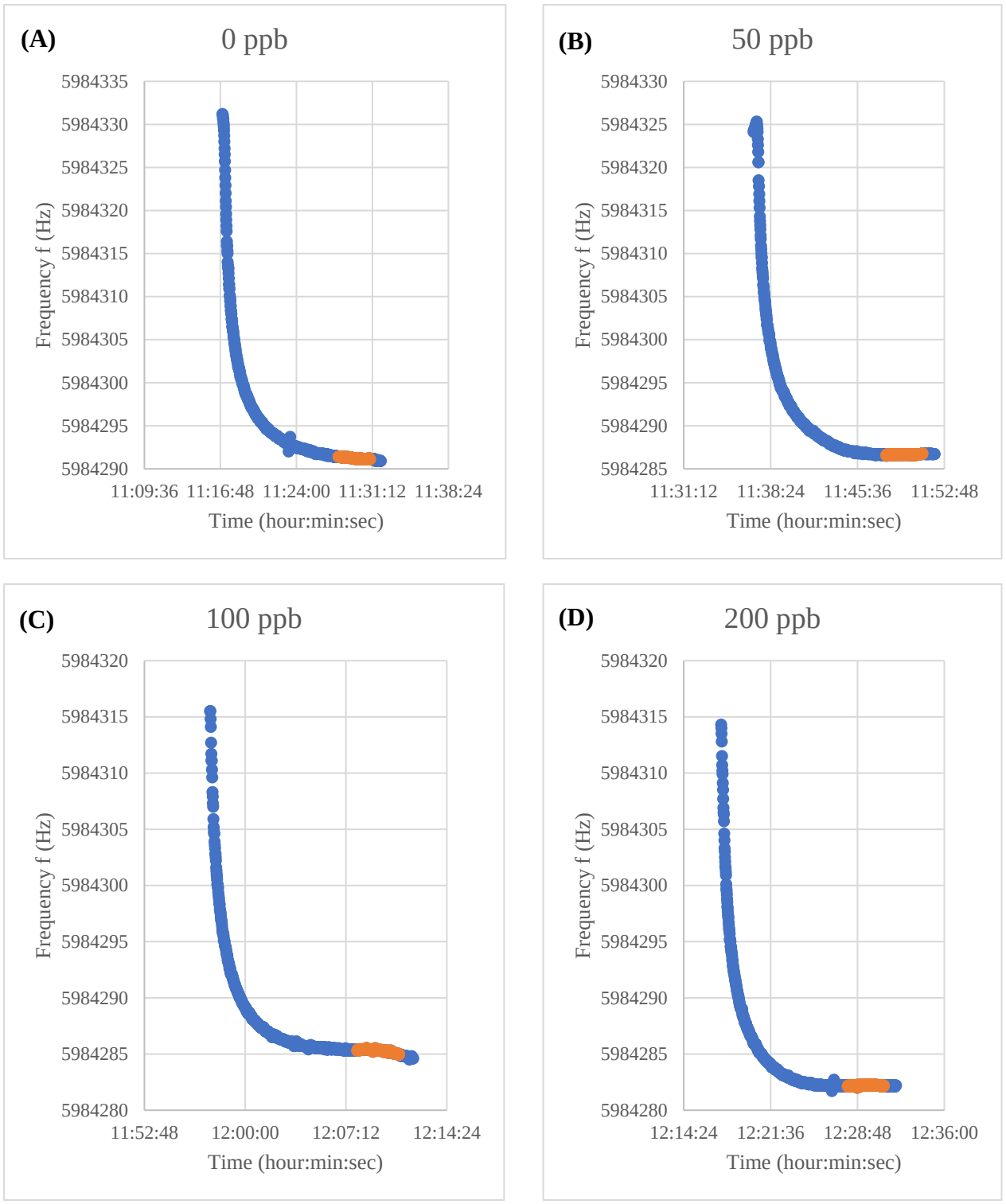

Figure A.4 Frequency vs. time variations for four concentrations of arsenic in ultra-pure water experiment 4 conducted on November 15, 2021, with 15 minutes stabilization time. (A) 0 ppb. (B) 50 ppb. (C)100 ppb. (D) 200 ppb.

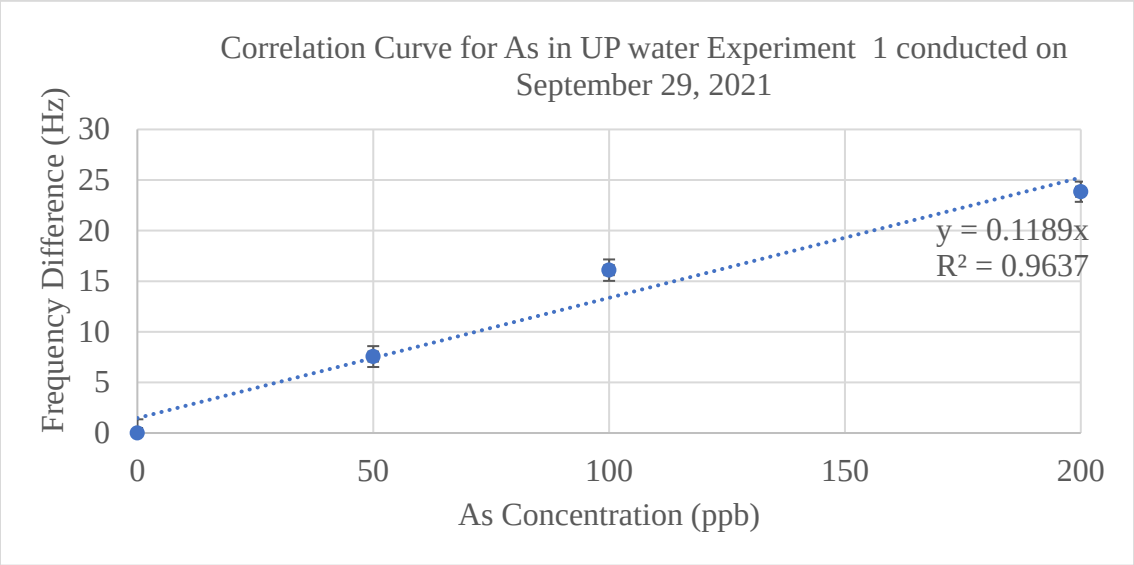

Figure A.5 Linear correlation curve for arsenic in ultra-pure water experiment 1 conducted on September 29, 2021. (Error bars show standard deviation of observation within experiment 1)

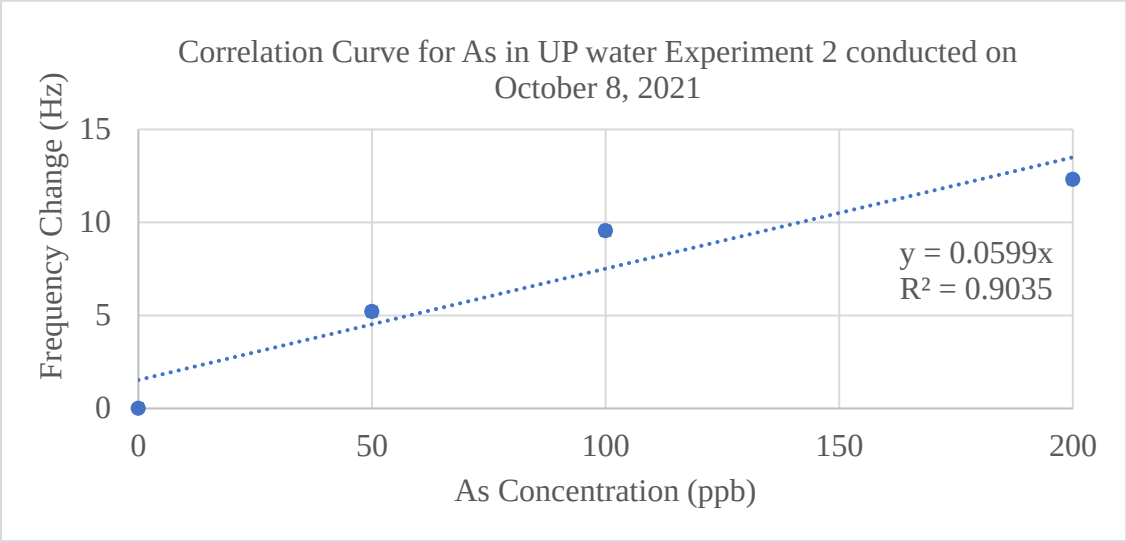

Figure A.6 Linear correlation curve for arsenic in ultra-pure water experiment 2 conducted on October 8, 2021. (Error bars show standard deviation of observation within experiment 2)

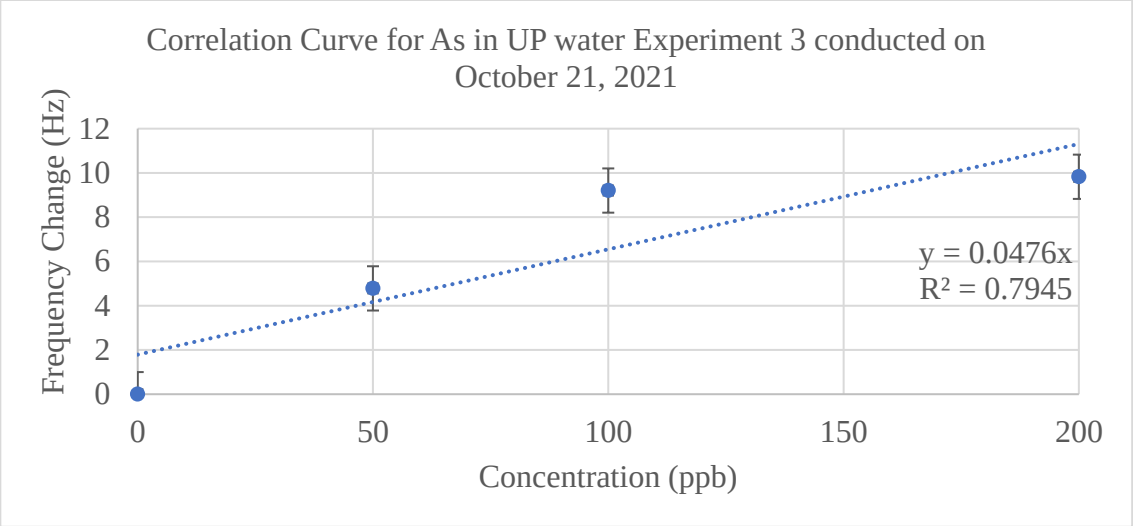

Figure A.7 Linear correlation curve for arsenic in ultra-pure water experiment 2 conducted on October 21, 2021. (Error bars show standard deviation of observation within experiment 3)

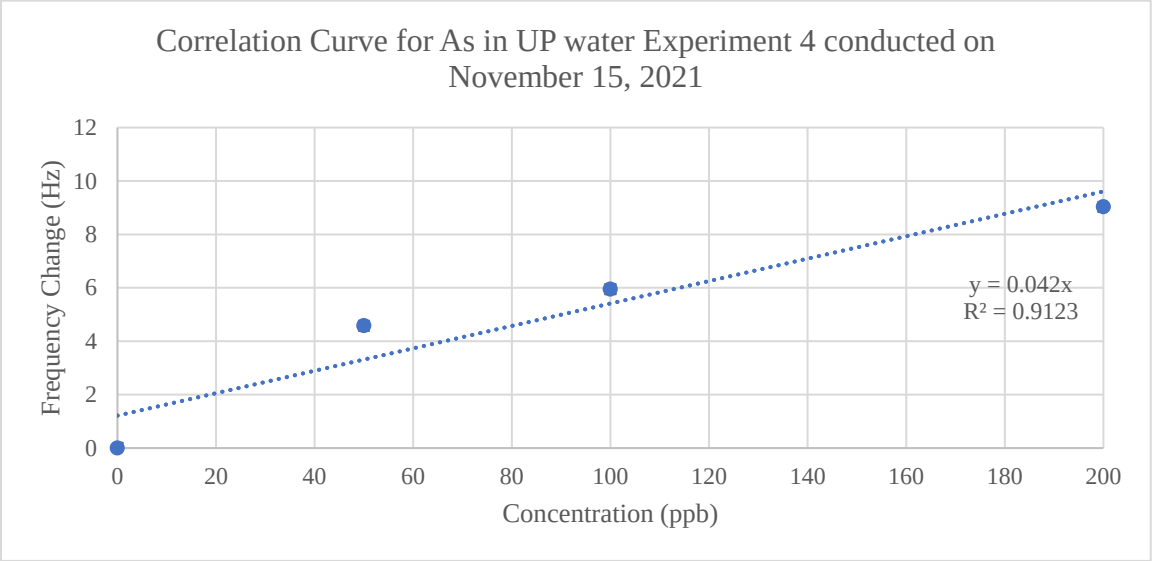

Figure A.8 Linear correlation curve for arsenic in ultra-pure water experiment 2 conducted on November 15, 2021. (Error bars show standard deviation of observation within experiment 4)

APPENDIX B

The QCM system recorded frequency vs. time variation of 0, 50, 100, and 200 ppb arsenic in 0.5% HNO_3. *Figure B.1–Figure B.2* shows frequency vs. time variation of arsenic samples in 0.5% HNO_3 from two experiments. The data highlighted in orange was the three-minute frequency value used for data analysis.

Figure B.3-Figure B.4 shows individual linear correlation curves for two experiments with four different concentrations of arsenic in 0.5% HNO_3.

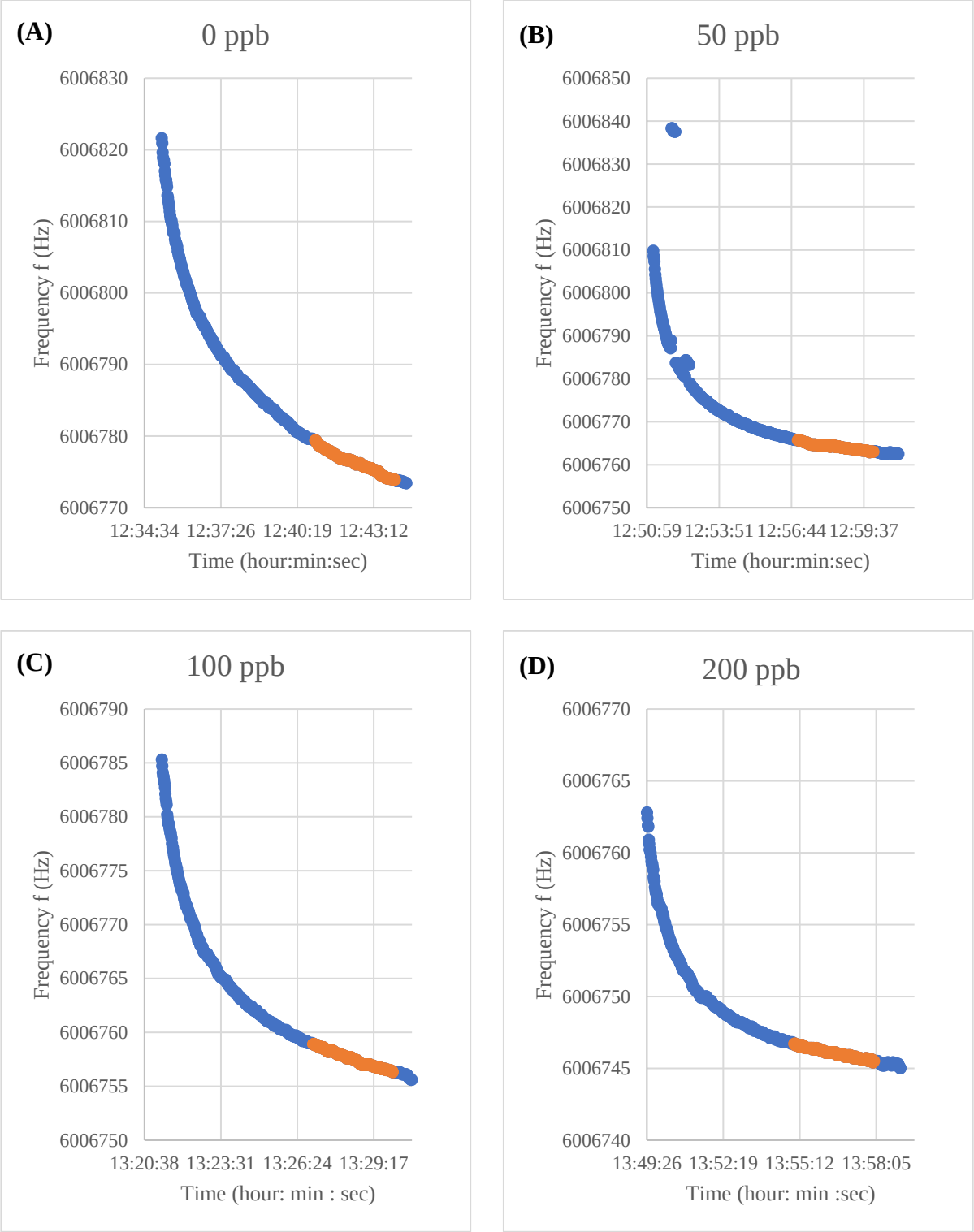

Figure B.1 Frequency vs. time variations for four concentrations of arsenic in 0.5% HNO_3 experiment 1 conducted on September 17, 2021, with 10 minutes stabilization time. (A) 0 ppb. (B) 50 ppb. (C)100 ppb. (D) 200 ppb.

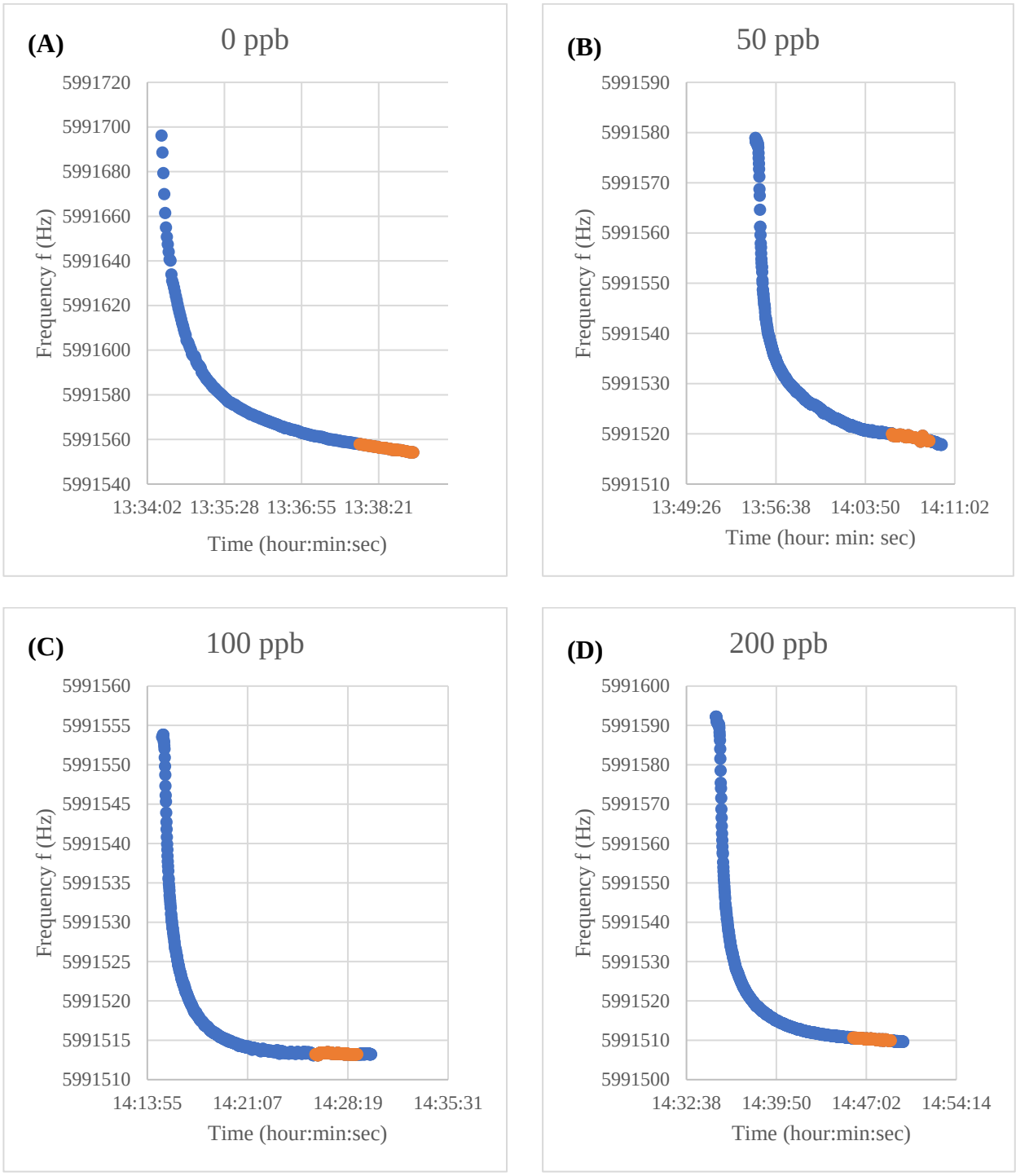

Figure B.2 Frequency vs. time variations for four concentrations in arsenic in 0.5% HNO_3 experiment 2 conducted on October 1, 2021 with 15 minutes of stabilization time. (The 0 ppb's resting time was only 10 minutes. Therefore, only the last 1 minute of the 0-ppb sample was used for analysis to maximize the time consistency of the remaining arsenic samples in this experiment) (A) 0 ppb. (B) 50 ppb. (C)100 ppb. (D) 200 ppb.

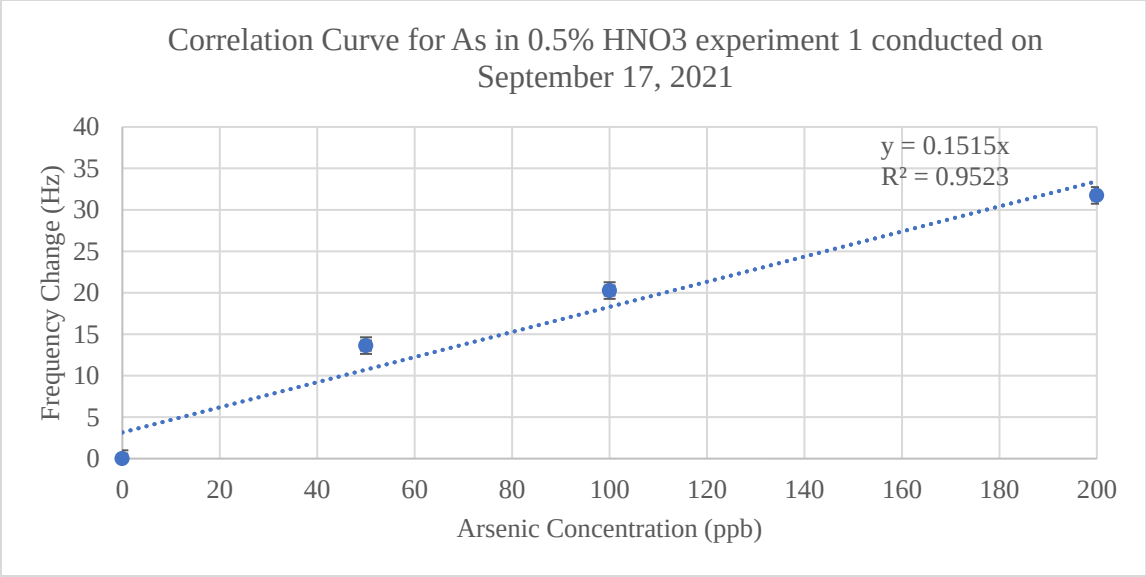

Figure B.3 Linear correlation curve for arsenic in HNO_3 experiment 1 conducted on September 17, 2021. (Error bars show standard deviation of observation within experiment 1)

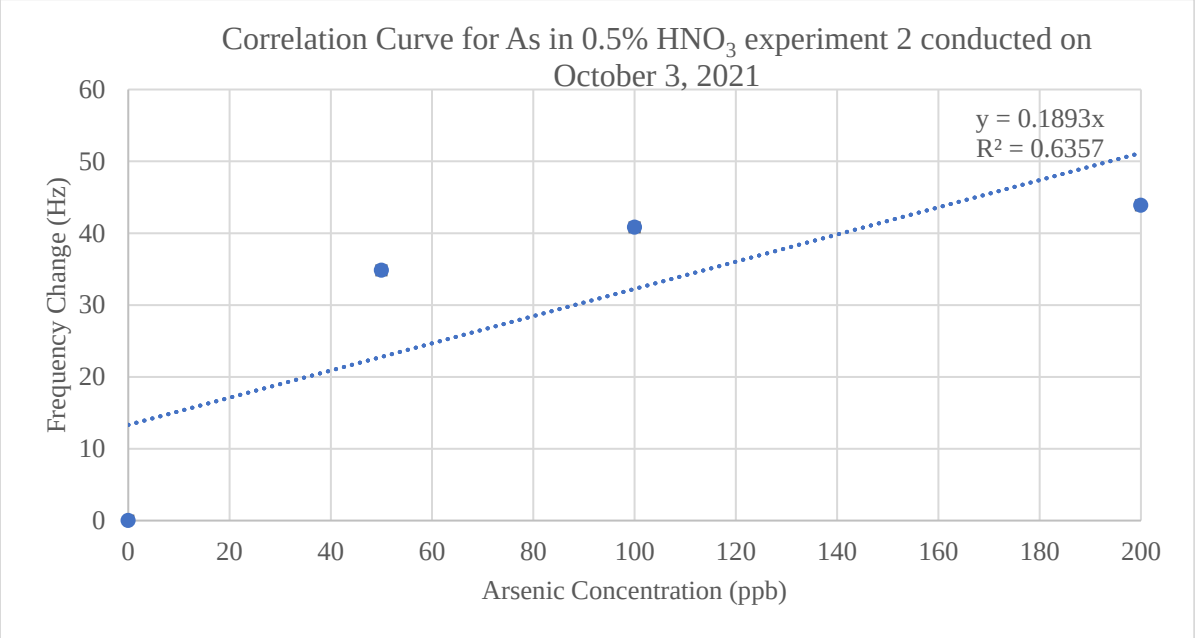

Figure B.4 Linear correlation curve for arsenic in HNO_3 experiment 1 conducted on October 3, 2021. (Error bars show standard deviation of observation within experiment 2)

APPENDIX C

The QCM system installed with drop-casted CGL ligand recorded frequency vs. time variation of 0 ppb lead in ultra-pure water. *Figure C.1* shows the frequency vs. time variation of 0 ppb lead samples in ultra-pure water from three separate quartz crystal gold electrodes.

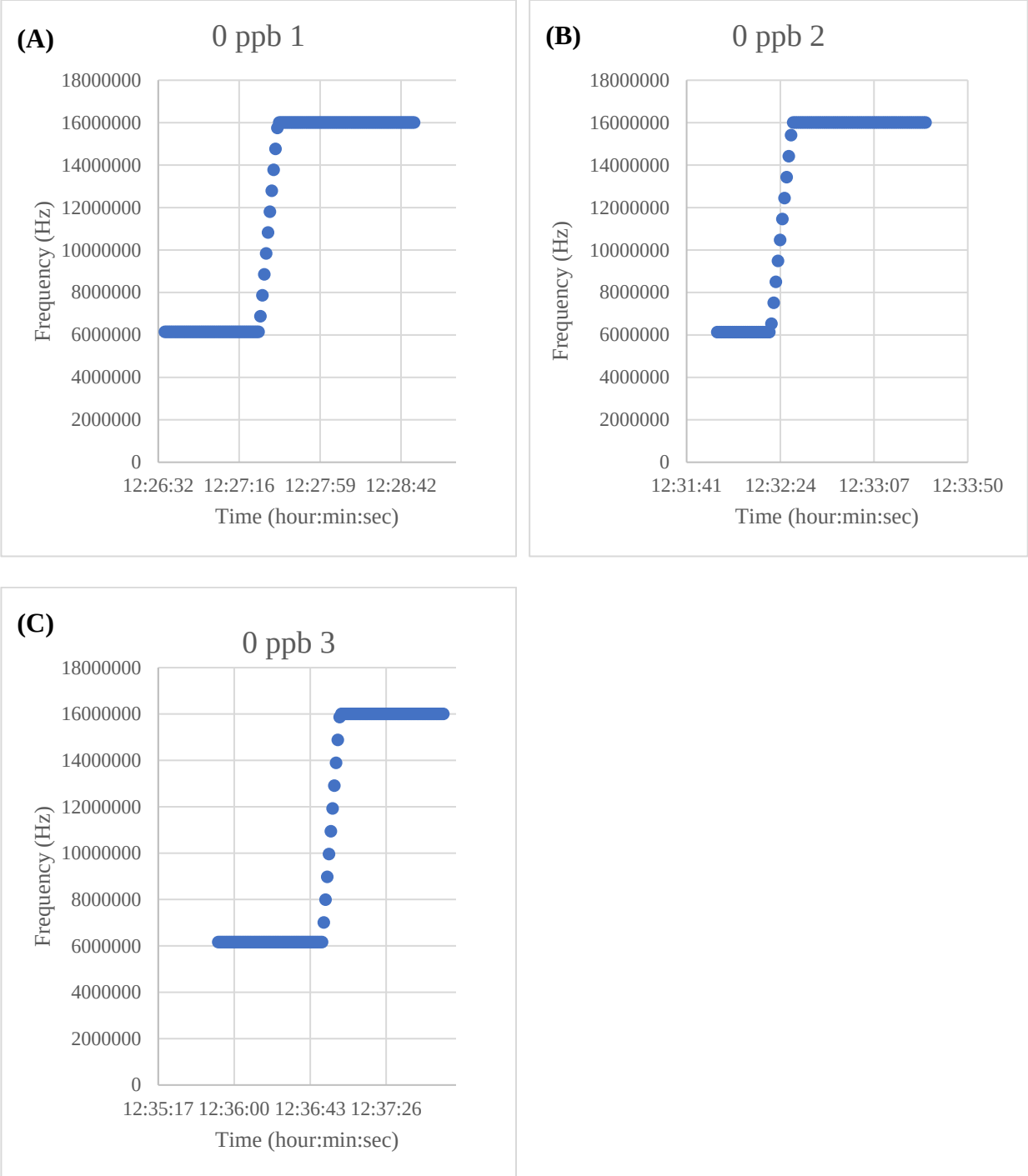

Figure C.1 The frequency vs. time variation after injection of 0 ppb (blank) in ultra-pure water using three separate CGL drop-casted quartz crystal gold electrode conducted on February 24, 2022. (A) Experiment 1. (B) Experiment 2. (C) Experiment 3.

APPENDIX D

The QCM system installed with CGL spin-coated quartz crystal gold electrode recorded frequency vs. time variation of 0, 100, 200 ppb lead in ultra-pure water. *Figure D.1 - Figure D.3* show frequency vs. time variation of five lead concentrations in ultra-pure water from three experiments. The data highlighted in orange was the three minute of frequency value used for data analysis. *Figure D.4 - Figure D.6* show the individual linear correlation curve for three experiments with three different concentrations of lead in ultra-pure water.

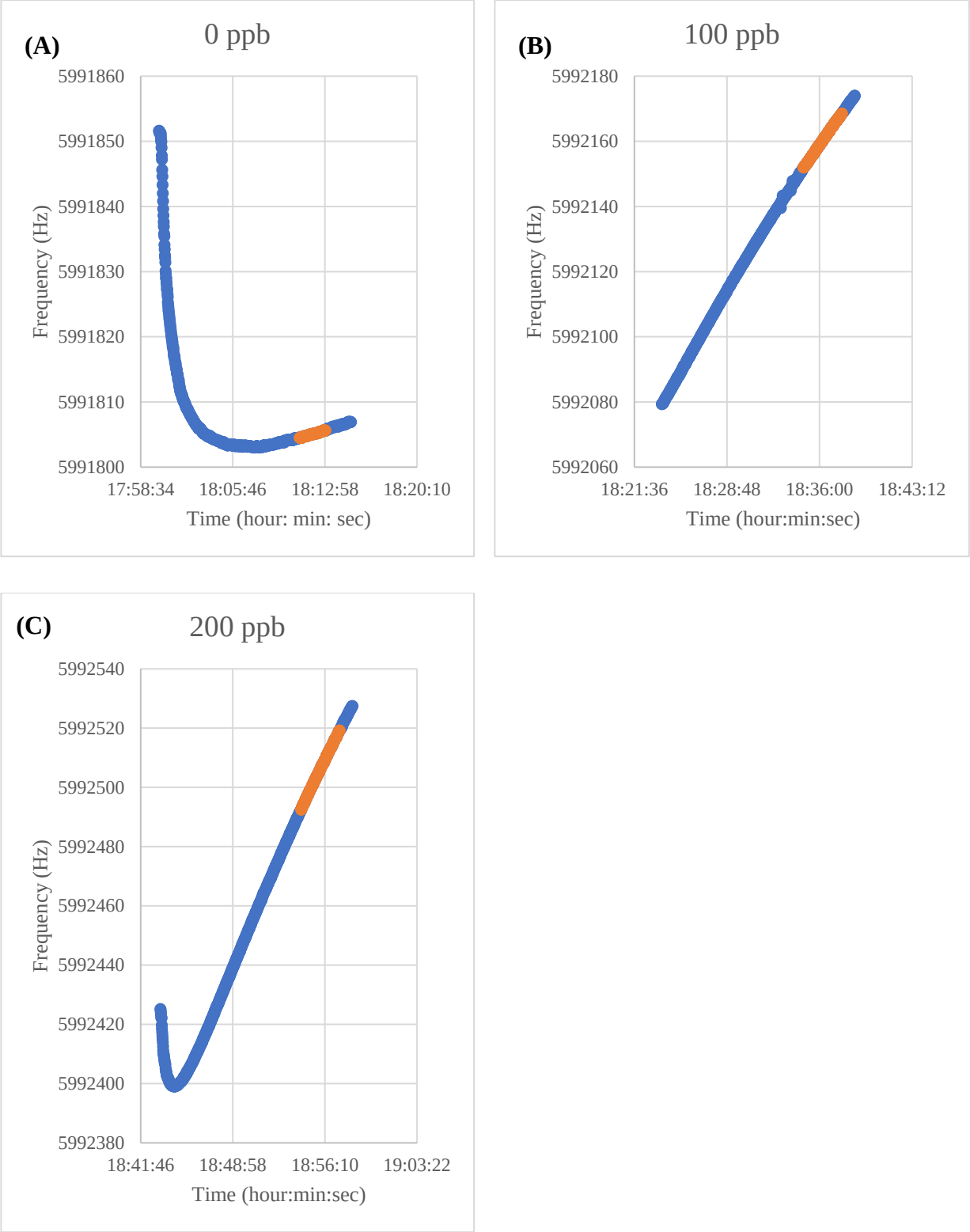

Figure D.1 Frequency vs. time variations for three lead concentrations in ultra-pure water experiment 1 conducted on March 7, 2022 with 15 minutes stabilization time. (A) 0 ppb. (B) 100 ppb. (c) 200 ppb.

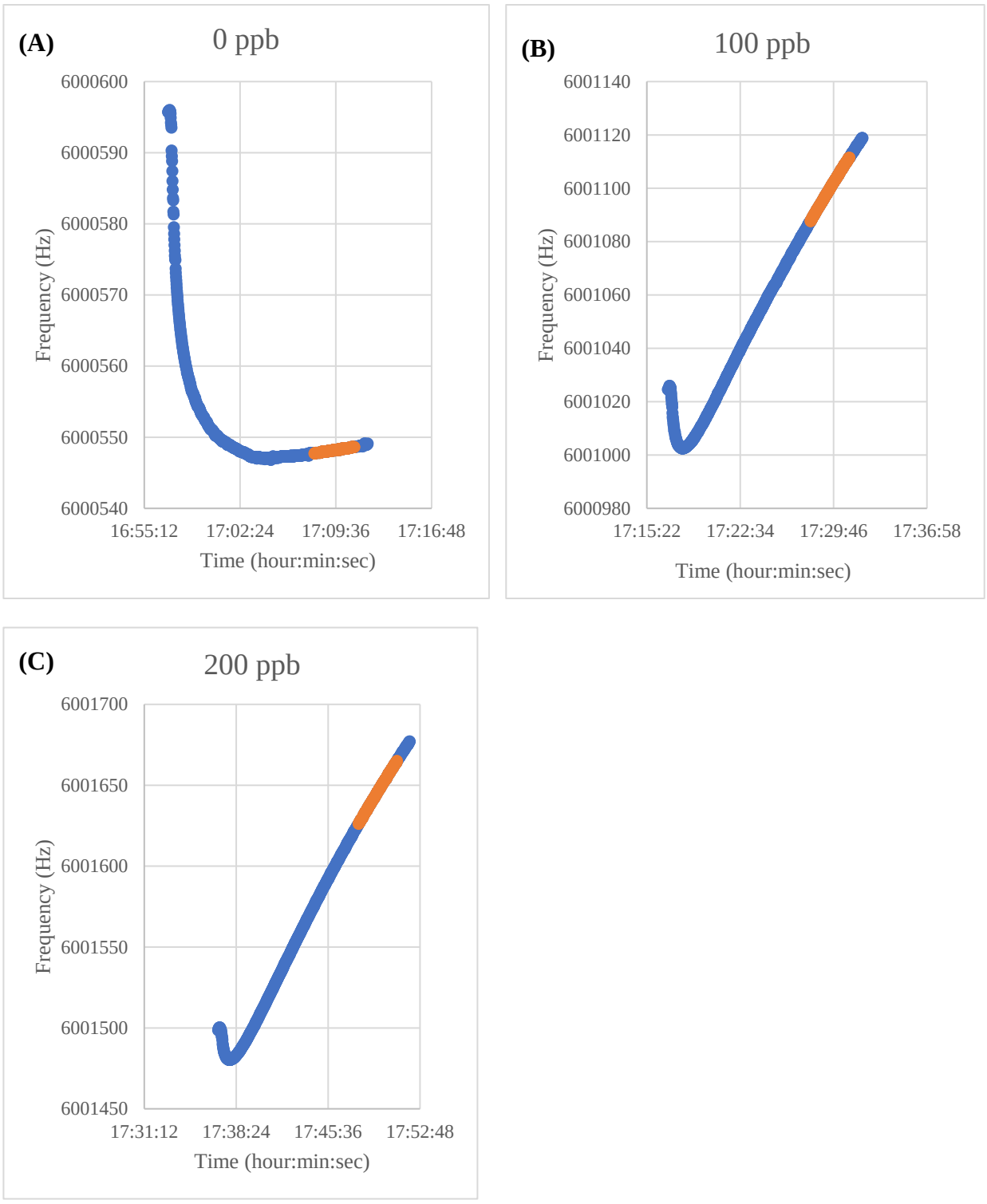

Figure D.2 Frequency vs. time variations for three lead concentrations in ultra-pure water experiment 2 conducted on March 7, 2022 with 15 minutes stabilization time. (A) 0 ppb. (B) 100 ppb. (C) 200 ppb.

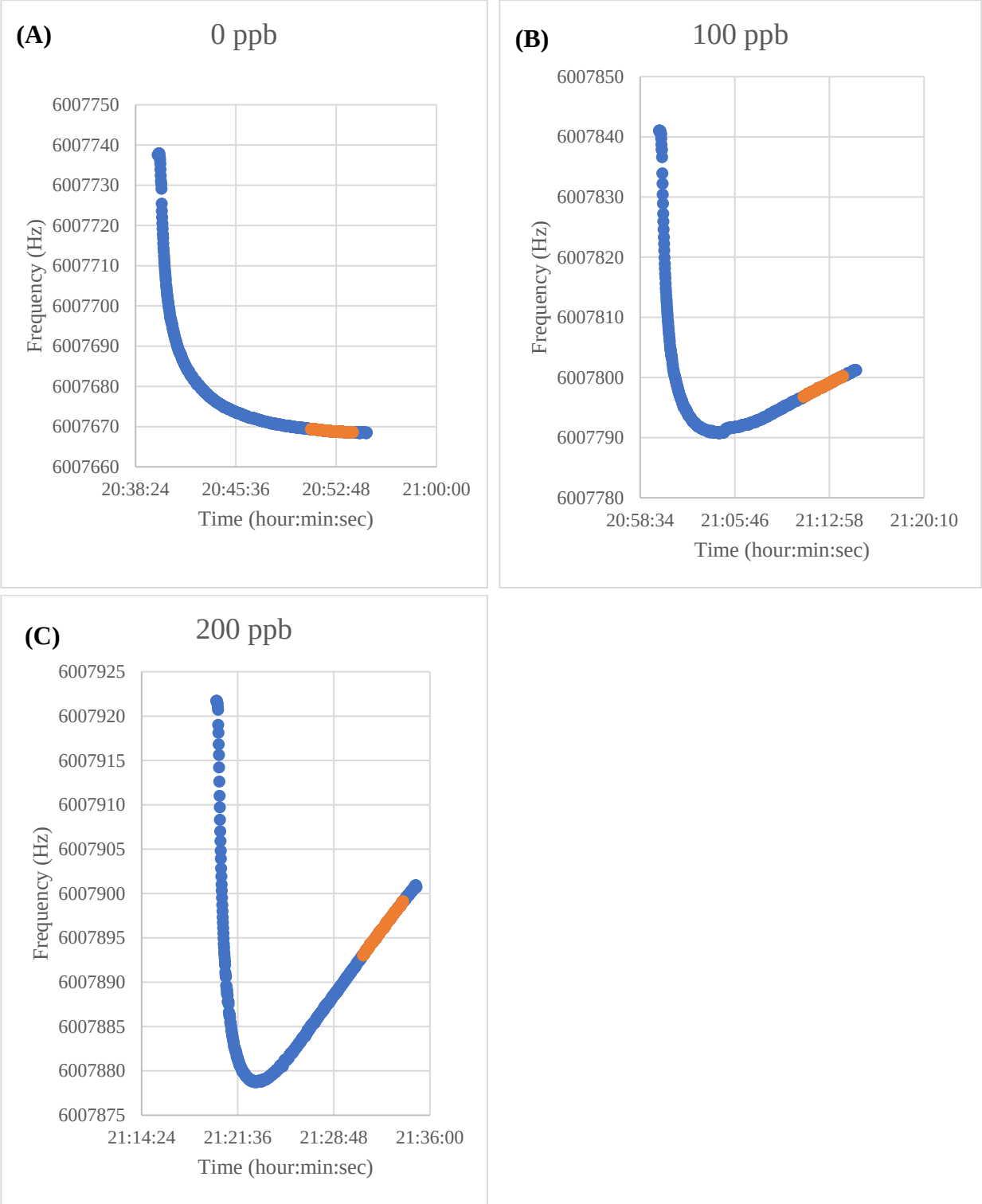

Figure D.3 Frequency vs. time variations for three lead concentration experiment 3 conducted on March 8, 2022 with 15 minutes stabilization time. (A) 0 ppb. (B) 100 ppb. (C) 200 ppb.

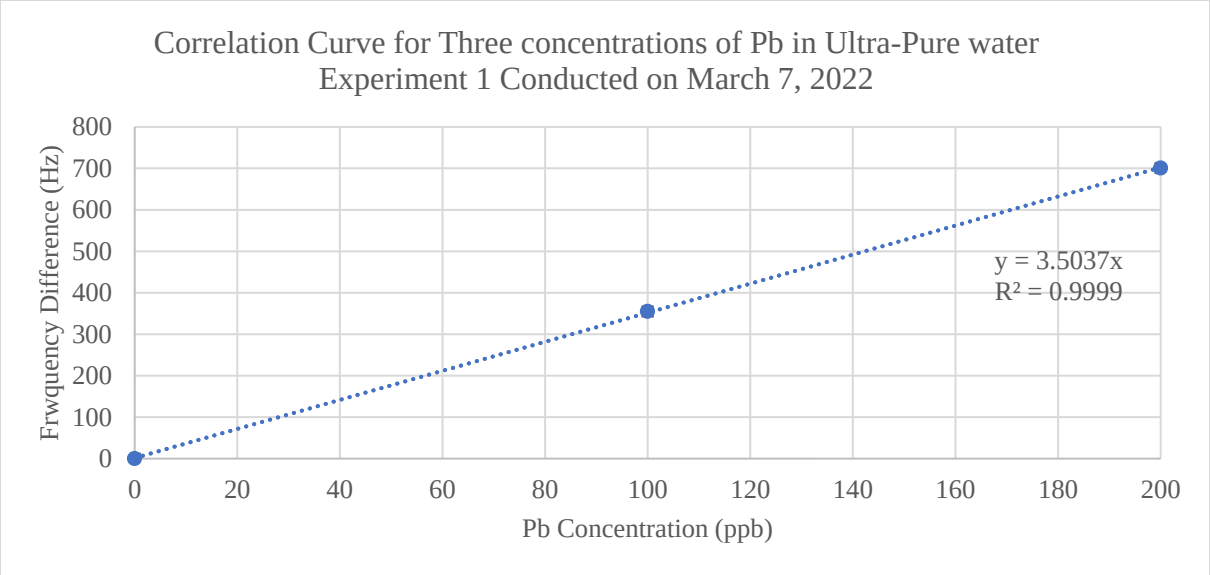

Figure D.4 Linear correlation curve for three lead concentration in ultra-pure water experiment 1 conducted on March 7, 2022. (Error bars show standard deviation of observation within experiment 1)

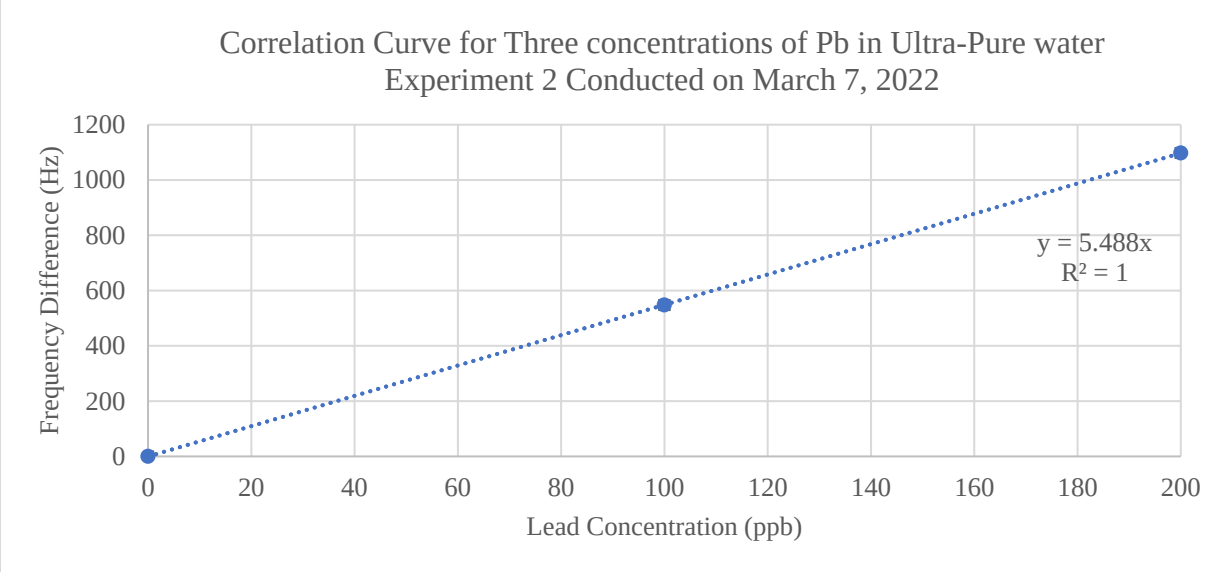

Figure D.5 Linear correlation curve for three lead concentration in ultra-pure water experiment 2 conducted on March 7, 2022. (Error bars show standard deviation of observation within experiment 2)

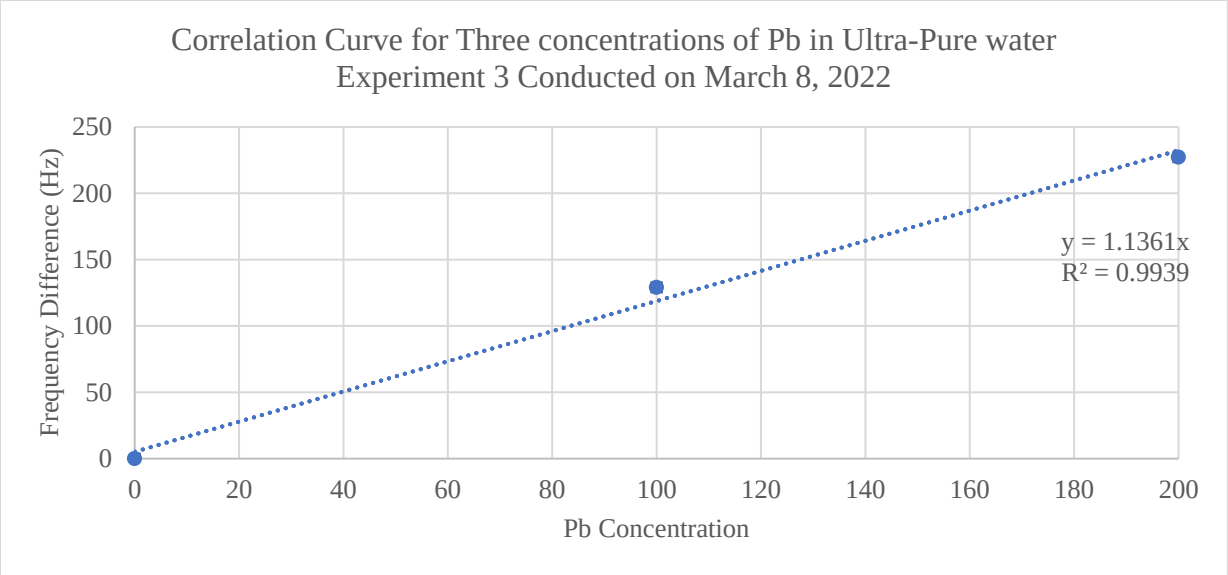

Figure D.6 Linear correlation curve for three lead concentration in ultra-pure water experiment 3 conducted on March 3, 2022. (Error bars show standard deviation of observation within experiment 3)

APPENDIX E

The QCM system installed with CGL spin-coated quartz crystal gold electrode recorded frequency vs. time variation of 0, 10, 25, 50, and 100 ppb lead in ultra-pure water. *Figure E.1 – Figure E3* show frequency vs. time variation of five lead concentrations in ultra-pure water from three experiments. The data highlighted in orange was the three-minute frequency value used for data analysis. *Figure E.4 – Figure E.6* show the individual linear correlation curve for three experiments with five different lead concentrations in ultra-pure water.

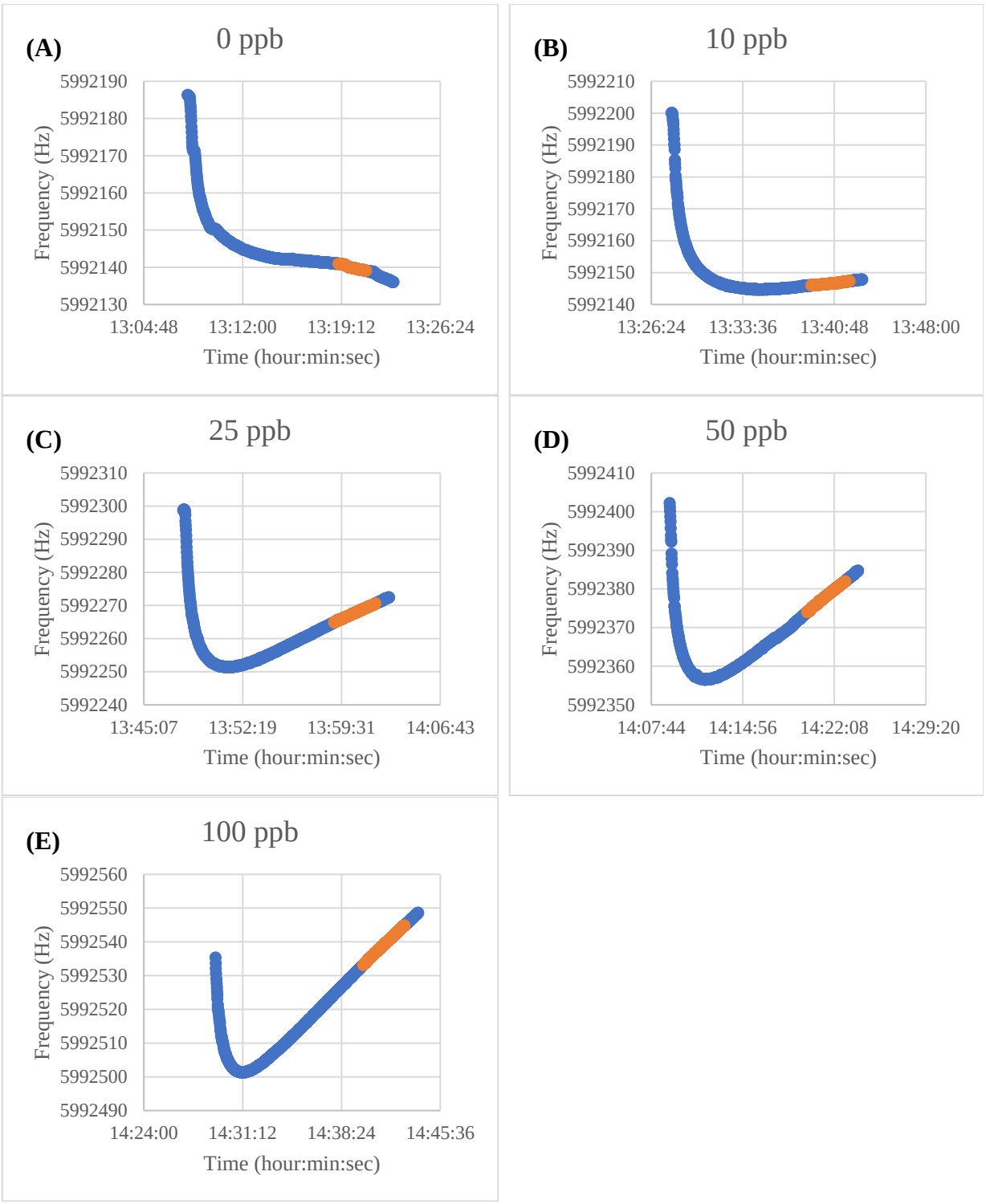

Figure E.1 Frequency vs. time variations with five lead concentrations in ultra-pure water experiment 1 conducted on March 8, 2022 with 15 minutes stabilization time. (A) 0 ppb. (B) 10 ppb. (C) 25 ppb. (D) 50 ppb. (E) 100 ppb.

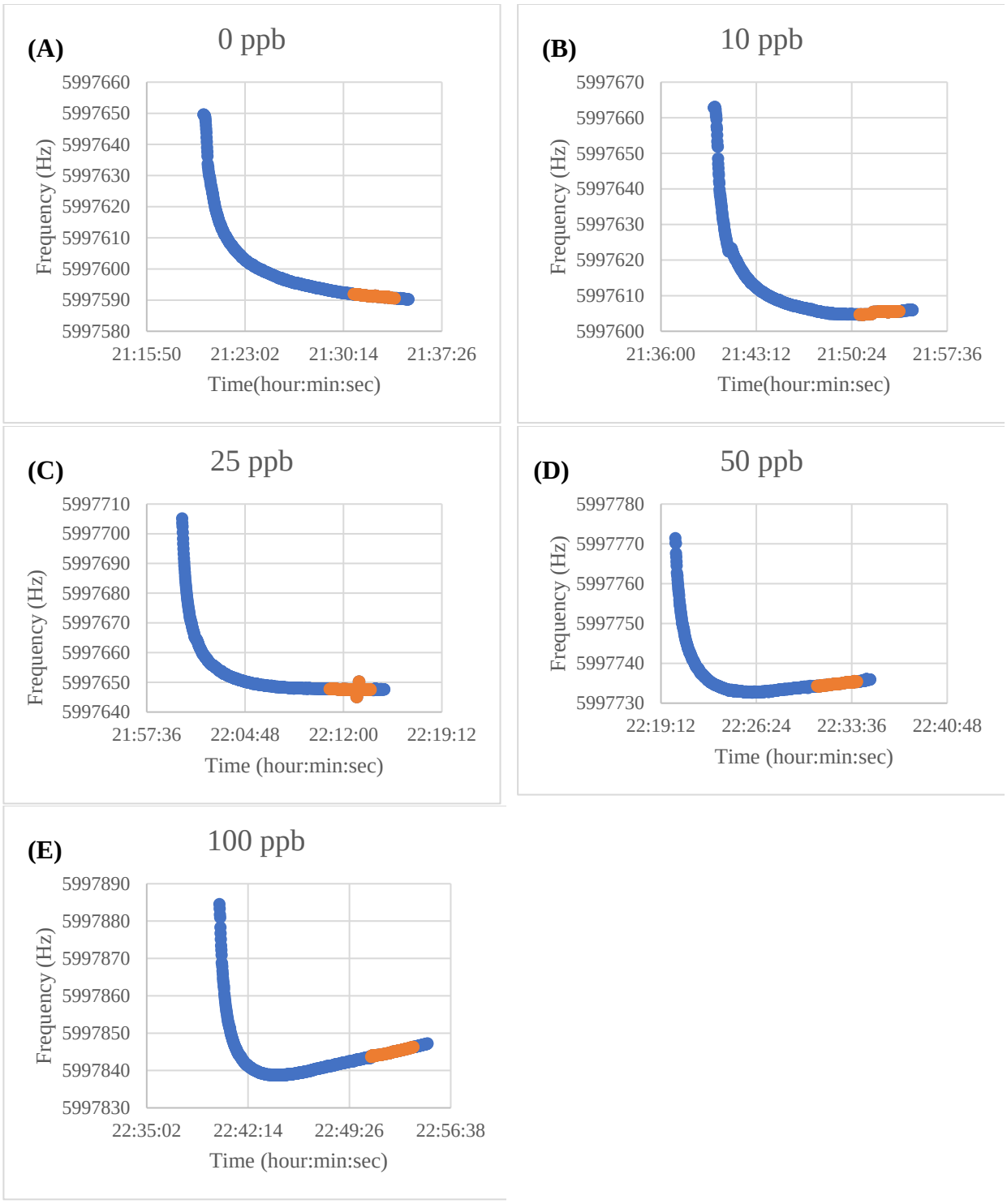

Figure E.2 Frequency vs. time variations with five lead concentrations in ultra-pure water experiment 2 conducted on March 9, 2022 with 15 minutes stabilization time. (A) 0 ppb. (B) 10 ppb. (C) 25 ppb. (D) 50 ppb. (E) 100 ppb.

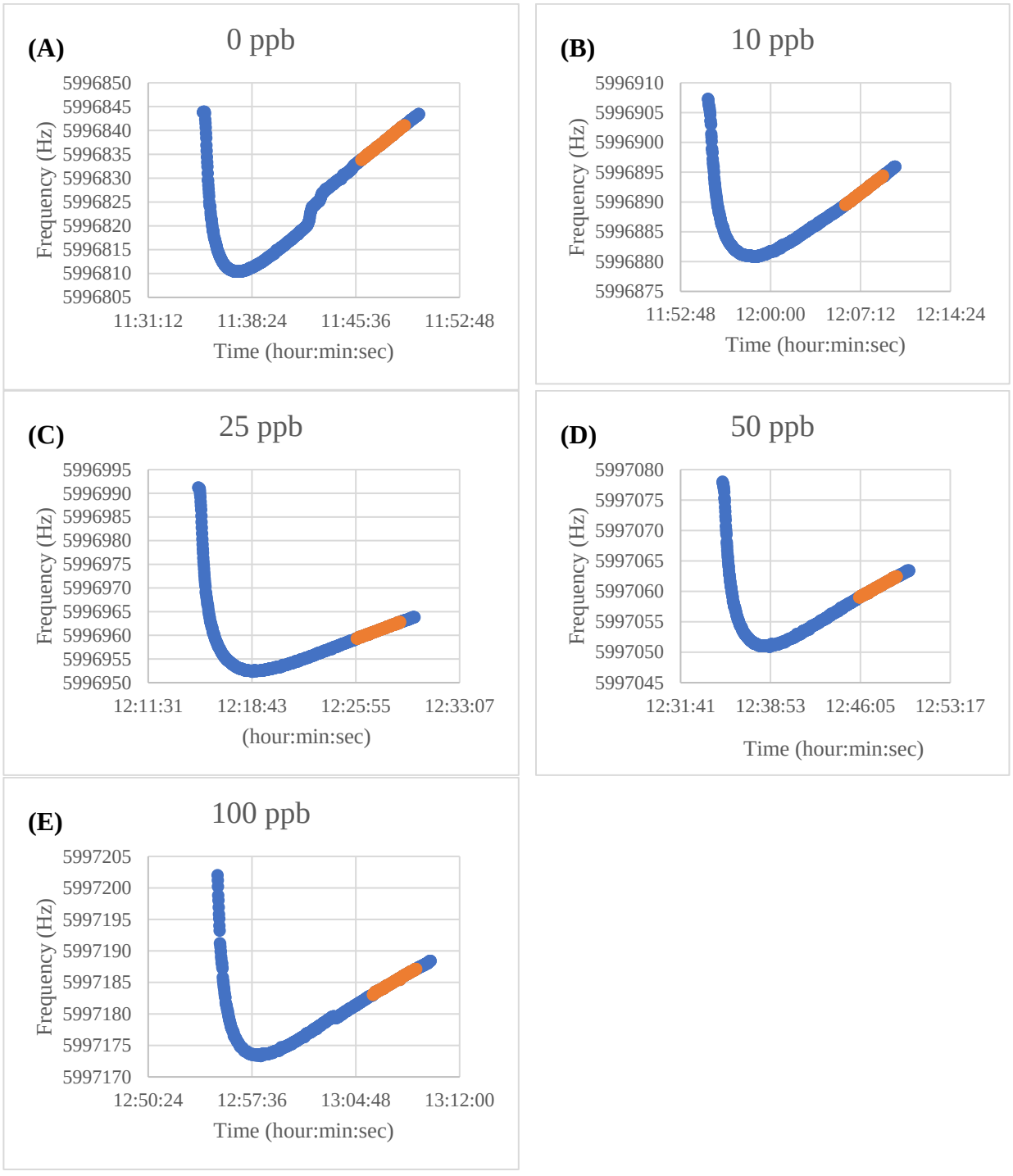

Figure E.3 Frequency vs. time variations for five lead concentrations in ultra-pure water conducted on March 10, 2022 with 15 minutes stabilization time. (A) 0 ppb. (B) 10 ppb. (C) 25 ppb. (D) 50 ppb. (E) 100 ppb.

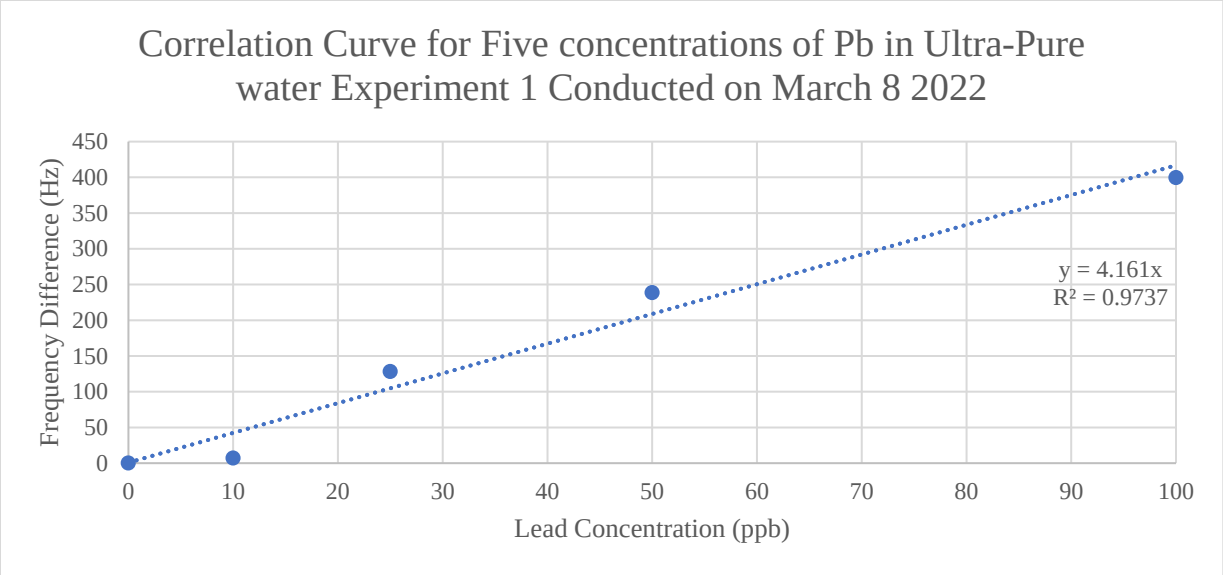

Figure E.4 Linear correlation curve for five lead concentrations in ultra-pure water experiment 1 conducted on March 8, 2022. (Error bars show standard deviation of observation within experiment 1)

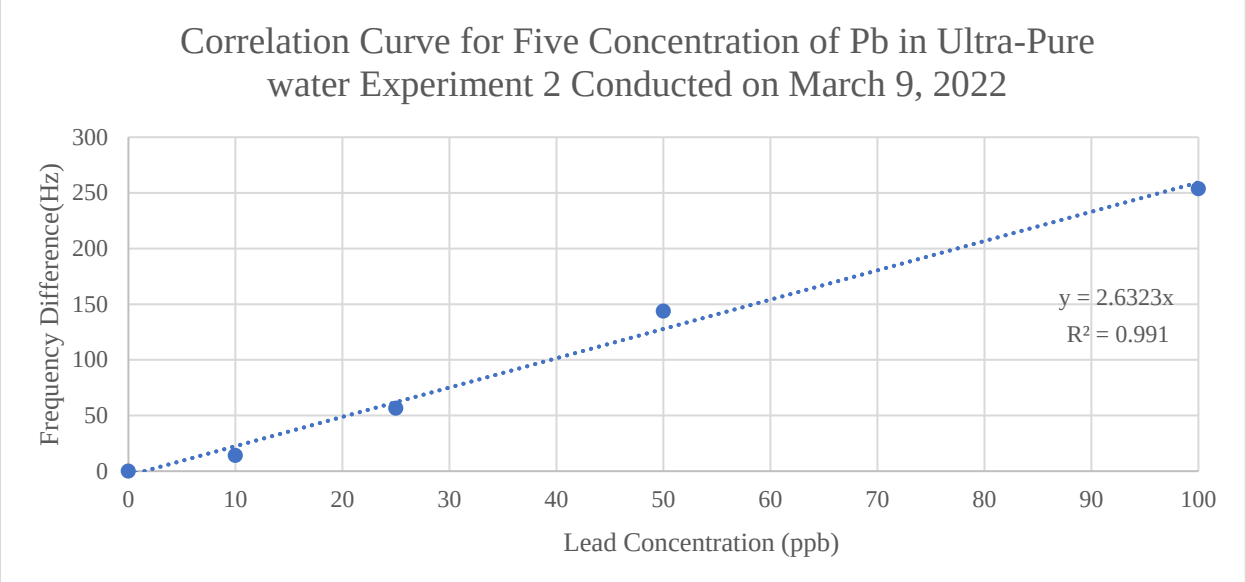

Figure E.5 Linear correlation curve with for five lead concentrations in ultra-pure water experiment 2 conducted on March 8, 2022. (Error bars show standard deviation of observation within experiment 2)

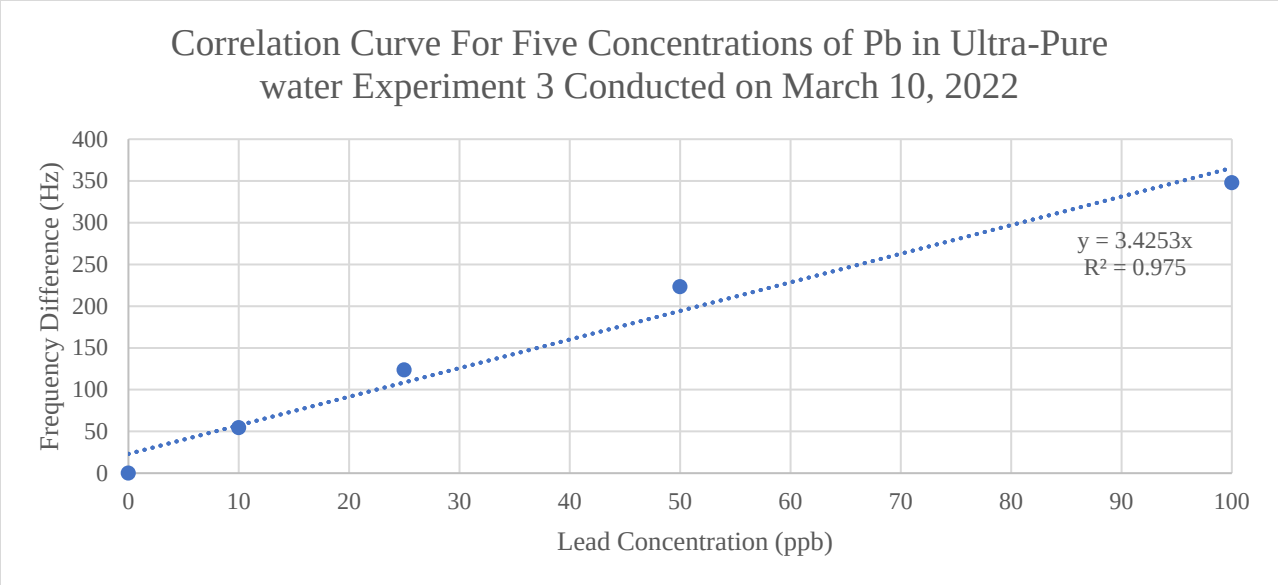

Figure E.6 Linear correlation curve for five lead concentrations in ultra-pure water experiment 3 conducted on March 10, 2022. (Error bars show standard deviation of observation within experiment 3)

APPENDIX F

The arsenic (As) and lead (Pb) samples in 0.5% HNO_3 and ultra-pure water were prepared using stock solutions containing 2% HNO3.

Reagent. The ultra-pure HNO3 for ICP analysis was obtained from Shimadzu Co. The 1,000-ppm arsenic in 2% HNO3 stock solution and 100-ppm was obtained from Exaxol Co. (Exaxol, USA).

0.5% HNO_3 solvent preparation. We first calculated the total volume of 0.5% HNO3 needed for the dilution (*Table F.1*). Then, a volumetric flask (100 or 500 mL) was rinsed with ultra-pure water at least five times, then 20 ml of ultra-pure water was added. Parallelly, five to six pipette tips were placed in the tip holder outside the bench hood. Subsequently, we pipetted an amount (*Table F.1*) of ultra-pure HNO3 in the Nalgene volumetric flask based on the volume needed. Finally, more ultra-pure water was added to the volumetric flask until the 100 / 500 mL mark line and the Nalgene flask were capped and shaken.

Table F.1 0.5% HNO_3 dilution table.

Ultra-pure HNO_3 ~68.5% (mL)	Ultra-pure Water (mL)	0.5 % HNO_3 (mL)
0.74	99.26	100
3.65	496.35	500

Arsenic sample preparation. The arsenic samples were diluted from the1,000 ppm arsenic stock solution containing 2% HNO_3 using a 100 ml Nalgene volumetric flask. The arsenic samples were diluted either with ultra-pure water or 0.5 % HNO_3. *Table F.2* shows the calculation table we used for the arsenic sample in the 0.5% HNO_3 calculation. *Table F.3* shows the calculation table for the arsenic samples in ultra-pure water calculation. The dilution was

conducted using a 5-50 μL micropipette obtained from Four E's Scientific Co. (Four E's Scientific, China). All arsenic samples only required the pipetting of the arsenic stock solution once to minimize the potential error.

Table F.2 The arsenic sample in 0.5% HNO_3 preparation table.

Arsenic concentration (ppb)	1,000 ppm arsenic in 2% HNO_3 pipetted (mL)	0.5% HNO_3 (mL)	Total Volume (ml)
0	0	100.000	100.000
50	0.005	99.995	100.000
100	0.010	99.990	100.000
200	0.020	99.980	100.000

Table F.3 The arsenic sample in ultra-pure water preparation table.

Arsenic concentration (ppb)	1,000 ppm arsenic in 2% HNO_3 pipetted (mL)	Ultra-pure water (mL)	Total Volume (ml)
0	0	100.000	100.000
50	0.005	99.995	100.000
100	0.010	99.990	100.000
200	0.020	99.980	100.000

Lead sample preparation. The lead samples were diluted from the100 ppm lead stock solution containing 2% HNO_3 using a 100 ml Nalgene volumetric flask. The lead samples were diluted with ultra-pure water. *Table F.4* shows the calculation table we used for the lead sample in ultra-pure water. The dilution was conducted using a 5-50 μL Four E's Scientific micropipette (Four E's Scientific, China) for concentrations between 10 ppb and 50 ppb. The dilution was conducted using a 100-1000 μL United Scientific micropipette (United Scientific, USA). All lead samples only required the pipetting of the lead stock solution once to minimize the potential error.

Table F.4 The lead sample in ultra-pure water preparation table

Lead concentration (ppb)	100 ppm lead in 2% HNO_3 pipetted (mL)	Ultra-pure water (mL)	Total Volume (ml)
0	0	100.000	100.000
10	0.01	99.990	100.000
25	0.025	99.975	100.000
50	0.050	99.950	100.000
100	0.100	99.900	100.000
200	0.200	99.800	100.000